



JOHANNES GUTENBERG
UNIVERSITÄT MAINZ



Designing multivalent nanoplatforms using antiviral peptides for therapy and diagnosis

Master's thesis

Siska Führer

Born June 29th, 1998 in Cuxhaven, Germany

Max-Planck-Institute for Polymer Research Mainz

Johannes Gutenberg University Mainz

Mainz, April 2021

Entwicklung von multivalenten Nanoplattformen zur Peptidassemblierung für die Therapie und Diagnose viraler Erkrankungen

von

Siska Führer

Zur Erlangung des akademischen Grads

Master of Science

Fachbereich 09 – Chemie, Pharmazie und Geowissenschaften

Johannes Gutenberg-Universität Mainz

Mainz, April 2021

Zusammenfassung

Die vorliegende Masterarbeit befasst sich mit der Entwicklung von multivalenten Nanokonstrukten für die Diagnostik und Therapie der viralen Erkrankungen, die durch HIV und SARS-CoV-2 hervorgerufen werden. Verwendet werden unterschiedliche Peptide, die durch ihre Bindung an virale Fusionsproteine das Eindringen des Pathogen in die Wirtszelle verhindern und auf diese Weise antivirale Wirkung besitzen. Im Zuge dieser Arbeit werden erwähnte Peptide gegen HIV und SARS-CoV-2 auf zwei unterschiedlichen Organisationsplattformen multimerisiert. Die erste untersuchte Plattform stellt das Streptavidin-Biotin-System da, welches über starke, nicht kovalente Bindungen zwischen dem Protein und seinem Liganden (Biotin) verfügt und durch die chemisch-synthetische Einführung einer Biotinfunktionalität an die antiviralen Peptide eine Möglichkeit zur Assemblierung von bis zu vier Äquivalenten biotinylierter Liganden an einem Protein bietet. Um eine Kombination von zwei verschiedenen Peptiden an einer Biotineinheit zu ermöglichen, wird ein trifunktionales Verbindungsmolekül synthetisiert und die jeweiligen Peptide chemoselektiv an dieses konjugiert. Die zweite untersuchte Organisationsplattform stellen Goldnanopartikel da, die über Ligandenaustauschreaktionen in der Lage sind mit thiolhaltigen, antiviralen Peptiden beschichtet zu werden. Auf diese Weise können viele Äquivalente verschiedener Peptide auf einer Plattform vereint werden und die modifizierten Goldnanopartikel sowohl therapeutisch als auch diagnostisch genutzt werden.

The fact that, with respect to size, the viruses overlapped with the organisms of the biologist at one extreme and with the molecules of the chemist at the other extreme only served to heighten the mystery regarding the nature of viruses. Then too, it became obvious that a sharp line dividing living from non-living things could not be drawn and this fact served to add fuel for discussion of the age-old question of "What is life?"

-Wendell Meredith Stanley (1946)

Eidesstattliche Erklärung
zum selbstständigen Verfassen der Masterarbeit

**Masterarbeit im Studiengang Chemie oder Biomedizinische
Chemie an der Johannes Gutenberg - Universität Mainz**

Ich, **Siska Führer**, Matrikelnummer **2732616**, versichere, dass ich meine Masterarbeit selbstständig verfasst und keine anderen als die angegebenen schriftlichen und elektronischen Quellen sowie andere Hilfsmittel benutzt habe. Alle Ausführungen, die anderen Schriften wörtlich oder sinngemäß entnommen wurden, habe ich kenntlich gemacht.

Mainz, 16. April 2021

(Ort, Datum)



(Unterschrift Siska Führer)

Acknowledgments

This work was made possible with the participation and support of so many people, who I want to thank at this point.

I want to express my deepest gratitude to PROF. DR. TANJA WEIL, who gave me the opportunity to work on such an interesting research topic in her inspiring research group. It has been a great experience to participate in her department.

I would like to thank PROF. DR. POL BESENIUS for taking his time again to be my second examiner.

I want to express my gratitude to PROF. DR. FRANK KIRCHHOFF for the profitable collaboration in this project.

My sincerest thanks I would like to express to DR. SEAH LING KUAN, for her supervision during my master's thesis, her support and guidance with her expertise and for always taking her time to help me, whenever problems were occurring.

I especially want to thank ASTRID HECK for supporting me professionally and mentally during this work and the past years, for always having an open ear for me and sharing her knowledge with me. I would like to thank LUJUAN XU for many helpful conversations when synthesis problems occurred and for her supply with chemicals.

Overall, I want to thank the whole WEIL DEPARTMENT for integrating me so nicely into the group right from my start as a research assistant in 2018 and for creating an inspiring and supportive working atmosphere in which I was able to develop as a researcher.

Finally, I want to thank my family for supporting me throughout my development during the past years and my partner, who has unconditionally strengthened my back, for his understanding support and making daily life so much easier.

Table of contents

| | |
|--|-----------|
| Zusammenfassung | II |
| Eidesstattliche Erklärung | IV |
| Acknowledgments | V |
| 1.1 Introduction | 1 |
| 1.1 VIRAL INFECTIONS | 1 |
| 1.2 ANTIVIRAL THERAPEUTICS AND DIAGNOSTICS | 3 |
| 1.2.1 Protein and peptide therapeutics | 5 |
| 1.2.2 Gold nanoparticles as theranostics | 9 |
| 1.3 SUPRAMOLECULAR NANOPLATFORMS AS THERAPEUTICS AND DIAGNOSTICS | 12 |
| 1.3.1 Avidin-Biotin Technology | 13 |
| 1.3.2 Strategies in organic chemistry for bioconjugation of biotinylated peptides | 17 |
| 1.3.2.1 Maleimide-thiol conjugation | 19 |
| 1.3.2.2 Reactions of alkynes with nucleophiles and in cycloadditions | 20 |
| 1.3.2.3 Click chemistry in development of multifunctional linker molecules | 22 |
| 2. Motivation and aim of this work | 23 |
| 3. Results and discussion | 26 |
| 3.1 SYNTHESIS OF A TRIFUNCTIONAL LINKER MOLECULE FOR PEPTIDE CONJUGATION | 26 |
| 3.1.1 Copper catalyzed azide alkyne cycloaddition of biotin-PEG4-alkyne | 27 |
| 3.1.2 Coupling of Biotin-PEG4-triazolo-lysine (2) to propargyl-PEG4-amine | 28 |
| 3.1.3 Deprotection of boc protected Biotin-PEG4-triazolo-lysine-PEG4-alkyne | 31 |
| 3.1.4 Coupling of Biotin-PEG4-triazolo-lysine-PEG4-alkyne to maleimide-PEG4-NHS | 33 |
| 3.2 CONJUGATION OF ANTIVIRAL PEPTIDES TO BIOTINYLATED LINKER MOLECULES | 39 |
| 3.2.1 Conjugation of EK1 peptide to bifunctional Biotin-PEG11-maleimide linker | 39 |
| 3.2.2 Conjugation of VIRIP to bifunctional Biotin-PEG11-maleimide linker | 42 |
| 3.2.3 Conjugation of VIRIP to trifunctional Biotin-PEG-maleimide-alkyne linker | 44 |
| 3.2.4 Azide-alkyne cycloaddition of EK1 to biotinylated VIRIP linker construct | 47 |
| 3.2.5 Reaction screening for thiol-yne reaction versus thiol-maleimide reaction with test peptides | 51 |
| 3.3 ASSEMBLY OF BIOTINYLATED PEPTIDES TO STREPTAVIDIN | 55 |
| 3.3.1 Assembly of biotinylated EK1 to Streptavidin | 56 |
| 3.3.2 Assembly of biotinylated VIRIP to streptavidin | 58 |
| 3.3.3 Characterization of multimerized peptides on streptavidin via SDS PAGE | 59 |
| 3.4 ASSEMBLY OF ANTIVIRAL PEPTIDES TO CITRATE STABILIZED GOLD NANOPARTICLES | 62 |
| 3.4.1 Assembly of EK1 and VIRIP to 5 nm gold nanoparticles | 62 |
| 3.4.2 Characterization of peptide coated gold nanoparticles | 63 |
| 3.5 IN VITRO STUDIES ON ANTIVIRAL ACTIVITY OF MULTIMERIZED ANTIVIRAL PEPTIDES | 70 |
| 3.5.1 Antiviral activity of streptavidin-based peptide constructs | 70 |
| 4. Conclusion and outlook | 73 |
| 5. Experimental Section | 75 |
| 5.1 INSTRUMENTS AND MATERIALS | 75 |
| 5.2 FREQUENTLY PRACTICED METHODS | 76 |
| 5.3 SYNTHESIS OF TRIFUNCTIONAL LINKER | 79 |

| | |
|---|----|
| 5.3.1 Synthesis of 2-((tert-butoxycarbonyl) amino)-6-(4-(15-oxo-19-((3a <i>S</i> ,4 <i>S</i> ,6a <i>R</i>)-2-oxohexahydro-1 <i>H</i> -thieno[3,4- <i>d</i>]imidazol-4-yl)-2,5,8,11-tetraoxa-14-azanonadecyl)-1 <i>H</i> -1,2,3-triazol-1-yl) hexanoic acid (2) | 79 |
| 5.3.2 Synthesis of tert-butyl (17-oxo-22-(4-(15-oxo-19-((3a <i>S</i> ,4 <i>S</i> ,6a <i>R</i>)-2-oxohexahydro-1 <i>H</i> -thieno[3,4- <i>d</i>]imidazol-4-yl)-2,5,8,11-tetraoxa-14-azanonadecyl)-1 <i>H</i> -1,2,3-triazol-1-yl)-4,7,10,13-tetraoxa-16-azadocos-1-yn-18-yl)carbamate (3) | 80 |
| 5.3.3 Synthesis of 17-oxo-22-(4-(15-oxo-19-((3a <i>S</i> ,4 <i>S</i> ,6a <i>R</i>)-2-oxohexahydro-1 <i>H</i> -thieno[3,4- <i>d</i>]imidazol-4-yl)-2,5,8,11-tetraoxa-14-azanonadecyl)-1 <i>H</i> -1,2,3-triazol-1-yl)-4,7,10,13-tetraoxa-16-azadocos-1-yn-18-amine (4) | 81 |
| 5.3.4 Synthesis of 1-(3-(2,5-dioxo-2,5-dihydro-1 <i>H</i> -pyrrol-1-yl) propanamido)- <i>N</i> -(17-oxo-22-(4-(15-oxo-19-((3a <i>S</i> ,4 <i>S</i> ,6a <i>R</i>)-2-oxohexahydro-1 <i>H</i> -thieno[3,4- <i>d</i>]imidazol-4-yl)-2,5,8,11-tetraoxa-14-azanonadecyl)-1 <i>H</i> -1,2,3-triazol-1-yl)-4,7,10,13-tetraoxa-16-azadocos-1-yn-18-yl)-3,6,9,12-tetraoxapentadecan-15-amide (5) | 82 |
| 5.4 BIOCONJUGATION OF ANTIVIRAL PEPTIDES TO BIOTINYLATED MOLECULES | 84 |
| 5.4.1 Conjugation of EK1 to maleimide-PEG11-biotin (6) | 84 |
| 5.4.2 Conjugation of VIRIP to maleimide-PEG11-biotin (7) | 85 |
| 5.4.3 Conjugation of VIRIP to trifunctional biotin-PEG-maleimide-alkyne linker (8) | 86 |
| 5.4.4 Conjugation of EK1 peptide to maleimide-PEG3-azide (9) | 87 |
| 5.5 ASSEMBLY OF BIOTINYLATED PEPTIDES ON STREPTAVIDIN | 89 |
| 5.5.1 Assembly of biotinylated EK1 on streptavidin | 89 |
| 5.5.2 Assembly of biotinylated VIRIP on streptavidin | 89 |
| 5.6 ASSEMBLY OF PEPTIDES ON 5 NM GOLD NANOPARTICLES | 89 |
| Literature | 90 |
| Abbreviations | 93 |
| List of figures | 94 |
| List of schemes | 96 |
| List of graphs | 97 |
| List of tables | 97 |
| List of appendixes | 97 |
| Appendix | 99 |

1.1 Introduction

In our modern society, life threatening diseases are often resulting of inflammation, cancer or infections with bacteria or viruses. The development of effective therapies for these lethal illnesses is of common interest, especially in times with global epidemics. A special case of diseases which can cause serious health problems are viral infections, since in contrast to bacteria or cancer cells, the pathogen causing the infection cannot be characterized as being alive^[1]. Nevertheless, viruses are able to adapt to their environment through mutations^[1]. In fact, they are highly specialized to the host organism they are infecting by having a steadily optimizing protein shell, which allows them to protect and store their genetic information and at the same time efficiently use the host cells infrastructure for their own replication^[2]. Besides the commonly mentioned pathogens that use mammalian cells as hosts, viral infections of plants, mushrooms (mycoviruses) and bacteria (phages) are known^[3]. The following work will focus on mammalian viruses especially the ones that infect human beings.

1.1 Viral infections

Viral diseases have been from great interest in medicine and science since centuries^[3]. One of the most prominent examples for an epidemic viral infection was the smallpox virus, whose spreading during the 18th century was a challenging task for scientist, but could be solved starting with the first vaccination by Edward Jenner and ending with the eradication of the smallpox virus in 1979^[3]. Today a variety of viral infections are spreading permanently or epidemic wise such as Rhino, Hepatitis C and Influenza or Ebola and SARS viruses. Typically viruses are divided into retro viruses which integrate into the human genome, RNA and DNA viruses whereas the last two describe in which form the virus genome is transferred to the host cell^[1,4].

One of the most challenging viral infections today are AIDS which is

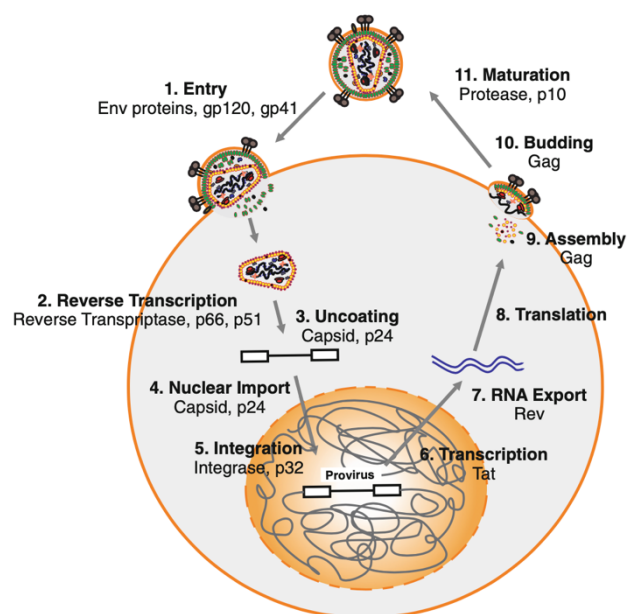


Figure 1: replication mechanism of HIV. Source:[4].

caused by the retrovirus HIV and SARS which is caused by the novel RNA coronavirus SARS-CoV-2^[5].

HIV originated in the zoonosis of a primate with human, SARS-CoV-2 in the one of bats and an unknown intermediate host with human^[3,5]. Both pathogens show a similar way of entering their host cell: HIV and SARS-CoV-2 connect to a coreceptor and use the available fusion machinery for a directed transfer of their genome through the cell membrane^[4,5]. Figure 1 shows the replication mechanism of HIV^[4]. The reproducing cycle of the HI virus starts with the receptor mediated entry of the particle to the cell, followed by its uncoating and reverse transcription of its genome from RNA to DNA, which is then able to be integrated into the host cell's DNA^[4]. In this state the viral

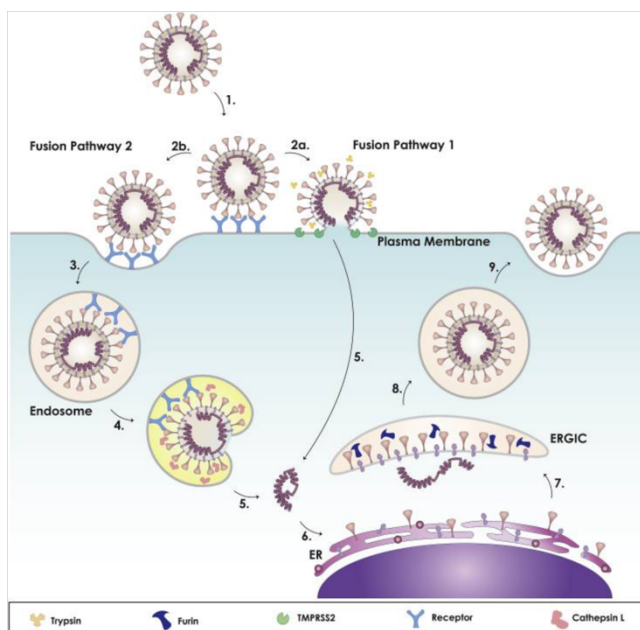


Figure 2: Fusion and replication mechanism of SARS-CoV-2.
Source:[5].

genome can rest for several years which makes HIV a lentivirus and a retrovirus^[4]. When replication of is triggered, the transcription of the integrated virus DNA to RNA and the translation of viral proteins is performed^[4]. The HIV preproteins assemble to a nonfunctioning virus particle that exits the host cell through budding and are afterwards processed through the viral protease to become a matured and infectious virus^[4].

The replication cycle of SARS-CoV-2 is slightly different to the one of HIV. Coronaviruses are able to enter their host cell in two different fusion pathways depending of the stage of infection^[5] (see Figure 2, fusion pathway 1 and 2). At early stage (fusion pathway 1), the pathogen is merging its own membrane with the outer membrane of the host cell, as it is for HIV^[5]. This fusion is proceeded receptor mediated as well, even though the receptor is different to the one HIV uses (see section 1.2)^[4,5].

At late-stage infection, the coronavirus is entering the cell to be infected through receptor mediated endocytosis and afterwards merging with the endosomal membrane to channel its genetic information into the cytosol^[5] (fusion pathway 2). Independently from how the pathogen entered its host, the RNA composed genome will be directly transcribed to viral preproteins that can mature to infection potent particles which exit

the cell through exocytosis^[5]. Compared to HIV, SARS-CoV-2 is not integrating into the human genome, which makes it a RNA virus^[5]. Taking into account the previously described mechanisms of replications, several kinds of interfering this cycle seem to be realistic to achieve a prevention of viral reproduction in the course of an infectious disease.

1.2 Antiviral therapeutics and diagnostics

As HIV causes the serious and often deadly disease AIDS, there is an urgency for efficient treatment of the infection. Since HIV itself is genetically unstable, it was not possible yet to develop a vaccination that can prevent a healthy person from being infected with HIV, but during the past decades different achievements were gained concerning the containment of virus spreading and even preventing infected persons from transferring the virus^[6]. The following Figure 3 shows the approaches of anti-HIV treatment since 1986^[6].

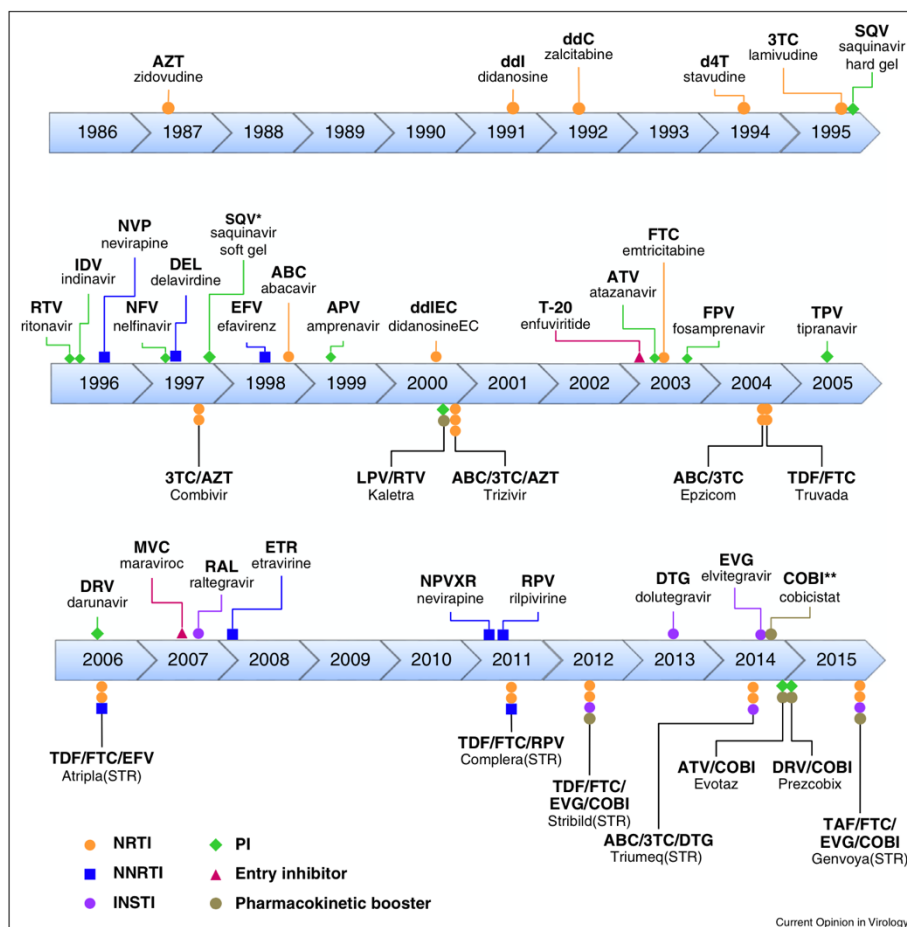
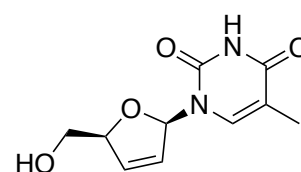
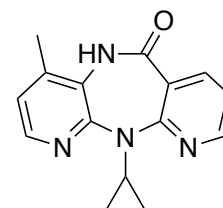


Figure 3: Approved antiviral drugs against HIV and AIDS since 1986. Source: [6].

Generally, antiviral drugs are classified by the way they block the virus replication^[6]. In the beginning of HIV treatment include mainly nucleotide reverse transcriptase inhibitors (NRTIs) like Zidovudine and Stavudine that inhibit the reverse transcription from HIV-RNA to DNA^[6]. This approach was followed by viral protease inhibitors (PIs) that inhibit the maturation of the virus particle after budding like Saquinavir, Amprenavir and Darunavir, but in contrast to NRTIs PIs cannot prevent the insertion of the viral DNA into the host cell's DNA^[6]. Since 1996 non nucleotide reverse transcriptase inhibitors (NNRTIs) are approved^[6]. This kind of drugs like Nevirapine have the same effect as NRTIs as they are inhibiting the reverse transcriptase, but do not base on nucleotide analogia^[6]. Integrase strand



Stavudine (NRTI)



Nevirapine (NNRTI)

Figure 4: The molecular structure of Stavudine and Nevirapine.

transfer inhibitors (INSTIs) like Raltegravir are used since the beginning of the 21st century and prevent the virus DNA from inserting into the human genome^[6]. One drawback, that NRTIs, NNRTIs and INSTIs have in common is that once a host cell is infected, they are not able to prevent a production of multiple viruses by one cell and therefore^[6]. The earliest way to pharmacologically interfere the HIV replication cycle is to prevent it from entering the cell. This can be achieved by entry inhibitors like Maraviroc, which is a small molecule or T-20, a peptide that is blocking the membrane fusion of HIV with the host cell^[6]. One of the greatest advantages of these antiviral agents is their ability to act as a therapeutic without a need to penetrate the host cells membrane, which in contrast is an indispensable criterium of therapeutics that interfere the viral replication cycle^[6,7]. Details of the inhibitory mechanism of entry inhibitors will be discussed in section 1.2.1. Today, antiretroviral therapies against HIV infections are usually performed through the combination of the previously mentioned drugs, as a combinatory treatment is more effective as one class of drug alone^[6]. Since 2014 for instance, the NRTIs Abacavir and Lamivudine are combined with the INSTI Dolutegravir in the preparation Triumeq^[6]. Recent studies show, that the triple therapy with antiretroviral drugs cannot only prevent an AIDS disease from outbreaking, it even is able to reduce the transferring of HIV to other persons by 95%^[6]. Nevertheless, there is no curative treatment for HIV^[6].

In 2019, a novel mutant of SARS virus SARS-CoV-2 began to spread in Wuhan, China^[8]. The rapid spread of the virus has reached the proportions of a pandemic with

severe consequences for healthcare and society. Thus, appropriate treatment of the disease was urgently needed. Although most cases of an infection with SARS-CoV-2 are not of a deadly nature, some patients suffer from the acute respiratory distress syndrome (ARDS) as a result of a SARS-CoV-2 infection^[9]. The resulting pneumonia has an overall mortality of about 60% which makes SARS-CoV-2 a huge health problem for people suffering from previous illnesses or aged persons^[9]. In addition to that, even recovered patients appear to have remaining organ damages^[9].

Today, vaccines against SARS-CoV-2 are already approved, but barely available, so critical cases of the disease will remain to occur, which makes an efficient drug an emerging need^[9]. Studies showed that the treatment of ARDS suffering patients with the monoclonal antibody Tocilizumab, which antagonizes interleukin-6 and is already approved for anti-immunogenic therapy, shows success in reducing the cytokine storm of patients that have to be mechanically ventilated, but does not provide a cure against an SARS-CoV-2 infection^[9]. Another suggested treatment of the coronavirus was the usage of the previously developed anti-Ebola drug Remdesivir^[10]. Inhibiting the viral RNA depending RNA polymerases, Remdesivir was a promising candidate for already approved treatment, but no significant curing effect of an SARS-CoV-2 could be observed^[10]. To date, some vaccinations against SARS-CoV-2 are available, but like it is for HIV, no cure of the disease, so in the end it is still necessary to find a reliable drug against the SARS infection which is able to eliminate the disease's symptoms and prevent the patient from long term damages. To meet these requirement, protein or peptide therapeutics could play an important role, as the examples of Maraviroc or T-20 as efficient and approved entry inhibitors against HIV show^[6].

1.2.1 Protein and peptide therapeutics

Since the field of biologics as treatments evolved in the early 1980s, they steadily established in research and the pharmaceutical market and kept their spotlight over the past decades^[11]. Not only because of their high potential in personalized medicine, but their highly specific set of function, accompanied by a less tendency to cause immune responses, which is not possible to achieve by small-molecule drugs, that often come with side effects^[11].

Since monoclonal antibodies are meanwhile well established in cancer immunotherapy or the treatment of rheumatoid arthritis, the potential of these biologicals is undeniable, but also still has some drawbacks, as the genetic engineering of biologicals is

accompanied by limitations such as laborious purifications processes with low yields, misfolding or immunogenic aggregates^[12]. Therefore, alternative strategies without reduction of the targeting efficiency are of great interest. This can be performed by using endogenous proteins or peptides that show biotherapeutic activity or can be modified to do so^[11].

Concerning the previously discussed entry inhibitors (see section 1.2) antiviral peptides were discovered, that can interfere at different stages of the viral fusion mechanism and therefore play an important role for the development of antiviral treatment, even though they often were overlooked because of their stability^[7]. To underline the different points of action, Figure 5 is showing the fusion mechanism of HIV with its host cells membrane^[7].

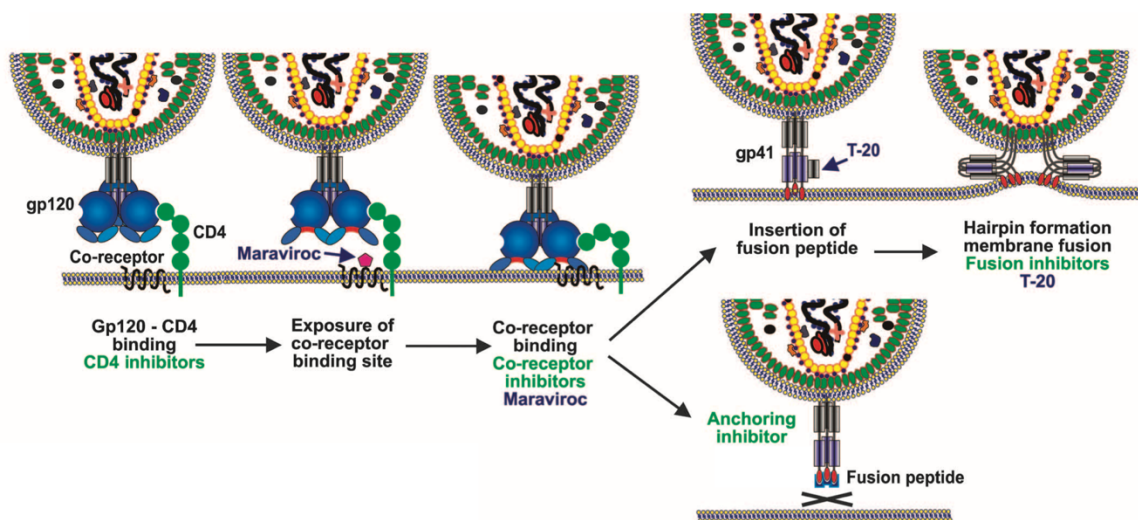


Figure 5: Fusion mechanism of the HI virus with host cell membrane and interfering points of entry inhibitors. Adapted from source [13].

To bind to the host cell, HIV first interacts with the cell membrane receptor CD4 over its glycoprotein (gp) 120^[7]. As a next step a coreceptor bound is formed via the viral coreceptor binding site exposure, which can be inhibited by the previously mentioned small molecule drug Maraviroc^[7]. If an interaction between the coreceptor, which is the chemokine receptor CXCR4 in the case of HIV^[13], is formed the fusion peptide of the virus is inserting into the host cell membrane and forms a hairpin which is leading to the membrane fusion^[7]. In this mechanism it is either possible to interfere through peptide fusion inhibitors, like the already approved T-20 or to block the viral fusion peptide^[7].

During the past years it was possible to obtain several antiviral peptides that show activity against HIV from the hemofiltrate from dialysis patients^[13,14]. One example is the human serum albumin fragment WSC02, which was found to be a potent antagonist of the CXCR4 and therefore is able to prevent the entry of HIV to the cell as well as inhibit the migration of pancreatic cancer cells, which are known to overexpress CXCR4^[15,16].

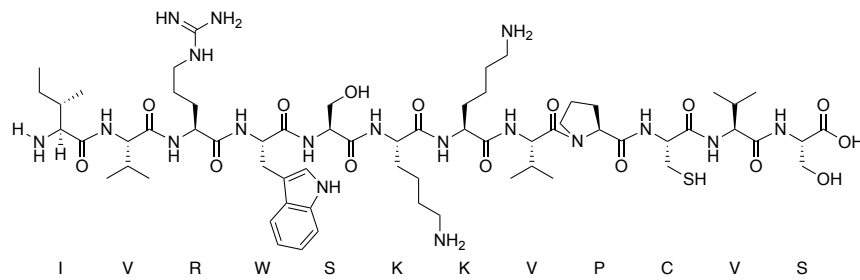


Figure 6: Molecular structure of CXCR4 antagonist WSC02^[15].

Another potent entry inhibitor that was found in hemofiltrate is a α_1 -antitrypsin fragment called VIRIP^[14]. This peptide is able to block the HIV membrane fusion by interacting with the viral fusion peptide and thereby inhibit the insertion process of fusion peptide to the membrane^[14,17].

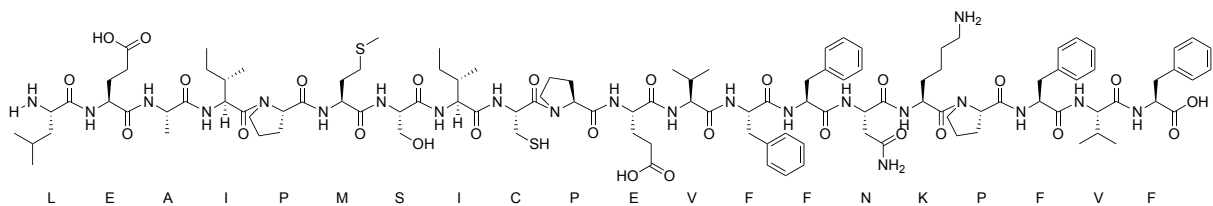


Figure 7: Molecular structure of fusion protein inhibitor VIRIP^[14].

Both peptides showed great activity against HIV and are promising candidates for future antiviral treatments, as they are way easier and cheaper to obtain than monoclonal antibodies^[7,13]. Not only for HIV also for SARS-CoV-2 some bio-based Substances that show antiviral activity were found^[18]. To describe the potential points of action of antiviral substances, Figure 8 is giving an overview on how the fusion mechanism of SARS-CoV-2 with its host cell is proceeding.

The viral spike protein is containing a trimer of two domains S1 and S2^[19] (Figure 8 a)). Whereas the S1 domain is essential for the interaction with the fusion coreceptor ACE2, the S2 domain contains two subdomains HR1 and HR2, that form a fusion core (6-HB) ^[19]. After S1 built up an interaction between the coreceptor, HR1 and HR2 are

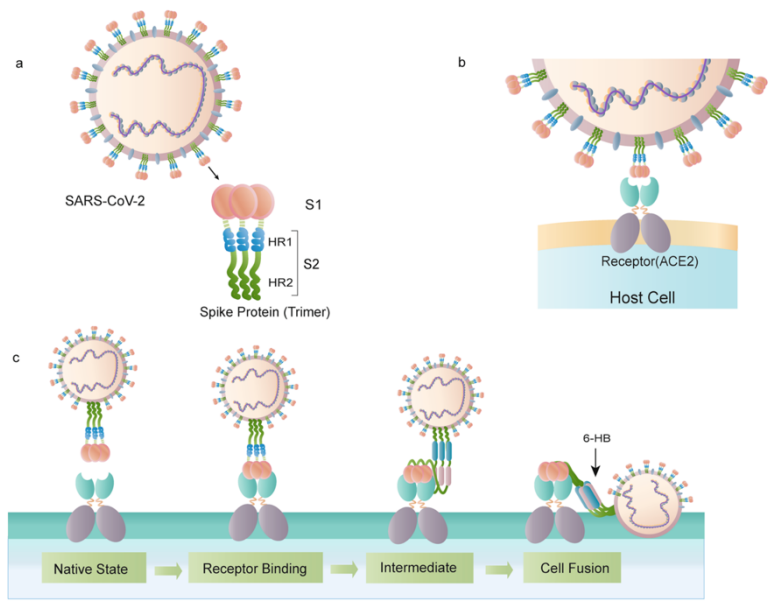
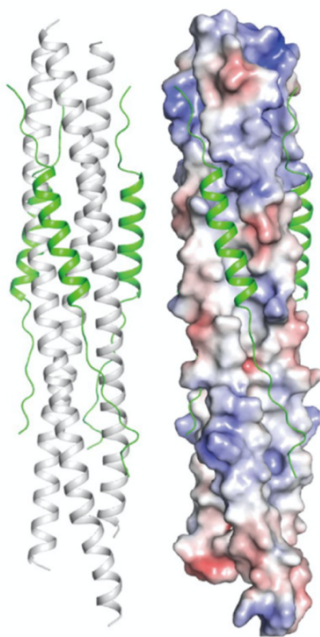


Figure 8: **a)** Structure of SARS-CoV-2 spike protein, **b)** Interaction between S1 subdomain of the virus with host cells ACE2 receptor, **c)** Fusion mechanism of SARS-CoV-2 with host cell membrane via its spike protein. Source: ^[19].

assembling to a multimeric fusion core that enables the virus to fuse with the host cell^[19]. To develop an entry inhibitor, different approaches could be followed, such as



HR1(SARS)-EK1

Figure 9: Model of interaction between EK1 (green) in complex with the HR1 domain of SARS-CoV. Source: ^[20].

targeting S1, HR1 or HR2 domains with suitable peptides or antibodies. The addressing of the S1 domain reveals to be not an efficient target, as it tends to mutate frequently ^[19]. In contrast to that, the S2 domain is highly conserved in different coronaviruses including SARS-CoV, MERS-CoV and SARS-CoV-2, which makes it a highly attractive target^[19]. Besides other candidates, the peptide EK1 was found to target the HR1 subdomain of the S2 domain with an IC₅₀ value of 287 nM^[8]. With this peptide it was possible to prevent the virus-cell fusion in a dose dependent manner up to 100%^[8]. In addition to that, EK1 shows antiviral activity not only against SARS-CoV-2 but against SARS-CoV and MERS-CoV, so the peptide can be claimed to be a pan coronavirus inhibitor^[20]. The following figure shows the molecular structure of the EK1 peptide.

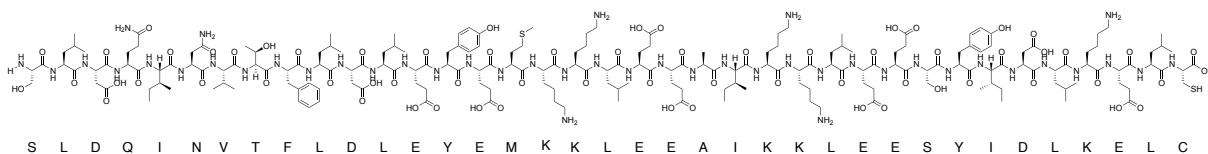


Figure 10: Molecular structure of the EK1 peptide containing 37 amino acids^[20].

The C-terminal cysteine was added to the native EK1 structure found in literature^[8] to enable thiol selective modifications and conjugations on the peptide.

All antiviral peptides previously presented contain a thiol group in form of an internal or terminal cysteine which opens a great opportunity in terms of bioconjugation reactions (see section 0), that can be used for connection or multimerization of different peptides and proteins in antiviral therapy.

1.2.2 Gold nanoparticles as theranostics

Gold nanoparticles obtained great interest during the past years^[21]. Being available in different diameters and shapes like rods, cages and stars, they provide a large surface for different functionalization and formulations^[21]. Standardized protocols can be found in literature to synthesize gold nanoparticles from HAuCl₄ and sodium citrate in solution and a short amount of time yielding citrate stabilized particles that can undergo ligand exchange reactions^[22]. Figure 11 gives an overview of established modification methods^[21]. As it is shown, besides agents that help visualizing the particles or have an effect on their *in vivo* circulation time like pegylation, gold nanoparticles (GNPs) can be loaded with a variety of bioactive molecules^[21].

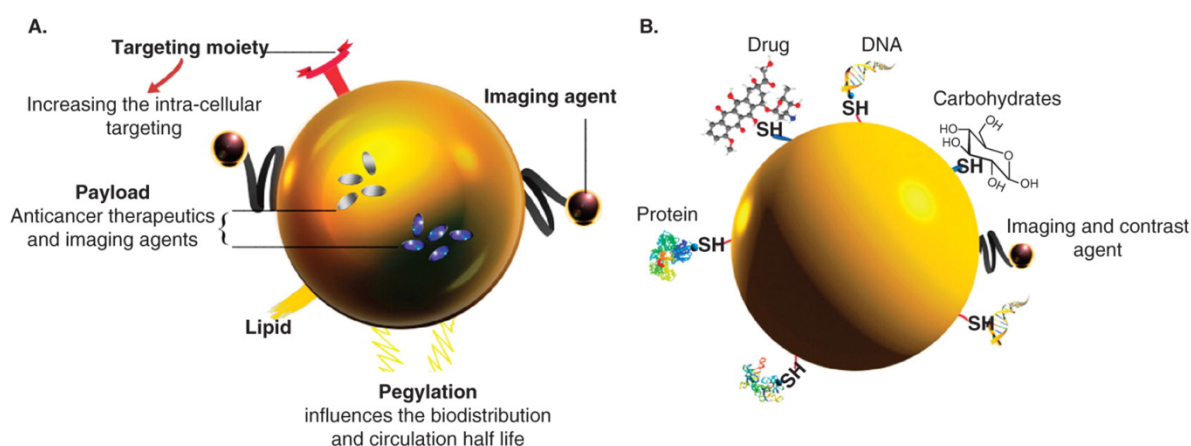


Figure 11: Varieties of possible surface modifications of gold nanoparticles either **A.**: noncovalently or **B.**: covalently via thiol-gold-bonds. Source: ^[21].

Targeting agents like antibodies can influence the biodistribution of GNPs and cause an efficient delivery to the desired cell type/protein like in carcinomas, whereas actual drugs can be payloads to be released in the targeting tissue^[21]. With respect to the

composition of the possible coating substances it is important to mention, that multiple organic molecules like proteins, peptides, sugars and DNA could be successfully attached to the gold nanoparticles [21].

Ligand exchange reaction can also be performed using a thiol containing payload, which is able to displace a citrate molecule that stabilizes the GNP through forming a stable sulphur-gold binding[23].

The adaption of this technique to several problems in biomedicine gave promising results: Peptide coated gold nanoparticles were able to prevent macrophage initiated lung injury in *in vivo* mouse models through manipulating the macrophage polarization[23]. GNPs that were modified with anti-inflammatory peptides could inhibit the immunogenic signaling of Toll-like receptor (TLR) 4[22] and conjugates of anticancer drugs with GNPs show improved activity and less side effects as the native substances[21].

Concerning viral diseases, it was found that gold nanoparticles that were coated with small interfering RNA (siRNA) were able to prevent an infection with the dengue virus, which is able to cause hemorrhagic fever[24]. In some cases GNPs coated with 3-mercaptopethanesulfonate were even able to destroy the virus itself, making it non-infective, as it is shown in Figure 12[25].

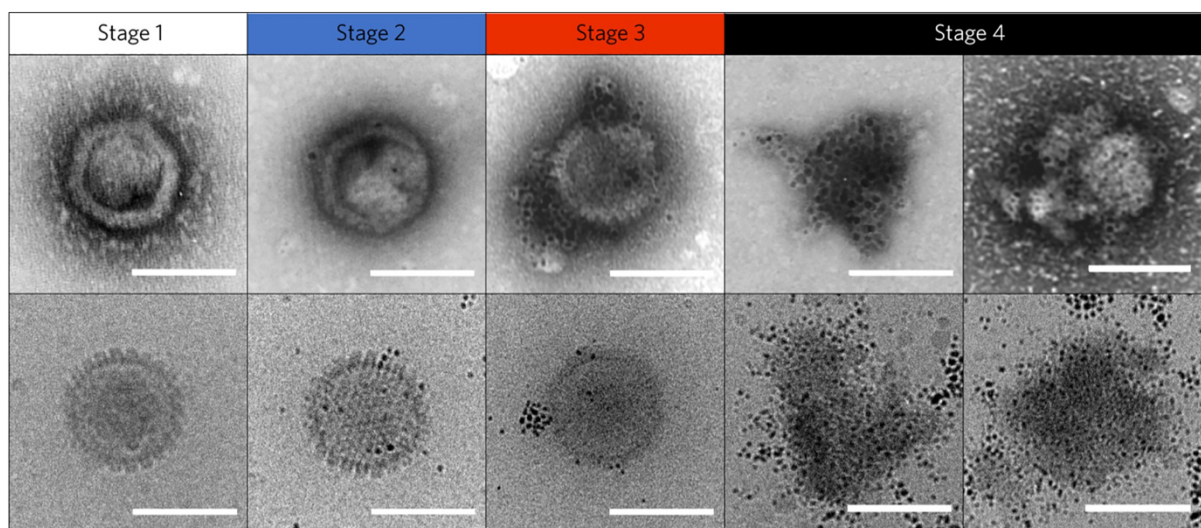


Figure 12: TEM images of herpes simplex viruses type 2 (HSV-2) treated with 3-mercaptopethanesulfonate coated gold nanoparticles for 90 min. Source: [25].

Besides their advantages as an multimerization platform, GNPs are versatile tools in terms of diagnostics or in photothermal therapy[21]. The irradiation of gold nanostructures with light in the near infrared area can cause the excitation of electrons in gold, of which relaxation to ground state can emit energy in the form of heat[21]. In combination with a targeting structure that is specified for a tumor, such as antibodies

appear to be, GNPs can be delivered to a pathogenic tissue, for example a tumor and disrupt the surrounding cells through heat development^[21]. Another advantage of gold

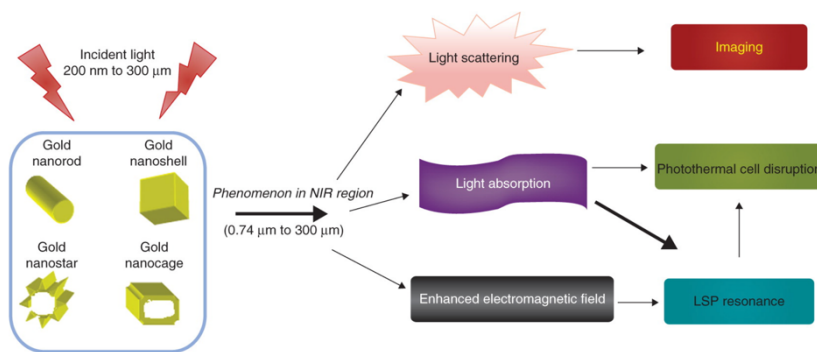


Figure 13: Effects of near infrared light irradiation of gold nanostructures.
Source: ^[21].

nanoparticles is that because of their high electron density, GNPs are easy to detect through light scattering or TEM imaging, which can be used for *in vitro* and *in vivo* diagnostics, for

example of antigens found on the surface of bacteria such as *salmonella*^[21,26].

All these approaches make the modification of gold nanoparticles with antiviral peptides a promising tool in terms of developing effective antiviral treatments.

1.3 Supramolecular nanoplateforms as therapeutics and diagnostics

Besides the metal based or inorganic nanoplateforms, there are several approaches to multimerize bioactive molecules or link a supramolecular functionality with another.

One of the most common natural bioconjugates are lectins interacting with glycosylated peptides or proteins [27]. In nature, lectins are generally characterized as proteins that are able to catch sugars from solution or help bacteria in interacting with other cells trough the binding of surface accessible glycoproteins[27]. This natural phenomenon can be used for several applications in biochemistry. To give an example, the formation of large supramolecular assemblies by the addition of lectins to glycosylated nanoparticles can be mentioned, as it is shown in the following figure[27].

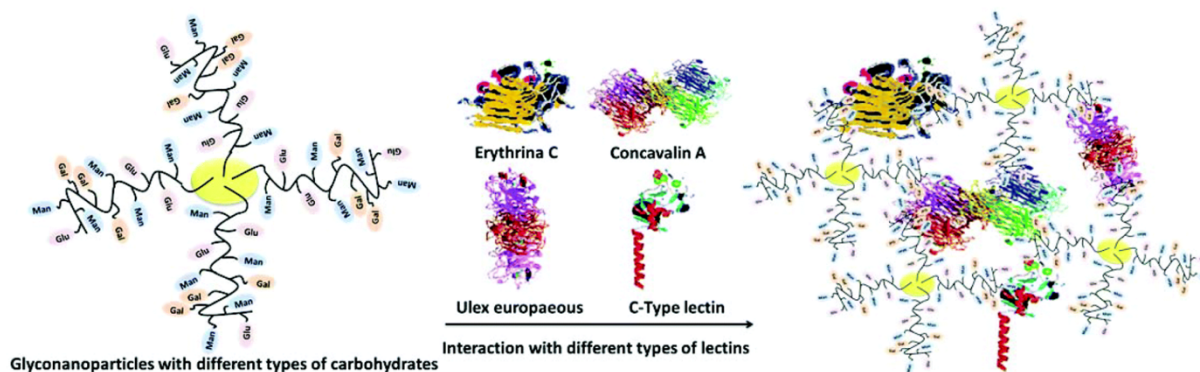


Figure 14: Formation of lectin-carbohydrate-conjugates through glyconanoparticles. Source: [27].

On the basis of these achievements, it was possible to generate glycopolymeric nanocarriers that form structures of vesicular or fibril shape, which allow targeted transport of biologicals such as DNA or monoclonal antibodies [27].

In addition to that, lectins can be used to identify glycosylated proteins through conjugates with quantum dots, which for instance allows the *in vivo* imaging of brain activities[28].

Another approach to combine several therapeutically relevant molecules is to covalently attach a functional group that allows supramolecular interaction to a native protein, such as human serum albumin (HSA).

HSA is one of the main proteins circulating in human blood with a molecular weight of about 65 kDa, acting as a transport protein via hydrophobic interactions[29]. Due to its low immunogenicity and good degradability it has been a versatile tool in connecting different bioactive functionalities on one protein[29].

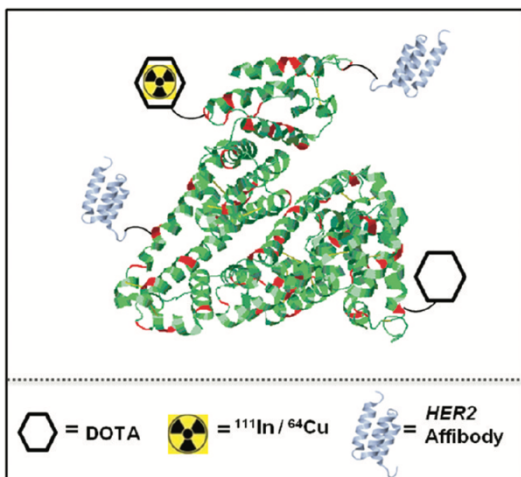


Figure 15: Different functionalities united on one HSA molecule to provide tumor targeting through an HER2 Affinity body and a cancer treatment through chelator DOTA in complex with a radioactive nuclide. Source:[29].

The high clearance of HSA in the kidneys allow an increased circulation time of the bioconjugates and improve the drug's solubility^[29]. The modification of HSA can be achieved by covalent reactions between its surface accessible amines or thiols and reactive forms of the species that have to be introduced, such as maleimides or NHS-esters^[29]. Figure 15 is giving an example of an HSA conjugate with an HER2 affinity body that targets cancer cells and the covalently bound chelator DOTA, which undergoes complexation of radioactive nuclides for PET imaging or radioactive cancer treatment^[29].

The resulting complex was successfully tested in *in vivo* mouse models for their anticarcinogenic activity^[29].

1.3.1 Avidin-Biotin Technology

One of the most used protein based supramolecular organization platforms is the system of avidin analogues and their natural ligand biotin^[11]. The association strength between biotin and avidin is the strongest non-covalent binding known in nature, possessing a K_D value of around 10^{-15} M^[30]. Besides Avidin, which can be derived from chicken eggs, streptavidin, which is originated from microorganisms and therefore has a different glycosylation pattern is another versatile biotin binding platform used for supramolecular assemblies^[30,31]. Figure 16 shows the ribbon diagram of native tetrameric streptavidin binding four biotin molecules within its β -barrel secondary structures^[32].



Figure 16: Ribbon diagram of tetrameric wild type streptavidin in complex with four Biotin molecules. Source: RCSB protein data bank, entry 6M9B. Source: [32].

Another avidin-like protein is its deglycosylated derivative neutravidin^[33].

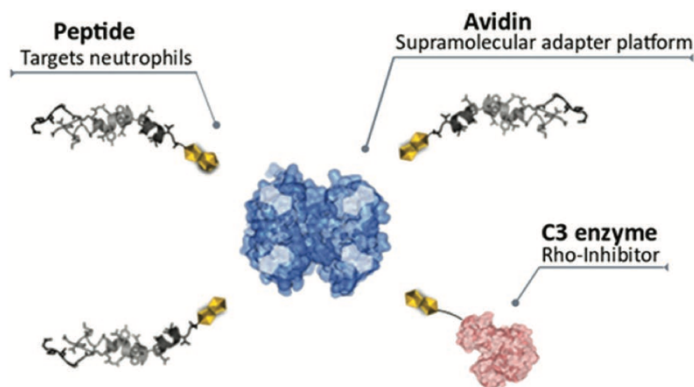


Figure 17: Combination of different biotinylated targeting identities on one avidin to inhibit Rho activity in neutrophils. Source: [34].

Compared to avidin derived from chicken egg white, streptavidin and neutravidin both show clear advantages in terms of biocompatibility concerning for example immunogenicity and bioactivity, such as solubility.

First, avidin has an isoelectric point of around 10, which makes it positively charged in physiological conditions and

most likely to bind unspecifically in *in vivo* conditions, whereas streptavidin and neutravidin are non-glycosylated and therefore have an isoelectric point near neutral, slightly acidic pH, which makes bio-applicability more likely and reduces unspecific binding^[33]. In addition to that, several streptavidin mutants were reported, being able to show increased thermostability and facilitated expression methods in different bacterial strains, which is making the protein more readily available^[30].

As they are able to bind up to four equivalents of biotin per tetramer, streptavidin or neutravidin appears to be very attractive in terms of supramolecular conjugation using the avidin derivatives as a connecting tool^[34].

Recent findings prove, that the combination of targeting peptides, like for neutrophile cells and a therapeutically active protein, like the Rho inhibiting toxin C3 is a promising approach to achieve highly specified treatments for several medical problems, such as reduction of inflammatory processes after traumatic

injuries^[34]. Notably, biotin being a small molecule is unlikely to influence the biologic activity of a substance^[35]. In addition to that, biotin contains a carboxylic functionality, which can be easily used for conjugation to different species. Besides biotin, other molecules are known to also bind to streptavidin/neutravidin, even though in a weaker manner concerning binding strength^[36,37]. One of these molecules is 2-iminobiotin, which occupies the biotin binding pocket of (strept)avidin in a pH dependent manner^[38].

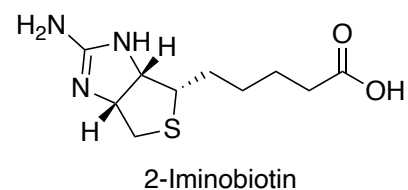
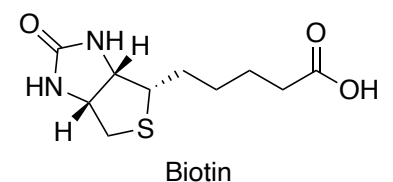


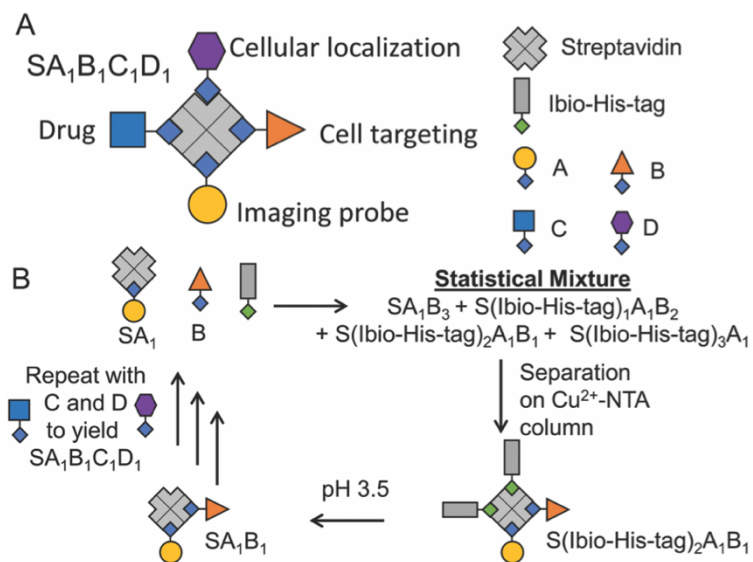
Figure 18: Molecular structures of biotin and 2-iminobiotin.

As a multivalent platform, avidin-like proteins (ALP) are not only useful for biotherapeutic applications, but for analytical or preparative^[39,40]. As examples, the counterstaining of biotin containing samples with R-phycoerythrin streptavidin^[40] as well as the purification of iminobiotin labeled proteins via immobilized avidin can be stressed^[36].

Independently of the field of application, the precise assembly of different biotinylated molecules to streptavidin/neutravidin with respect to stoichiometry is a challenging task^[39]. Adding more than one species to an unoccupied ALP usually causes a statistical mixture of differently occupied proteins that are almost impossible to separate via common chromatographic techniques^[39]. One approach to solve this problem was the usage of iminobiotinylated His-tags, that were added to each assembling step during a multi-step procedure for the creation of a tetravalent streptavidin hybrid, as shown in Scheme 1^[39]. In a first step, only one of the four biotinylated species were added to SAV in combination with the iminobiotin His-tag^[39]. Afterwards the different occupied SAVs were separated from each other on a copper NTA column, with which the His-tags interact,^[39]. Depending on how many His-tags were assembled per SAV molecule, the interactions between the immobilized phase

was increased, causing the mono-biotinylated SAV eluting after the double and triple biotinylated proteins^[39]. The mono-biotinylated product was recovered and iminobiotin was cleaved off from SAV through a change of the buffering pH to acidic conditions (pH 3.5, see Scheme 1), leaving only the desired

monofunctionalized protein^[39]. This procedure was repeated with the remaining biotinylated functionalities until the desired tetrafunctional streptavidin was obtained^[39]. However, even though this approach is promising, the procedure is tedious. As Ni-NTA columns do not offer high separation resolutions, 12 His-tags per iminobiotin unit are



Scheme 1: reaction scheme for the assembly of different functionalities to one streptavidin molecule with precise stoichiometry. Source: ^[39]

required for purification, limiting the yield of the desired product through a loss of material during each purification step.

Considering the eventual necessity for larger scales for an approved biological drug for the treatment of viral infections, a simpler procedure with minimal purification procedure would be more desirable. At the same time, it should be possible to assemble multiple (up to four) different units on one ALP, enabling targeted delivery to the affected tissue and treatment of the corresponding disease.

To meet these requirements, a possible approach could be the design of a multivalent linker molecule that connects two or more bioactive molecules like peptides on the one side and a biotin functionality on the other side, allowing to assemble the pre-linked therapeutics on streptavidin and neutravidin, which then could cause a multimerization effect and enhanced pharmacokinetic and pharmacodynamic parameters.

1.3.2 Strategies in organic chemistry for bioconjugation of biotinylated peptides

With respect to the previously mentioned requirements for an efficient biotherapeutic agents, it is possible to address the problem from a chemically point of view. To assemble different moieties on an ALP, it is mandatory to introduce a biotin functionality onto the bioactive molecule. Biotinylation is a well-known procedure in literature and often performed by site selective protein or peptide modifications in a post-translational manner^[41]. In order to modify native proteins or peptides, it is important to choose a suitable functionality on the molecule, avoiding non-selective or multiple conjugations. Considering the twenty proteinogenic amino acids, several functional groups appear to be modifiable, such as primary amines, as they occur in lysine, arginine and N-terminal residues, alcohols, like in serine or threonine, thiols from cysteine or carboxylates, as they can be found in glutamate, aspartate or C-terminal residues^[42]. Besides their amino acids, proteins often contain glycosylated structures, which can be modified over their aldehydes from carbohydrates after treatment with periodate^[42]. Whereas the mentioned amines often react with activated esters, such as NHS-esters, aldehydes are reacted with hydrazines and carboxylate

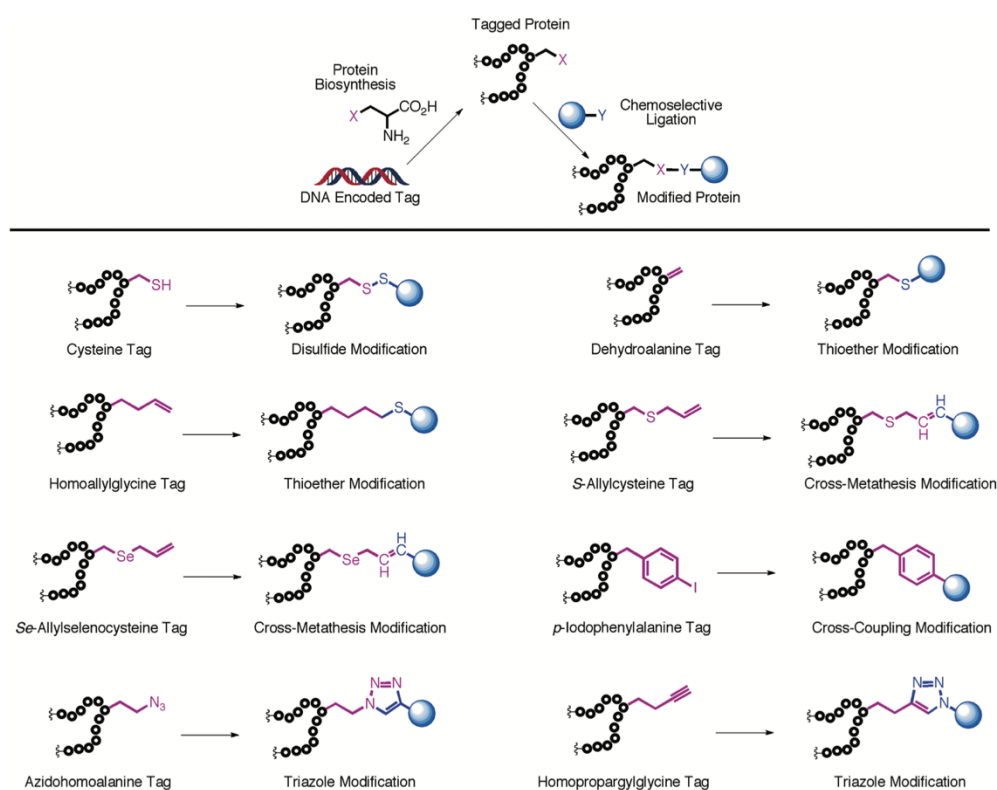
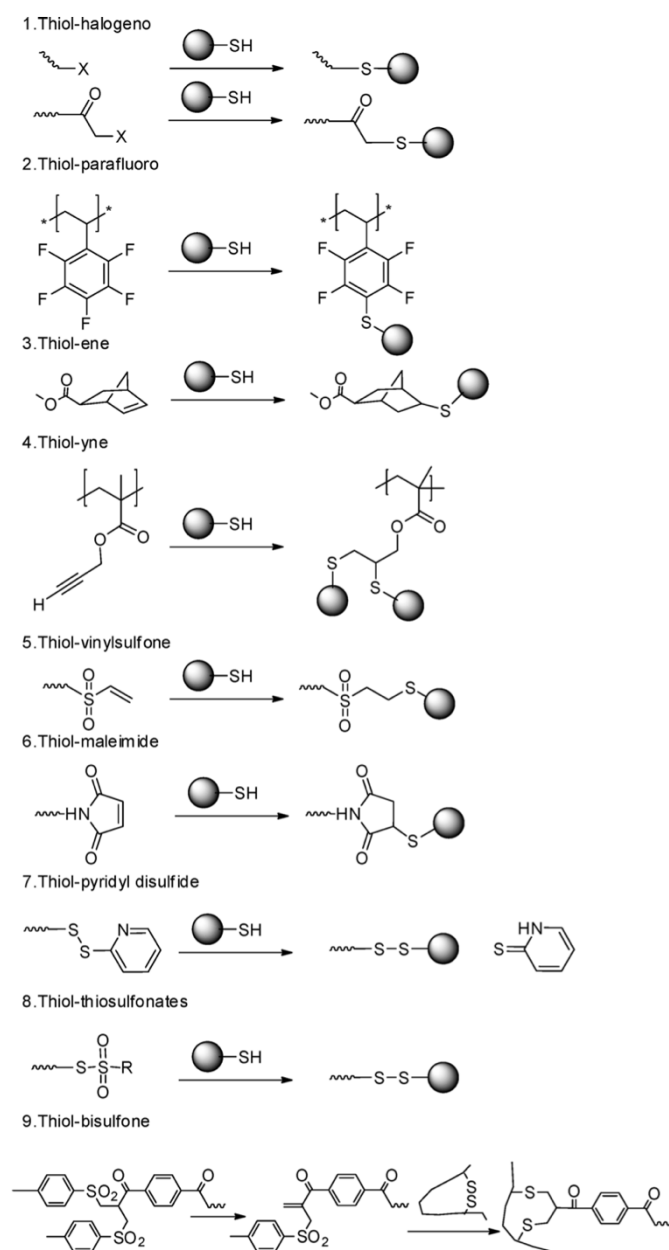


Figure 19: Possible tags and their reaction in order to chemoselectively modify proteins or peptides. Source:[43].

residues on proteins or peptides are mainly used for modifications with amines under formation of amide bonds^[42].

In addition to the employment of natural amino acids, another approach is the biosynthesis of pre-tagged proteins or peptides, allowing chemoselective reactions on single residues, as shown in Figure 19^[43].

It is clear that, besides proteins or peptides that already contain one of the tags shown



Scheme 2: Overview of common thiol selective bioconjugation reactions. Source:[44].

above, cysteines seem to offer a quite specific position to undergo covalent conjugations^[41]. Thiol functionalities from cysteines represent an important nucleophile in many covalent protein or peptide linkages via alkenes, alkynes, sulfones and 1,4-unsaturated carbonyl systems^[41].

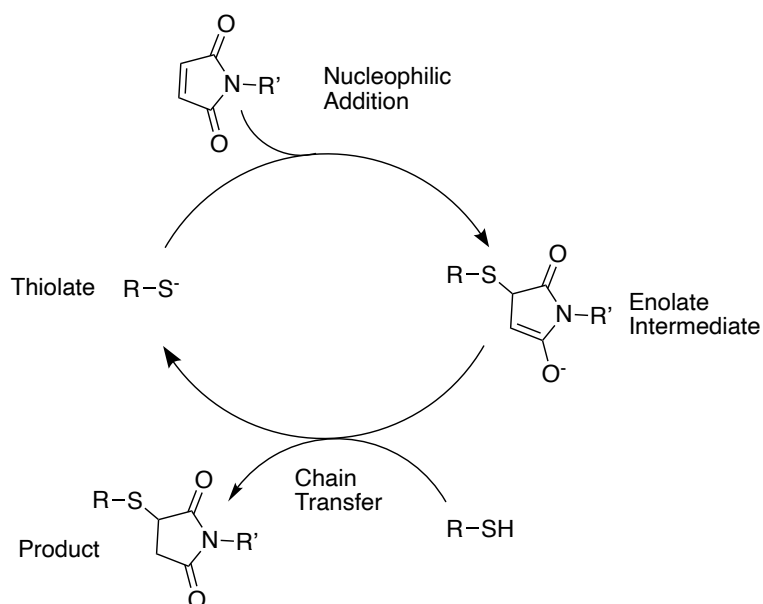
As it is shown in Scheme 2, thiols are able to react in several substitution reactions on aliphatic or aromatic carbon centers with halogens as leaving groups, as well as in addition reactions on π bonds in unsaturated systems^[44]. A reaction, which should be stressed is the targeted production of disulfide bridges from pyridyl disulfides or thiosulfonates, as their reaction product with cysteines imitates a natural protein link, a disulfide bridge, which therefore can be cleaved *in vivo*^[41,44,45].

Another advanced approach is the intercalation into disulfide bridges, that uses bisulfones, which are able to eliminate to an allylsulfone, providing a bivalent electrophilic system^[46]. Through the reduction of thiol bridges with TCEP, two nucleophiles are generated, which then can react with the

linker molecule under scission of two *p*-toluenesulfonic acid molecules, rebridging the former disulfide with an additional functionality, for example a biotin^[46]. With respect to applicability and yield, this work will employ the well-established thiol-maleimide, thiol-yne and cycloaddition reactions

1.3.2.1 Maleimide-thiol conjugation

Maleimides are the most frequently used thiol selective conjugation functionality, due to its rapid reaction with nucleophiles and often easy to perform reaction conditions^[41,44]. Thiol-maleimide-additions do not require harsh conditions such as transition metal catalysts or heat, which makes it very suitable for couplings with



Scheme 3: Reaction mechanism of the thiol-maleimide reaction. Adapted from source [47].

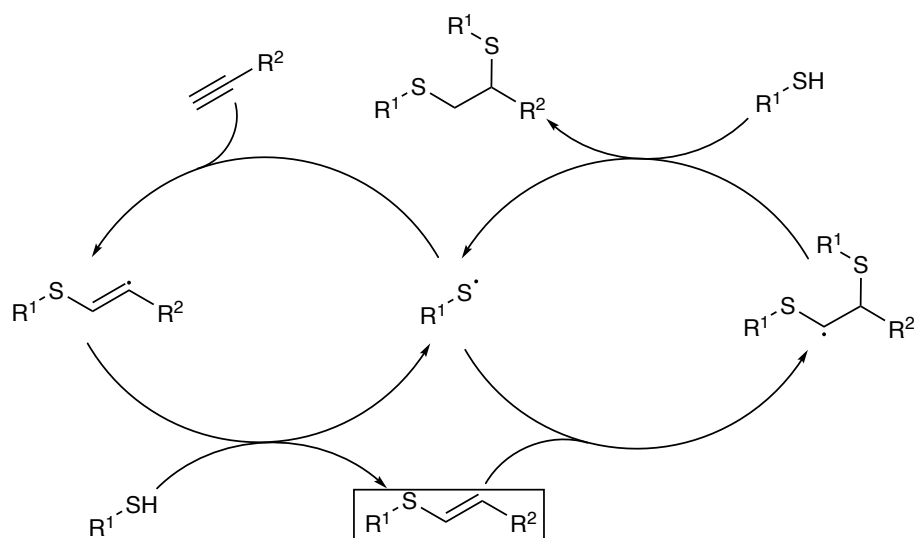
sensitive materials like proteins^[44]. This system has been used successfully for bioconjugation reactions of antibodies, DNA, ALPs, peptides and many more^[34,44]. The reactivity of maleimides is caused by their Michael system, which provides a electrophilic 1,4-unsaturated carbonyl system, allowing different nucleophiles to be added easily^[47]. Scheme 3 is

illustrating the mechanism of the described reaction: The reactive thiol species in this case is the thiolate, which in a first step adds onto the 4-position of the maleimide carbonyl, resulting in an intermediate enolate^[47]. In the following step, the amide functionality is recovered through a chain transfer reaction during which another thiol becomes deprotonated and the once unsaturated 3-position of the maleimide is protonated to form a substituted succinimide^[47]. As the reaction mechanism may suggest, the selective addition of thiols to the maleimides is, especially in the presence of other nucleophiles like it is the case for proteins or peptides, is dependent from the pH value in which the reaction takes place, so usually, thiol-maleimide reactions are proceeded in neutral conditions, like physiological pH of 7.4^[48,49].

1.3.2.2 Reactions of alkynes with nucleophiles and in cycloadditions

Besides maleimides, alkynes represent an important functionality in bioconjugation chemistry too^[50]. Lately the focus of the usage of alkynes lied more in material science, such as photopolymerization^[51], but being able to react with several nucleophiles, especially thiols, under different conditions as well as in cycloaddition reactions, alkynes appear to be a versatile tool for several approaches in linker synthesis as well as modification of biomolecules^[44,49].

The first reaction type of alkynes that has to be mentioned is the reaction with nucleophiles, especially thiols that is of relevance in this thesis. Thiol-yne reactions usually proceed under radical conditions, mostly initiated by light and a suitable photoinitiator^[51]. The following scheme shows the reaction mechanism of thiol-yne reactions.



Scheme 4: Mechanism of radical initiated thiol-yne reaction. Adapted from source [51].

As Scheme 4 shows, the addition of thiols to alkynes can be separated into two reaction cycles, in which two different reaction products can be obtained, the mono and the double adduct of the thiol^[51]. The resultant product formed is dependent on steric demand^[44]. This fact can be exploited for the desired modification of cysteine-containing antiviral peptides (see section 1.2.1), as they appear to be bulky enough to enable mono addition, similar to the product surrounded by a black frame in Scheme 4. To activate the mechanism above, photoinitiators are often used^[44]. One

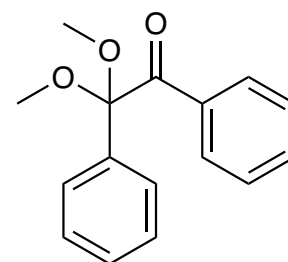
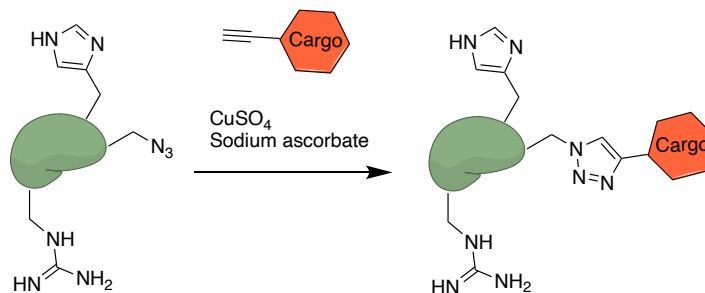


Figure 20: Molecular structure of DMPA.

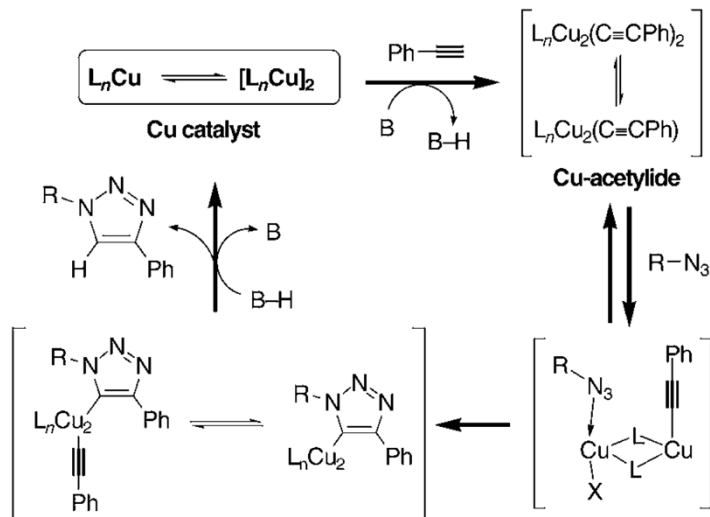
commonly used molecule is 2,2-dimethoxy-2-phenylacetophenone (DMPA), which is shown in Figure 20^[44].

The second type of reactions, in which alkynes are well established are [3+2]-cycloadditions with azides^[50]. Due to their low reactivity in basic or acidic reactions, alkynes and azides do almost not interfere with other biomolecules under physiological conditions, which makes them a really promising tool for *in vitro* bioconjugation reactions,



allowing targeted reactions at defined positions of

biomolecules^[50,52]. [3+2]-cycloadditions can be performed without a metal catalyst, being called Huisgen reaction or copper respectively ruthenium catalyzed^[50,53]. The following scheme shows the reaction mechanism of the copper catalyzed Huisgen reaction^[53]. As it becomes clear from Scheme 6, due to the coordination of copper to



Scheme 6: Mechanism of the copper catalyzed [3+2] cycloaddition of azides with alkynes. Source: [53].

the 5-position of the 1,2,3-triazole, the reaction selectively forms the 1,4-disubstituted product^[53].

Cu(I) is the catalytically active specie, but not the most stable oxidation level of copper. Thus, Cu(II) salts are used in combination with reducing agents like sodium ascorbate, to create Cu(I) *in situ*^[53].

Overall, copper catalyzed Huisgen reactions are known to result in high yields, even if proceeded in an multifunctional environment, such as large proteins or cells and therefore appear to be certainly useful for the synthesis of linker molecules or the functionalization of peptides and proteins^[50].

1.3.2.3 Click chemistry in development of multifunctional linker molecules

Recent studies showed, that dimerization of antiviral peptides can enhance their antiviral activity^[54]. To achieve such a dimerization, it is necessary to design a linker molecule, that is able to react with different functionalities through various triggers. The previously described reaction types in section 1.3.2.1 and 1.3.2.2 employing thiol-maleimide reactions, photoinitiated thiol-yne reactions and alkyne-azide cycloadditions can be used to selectively functionalize different antiviral peptides in a sequential manner with minimal cross reactivity. Biotinylation of the peptides is a prerequisite for subsequent assembly to an ALP, as mentioned in section 1.3.1. Consequently, a suitable linker molecule must contain three different functionalities including two reactive groups and biotin. Considering the steric demand of two peptides and one protein being connected with each other in the final supramolecular construct and to

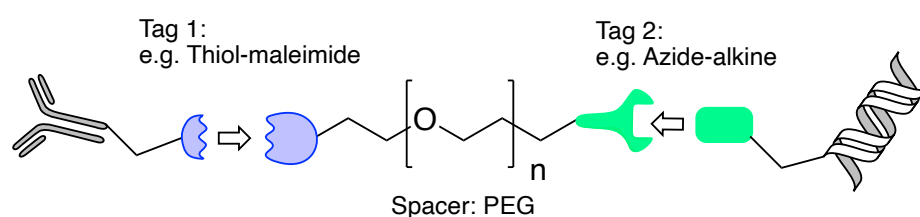


Figure 21: General idea of dimerization/functionalization of different biomolecules through click chemistry with PEG chain spacing units.

exclude a loss of biotin-binding to the ALP, a suitable spacer is required, which also introduce increased flexibility of the construct^[54]. A commonly used molecular building block is polyethylene glycol(PEG)^[55]. After being introduced to a bioactive molecule via a terminal functionality, such as amines, PEG chains do not only enhance the solubility of a conjugate, but could increase the overall circulation time in an organism^[55]. As they are nontoxic, PEGylation of nanocarriers has become a common technique in nanomedicine and therefore appears to be a suitable spacing moiety for a multifunctional linker molecule^[55]. In terms of dimerization of antiviral peptides, it was found, that the efficiency of entry inhibitors depends of the length of the spacing linker section^[54]. For peptidomimetics that inhibited the HIV fusion with its host cell, a linker length of 44 Å, accordingly nine PEG units (see Figure 21, $n = 9$) appeared to have the lowest IC_{50} value of all tested dimers^[54]. This knowledge is taken into consideration for the molecular design of peptide multimers. In summary, the mentioned molecular building blocks consisting of maleimides, alkynes and azides as peptide reactive functionalities and PEG chains as spacing units can be merged to a promising tool for

multimerization and functionalization of antiviral peptides to enhance their broad spectrum application or anti-infectivity.

2. Motivation and aim of this work

Viral diseases pose serious health concerns today, but there is no curative treatment. The overall aim of this work is the development of effective biotherapeutic treatments against virus infections, specifically HIV and corona. To achieve this, we seek to develop chemical tools for the assembly of different antiviral peptides to supramolecular nanoplatforms. Ultimately, the peptide nanomaterials will be evaluated for their antiviral activity.

The first approach of antiviral peptide multimerization is to biotinylate them via covalent bioconjugation reactions and furthermore, combine four equivalents of bispecifics on one streptavidin or neutravidin protein.

To achieve a combination of two different peptides on one avidin-like protein, a trifunctional linker molecule will be synthesized, containing one biotin functionality, one maleimide functionality and one alkyne group for chemo selective conjugation of the fusion inhibitors, as it is shown in the following figure.

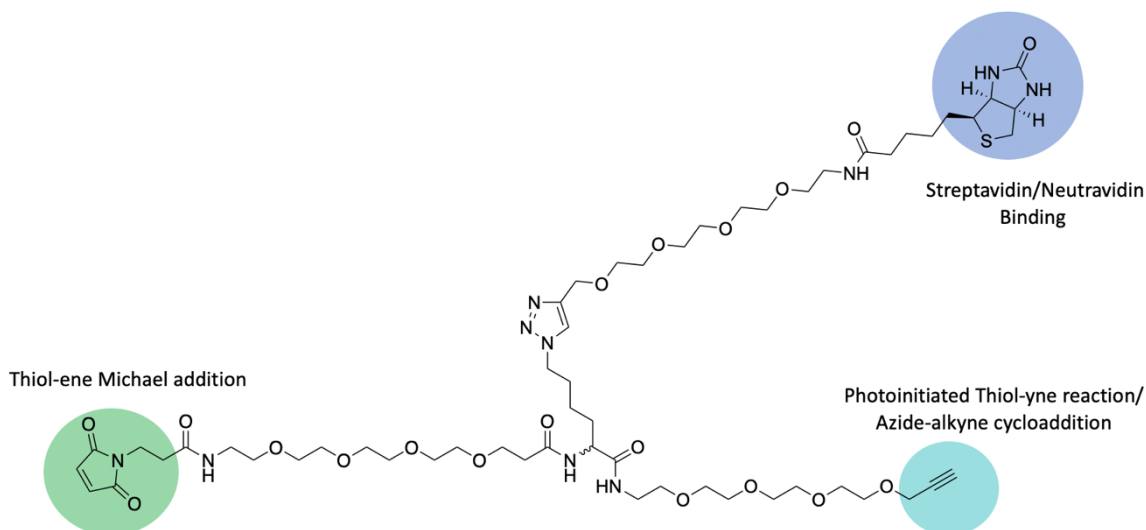
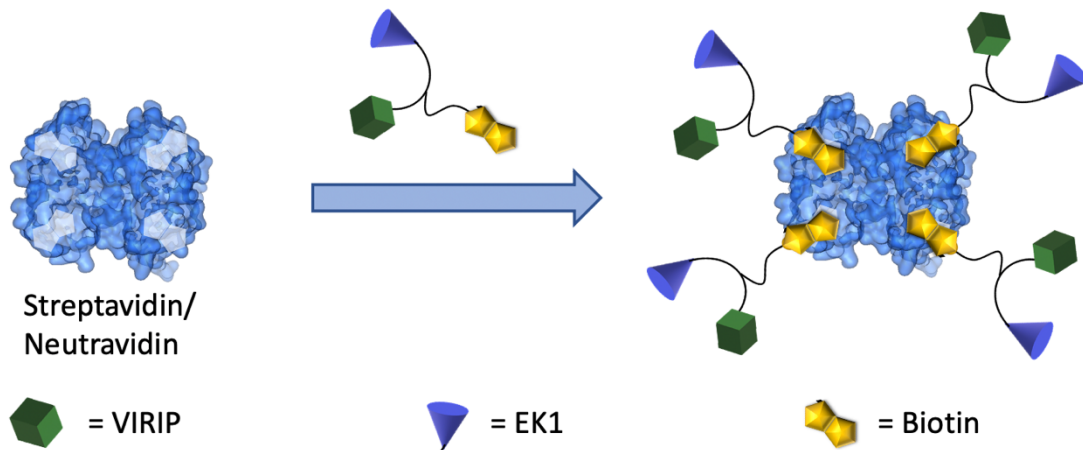


Figure 22: Envisioned molecular structure of the trifunctional linker molecule for chemo selective bioconjugation reactions.

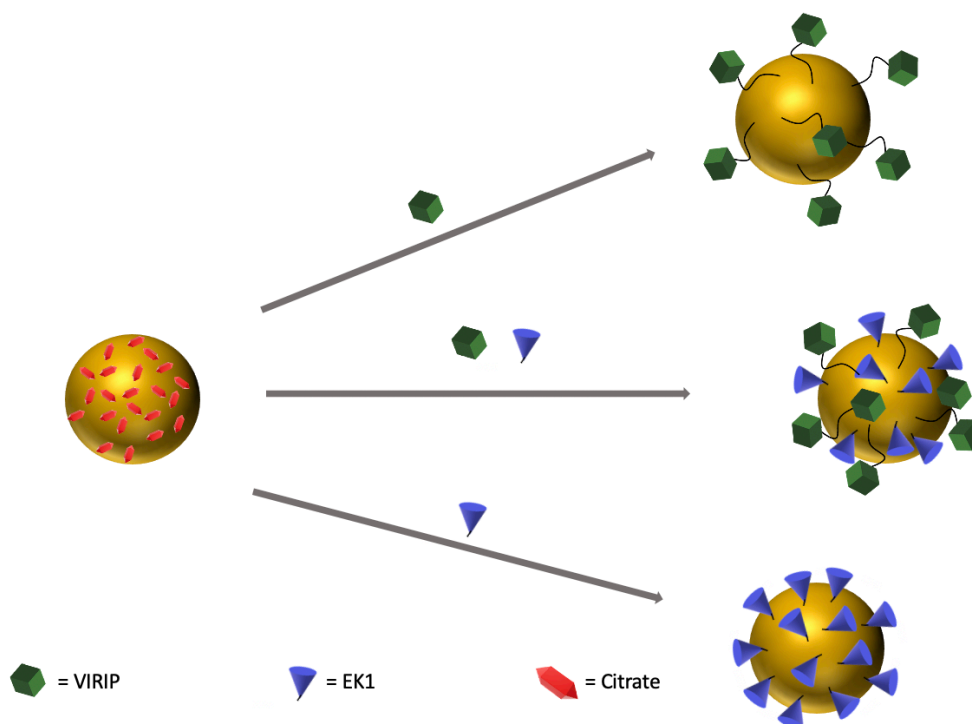
The trifunctional linker molecule will be used to conjugate one antiviral peptide to the maleimide group (see green circle Figure 22) and a second peptide to the alkyne functionality (see turquoise circle Figure 22).

After successful conjugation of each peptide, the biotin functionality (see blue circle Figure 22) will be used to assemble the trifunctional construct to streptavidin/neutravidin. The different protein nanoplatforms will be tested for their antiviral activity in *in vitro* cell experiments.



Scheme 7: General reaction scheme of supramolecular assembly of multimerized antiviral peptides to streptavidin/neutravidin.

The second approach for peptide multimerization in this work will be the ligand exchange reaction of citrate stabilized gold nanoparticles with cysteine containing fusion inhibitors. As described in section 1.2.2, the stable bond between sulfur and



Scheme 8: General reaction scheme of ligand exchange on the surface of gold nanoparticles with antiviral peptides.

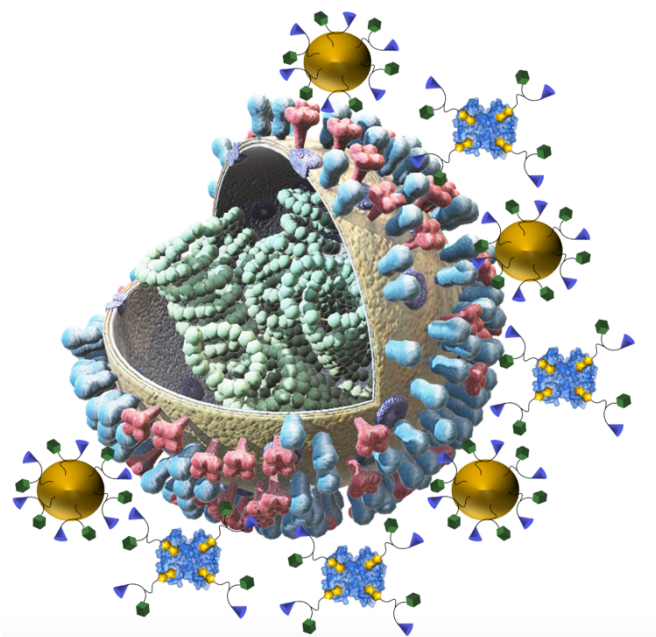


Figure 23: Model of potential inhibition of SARS-CoV-2 virus by peptide coated gold nanoparticles and streptavidin/neutralavidin conjugates.

gold will be used to coat the metal particles with a corona of either one kind of antiviral peptide or a statistical mixture of two different moieties, as it is shown in Scheme 8.

As the ligand exchange is completed, the particles will be characterized in terms of their antiviral activity in *in vitro* cell experiments.

As a last step, the antiviral nanoplateforms will be evaluated to determine their efficiency in the reduction of host cell infection with HIV and SARS-CoV-2.

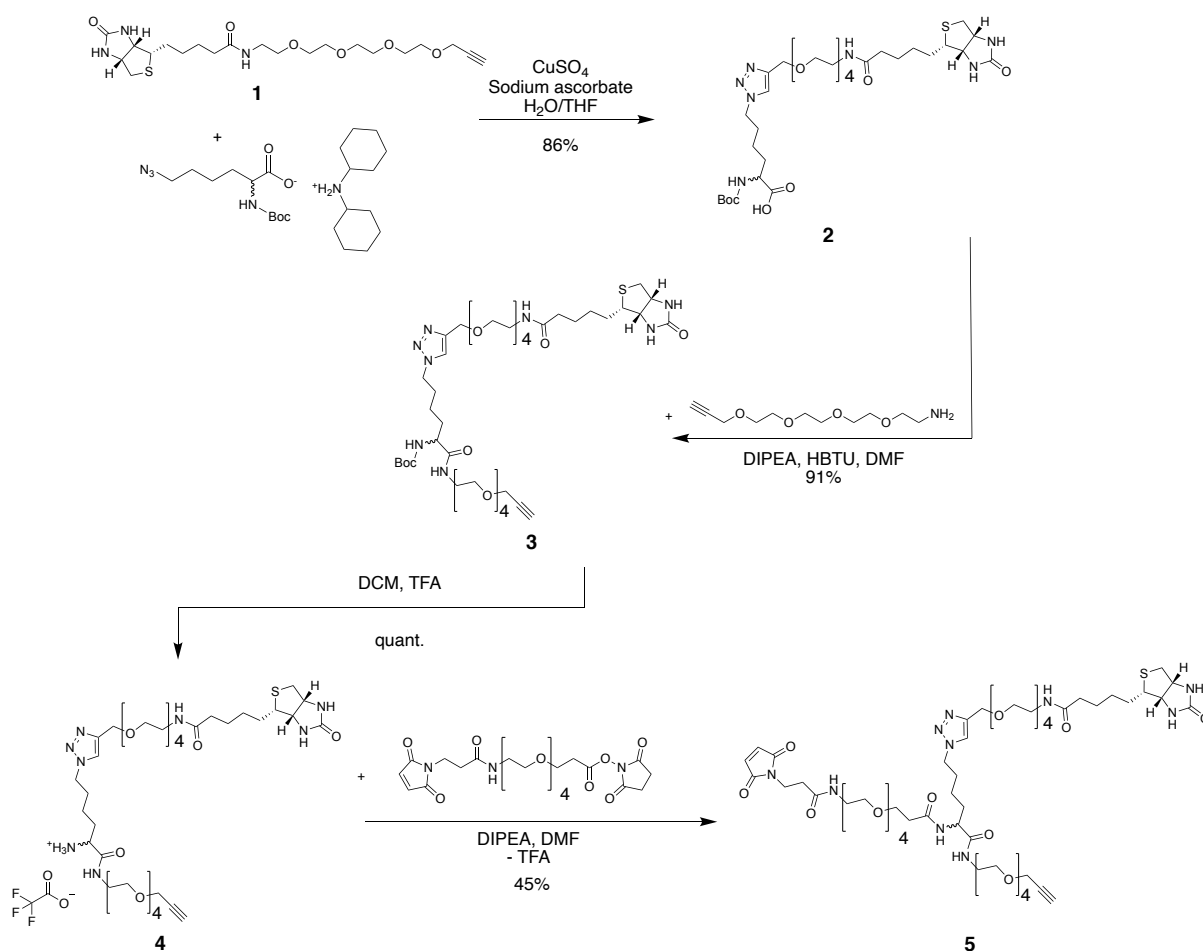
This research work will be performed in collaboration with Fabian Zech, PhD student at the institute of molecular virology, university medical center in Ulm and will be part of his PhD thesis as well as the PhD thesis of Astrid Heck, PhD student at the Max-Planck Institute for Polymer Research in Mainz.

3. Results and discussion

3.1 Synthesis of a trifunctional linker molecule for peptide conjugation

As described in the previous chapter, the covalent linkage of two different antiviral peptides and one biotin unit requires the synthesis of a trifunctional linker molecule on which the selective introduction of each functionality is possible.

This chapter focuses on the four-step synthesis of the designed linker shown in Figure 22. The performed reaction sequence is shown in the following scheme.



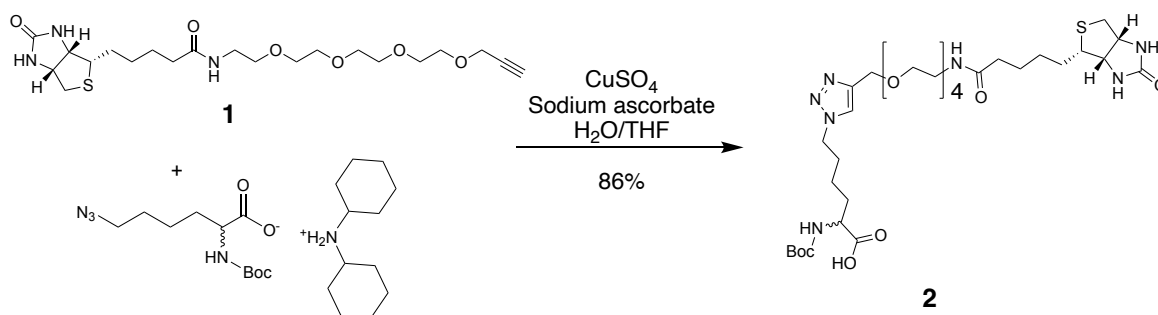
Scheme 9: Synthesis route performed to synthesize a trifunctional linker molecule.

The reaction sequence started with a copper catalyzed alkyne azide cycloaddition of a biotin containing PEG-4 chain including a terminal propargyl group with a *boc*-protected azido lysine. In the following step, a new alkyne functionality was introduced to the molecule via an HBTU assisted coupling between the lysine's carboxylate group and the primary amino functionality of propargyl-PEG-4-amine. The resulting molecule was deprotected to reveal the amine function of azido lysine, which was reacted with maleimide-PEG-4-NHS ester to obtain the final compound with an overall yield of 35%.

The synthesis of each intermediate compound and its characterization will be discussed in the following sections.

3.1.1 Copper catalyzed azide alkyne cycloaddition of biotin-PEG4-alkyne

To introduce the first of three functionalities to the linker molecule backbone based on a boc-protected azido lysine, the cycloaddition of biotin-PEG-4-alkyne was achieved using copper catalyzed Huisgen reaction as it was described in section 1.3.2.2 Scheme 6. The reaction was performed as shown in Scheme 10.



Scheme 10: Reaction equation of [3+2]-cycloaddition of biotin-PEG4-alkyne and N-boc-azidolysine.

After reaction for 40 h, the solvent was removed through lyophilization. As the LC-MS analysis showed full conversion of the starting material, purification could be achieved by removal of the excess copper salts by precipitation, followed by filtration to remove the basic copper carbonate. The reaction yielded in 86% of product 2 after filtration and lyophilization. For analytical purposes 10 mg of the product were purified by preparative HPLC to exclude any residual salts and dicyclohexylamine, whereas for the next reaction step, dicyclohexylamine will help to basify the reaction solution. Figure 24 shows the LC-MS TIC spectrum of the filtrated product (retention time 4.8 min) with the expected product mass of 730 m/z [M+H⁺] and 752 m/z [M+Na⁺]. The minor peak (retention time 2.4 min) represents dicyclohexylamine.

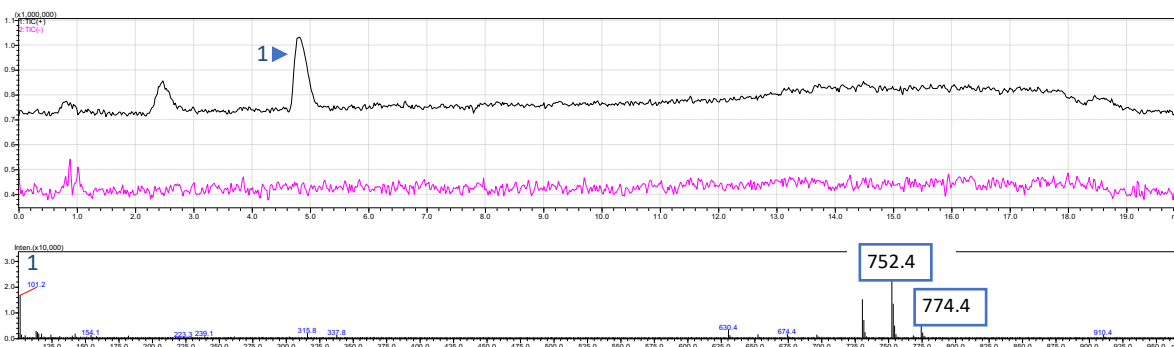


Figure 24: LC-MS analysis of the filtrated compound 2. Peak 1 in the upper TIC spectrum represents the desired product. The lower ESI⁺ mass spectrum shows the integrated mass peaks from peak 1 in the TIC spectrum.

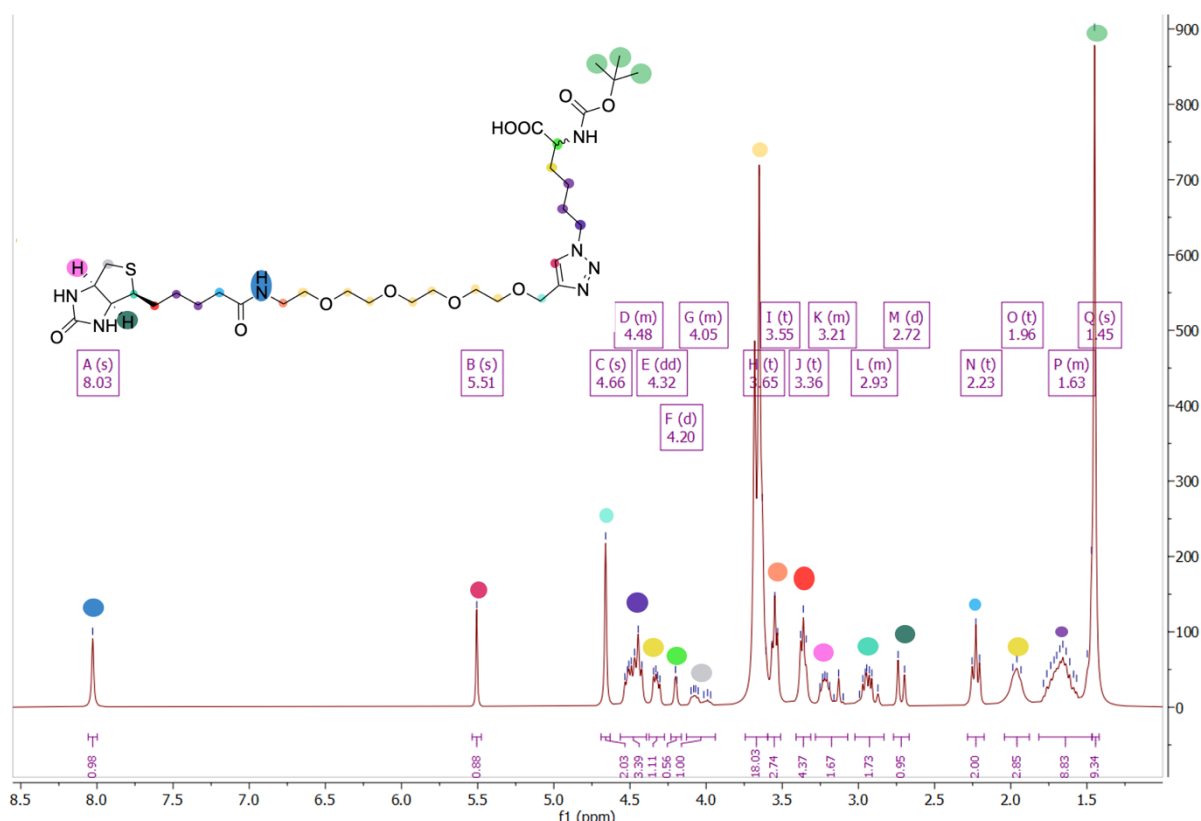
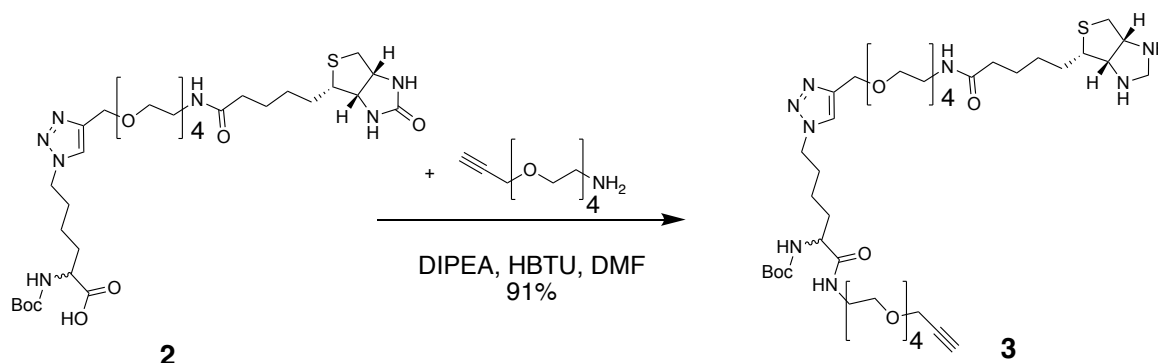


Figure 25: $^1\text{H-NMR}$ spectrum of purified compound **2**. Measured at 300 MHz in MeOD.

In Figure 25 it is shown that the product molecule contains the desired biotin signals in the $^1\text{H-NMR}$ spectrum as well as the characteristic signal of the boc protection group shifted to 1.5 ppm (light green), which proves that the reaction was successful. The obtained product was used in the second reaction step.

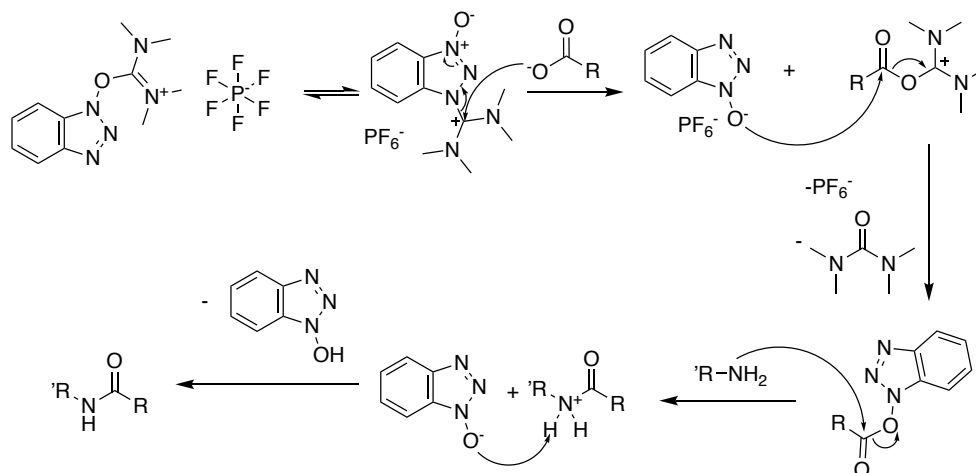
3.1.2 Coupling of Biotin-PEG4-triazolylsine (**2**) to propargyl-PEG4-amine

To introduce an alkyne function to the biotinylated linker backbone for thiol-yne click reactions or azide-alkyne cycloadditions as described in chapter 2, compound **2** was reacted with propargyl-PEG-4-amine via its carboxylate functionality, as shown in the following scheme.



Scheme 11: Reaction equation of biotin-PEG-4-triazolylsine with propargyl-PEG-4-amine.

To enable a nucleophilic substitution of the amine on the carboxylate's carbon atom, it has to be activated via the formation of a good leaving group^[56,57]. Therefore, the coupling agent HBTU was chosen. The general mechanism of the HBTU assisted formation of an amide bond is shown in the following scheme.



Scheme 12: General coupling mechanism between carboxylic acid and primary amine via HBTU as a coupling agent. Mechanism adapted from sources [57] and [58].

As it can be inferred from Scheme 12, the HBTU assisted coupling is facilitated in basic conditions, which is why the reactions shown in Scheme 11 was performed with the addition of Hünig's base (DIPEA). The crude reaction mixture was purified via preparative HPLC, affording molecule **3** in 91% yield.

The following figure shows the results of the LC-MS analysis of the isolated product fraction.

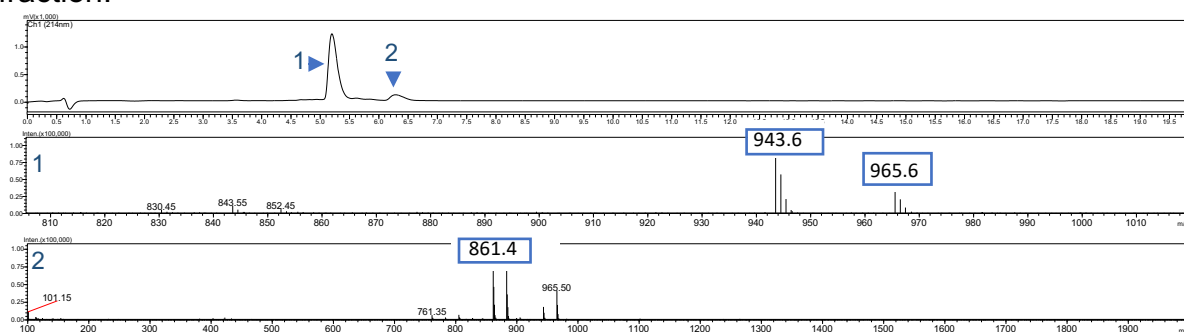


Figure 26: LC-MS spectrum of the purified product **3**. Peak 1 represents the product, peak 2 represents the boc-deprotected form of the product, that probably formed during HPLC purification under acidic conditions (0,1 vol% TFA). For clarity, only m/z from 800 to 1020 is shown here. Full MS is available in appendix 18.

As it becomes clear to see from Figure 26, the main peak in the photodetection chromatogram at 214 nm (**1**, retention time 5.3 min) shows the desired product mass of $m/z = 944$ [$M+H^+$] and $m/z = 966$ [$M+Na^+$]. A second peak appears in the LC spectrum (**2**, retention time 6.3 min) whose mass fits to the boc-deprotected form of the product with $m/z = 861$ [$M+Na^+$]. If this assumption is supported by the fact that the

HPLC purification of the product was performed under acidic conditions by addition of 0,1% of TFA to the chromatography solvent, which were then able to cleave off the boc protection group of the product molecule **3**. Under these circumstances, the contamination of the product with deprotected product would not have done any harm to the following reaction sequences, since the next synthesis step was the deprotection of product **3** in TFA acidic conditions. $^1\text{H-NMR}$ spectrum (Figure 27) further confirmed that there are no other impurities.

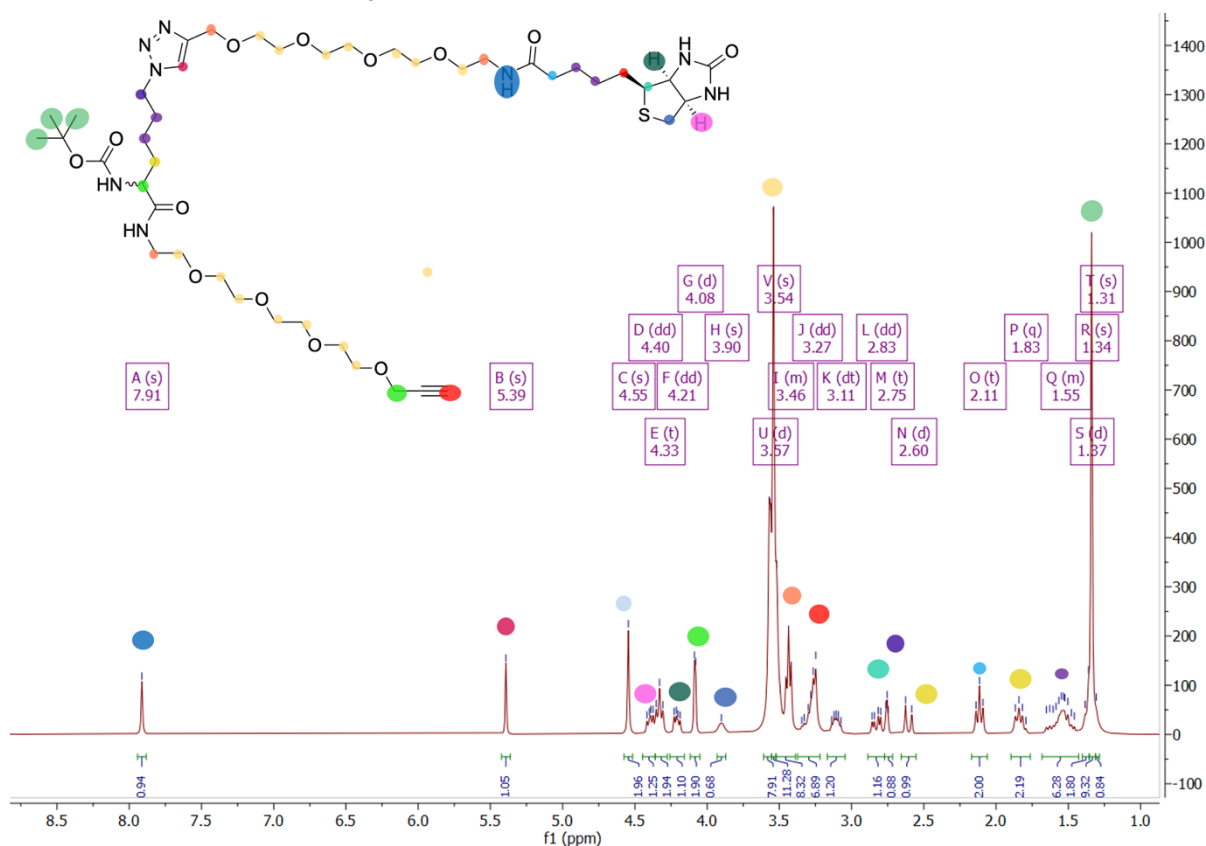


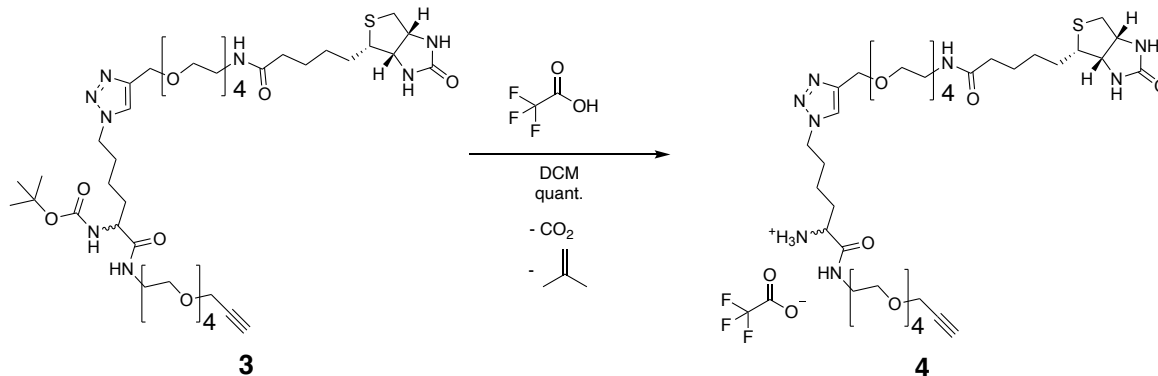
Figure 27: $^1\text{H-NMR}$ spectrum of purified compound **3**. Measured at 300 MHz in MeOD.

As the $^1\text{H-NMR}$ spectrum shows, the characteristic signals of biotin shifted to the high field become visible, as well as the characteristic triplet signal caused by the PEG chains (3.5 ppm). The boc protection group can be assigned to the characteristic singlet peak shifted to 1.3 ppm. Critically, a newly introduced alkyne signal, a singlet peak at 2.75 ppm, represented through the berry purple dot above it, confirms the successful introduction of an alkyne and the identity of compound **3**.

3.1.3 Deprotection of boc protected Biotin-PEG4-triazolo-lysine-PEG4-alkyne

To enable the introduction of further functional groups to the linker molecule, it was necessary to remove the amine protecting group in the triazolo-lysine residue.

This reaction was conducted after a literature procedure of *Pokorski et al. (2011)*^[58] with slight modifications as shown in Scheme 13 .



Scheme 13: Reaction equation of the deprotection step of product 3 to yield its free amine form 4.

After the procedure was completed, the product was concentrated and dried in vacuum to afford compound 4 in quantitative yield as a TFA salt. The purity of the

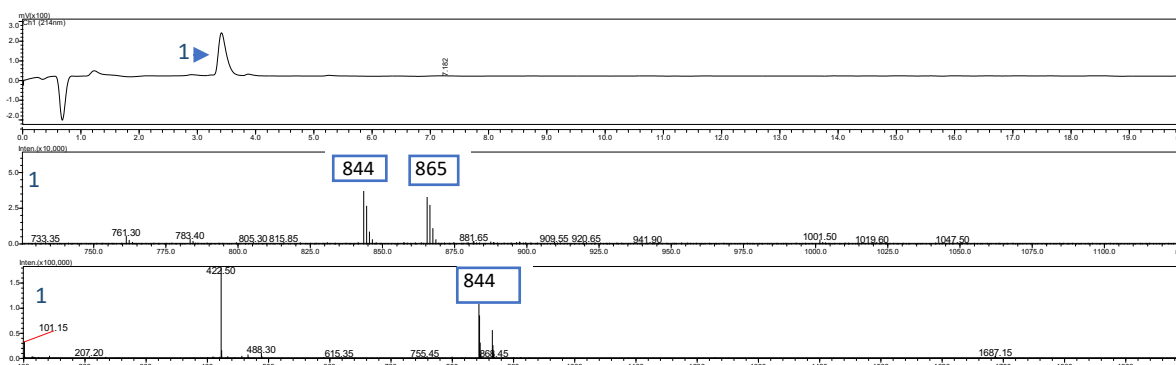


Figure 28: LC-MS spectrum of deprotected product 3 after removal of the solvent and excess TFA.

product was proven by LC-MS and NMR analysis, as the following figures show.

From Figure 28, only one characteristic peak becomes visible (1, retention time 3.4 min) where the corresponding mass fits to the expected product mass of molecule 4. One mass peak can be assigned to $m/z = 843$ [$M+H^+$], the other one to $m/z = 856$ [$M+Na^+$]. Only one peak was observed in the LC, indicating the purity of the product.

To substantiate the identity of the product, the $^1\text{H-NMR}$ spectrum of compound **4** was acquired and is shown below.

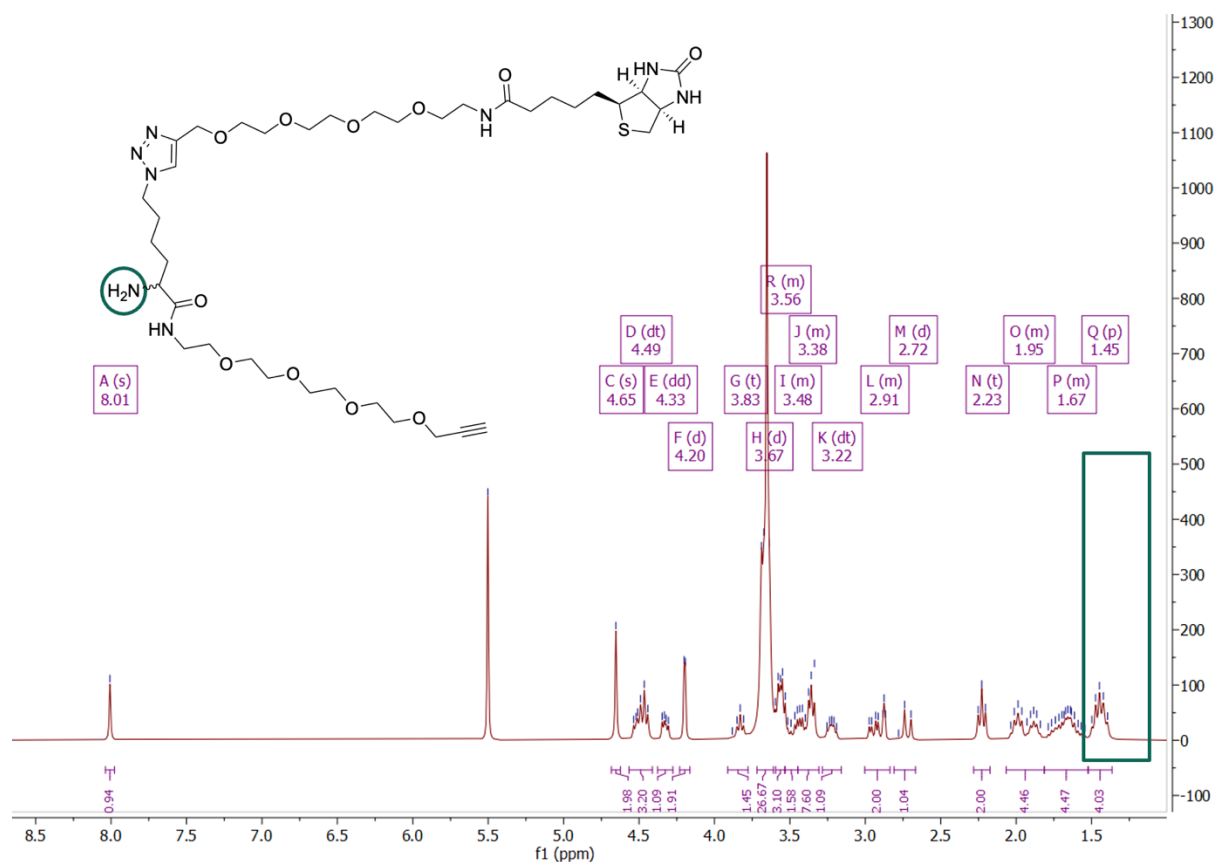
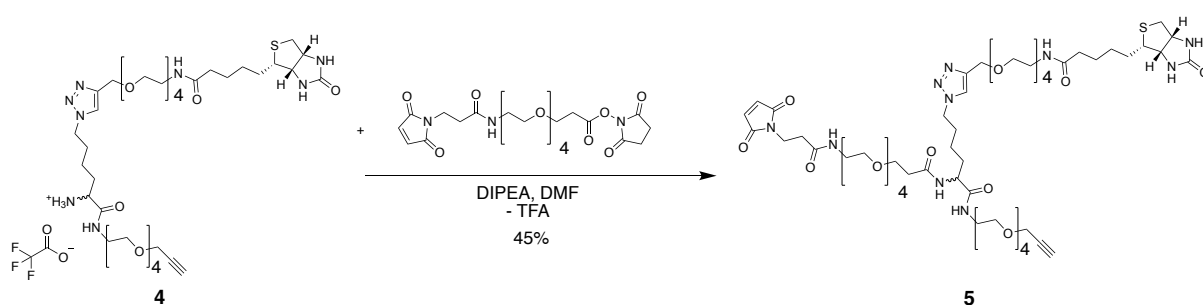


Figure 29: $^1\text{H-NMR}$ spectrum of compound **4**. Measured at 300 MHz in MeOD.

Compared to the $^1\text{H-NMR}$ spectrum of the protected compound **3** (see Figure 27), all characteristic signals remain present. Notably, the characteristic singlet signal corresponding to nine protons from the boc protection group is not observed in the high field. The absence of this peak shows that the protective *tert*-butoxy carbonyl is successfully cleaved off from the linker backbone, rendering the amine available for subsequent coupling reactions.

3.1.4 Coupling of Biotin-PEG4-triazolo-lysine-PEG4-alkyne to maleimide-PEG4-NHS

To obtain the final desired trifunctional linker molecule, the third bioconjugation enabling functionality had to be introduced to the previously synthesized compound. This was conducted through the usage of the amine group in a reaction of compound **4** with a bifunctional PEG chain containing maleimide and an electrophilic active ester. Through this commercially available NHS ester it became possible to merge the amine group of the linker backbone with the maleimide tag and its spacer group. The following scheme shows the reaction equation of the performed procedure.



Scheme 14: Reaction equation of the NHS coupling between compound **4** and maleimide-PEG-4-NHS.

As it becomes clear to see from Scheme 14, the amine in molecule **4** represents the nucleophile, which is able to add on the carbonyl's carbon atom under release of *N*-hydroxysuccinimide. To enhance the nucleophilicity of the amine by preventing it from being protonated, DIPEA as a passive base was added. After completion of the reaction, the crude product was subjected to preparative HPLC, resulting in 45 % of the theoretical yield. This observation can be explained by the fact that the purification by HPLC had to be repeated, because of remaining traces of the NHS ester, which contaminated the product fraction after the first run of preparative HPLC. This was proven by LC-MS analysis (see Figure 30 A). Another reason for the low yield of product **5** could have been the steric demand of the starting material, which influenced the accessibility of the amine. Nevertheless, the desired product could be purified completely after a second preparative HPLC procedure. This is corroborated in the following Figure 30, which shows the corresponding LC-MS analytics of the purification procedure.

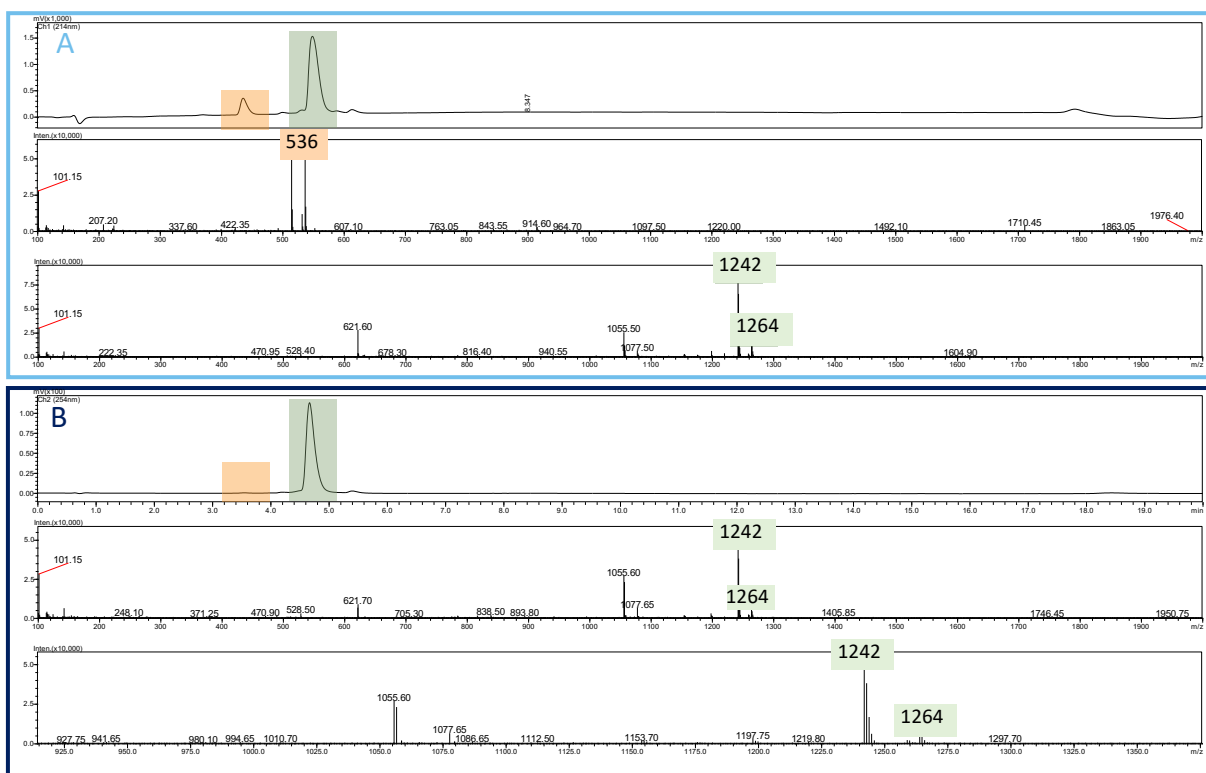
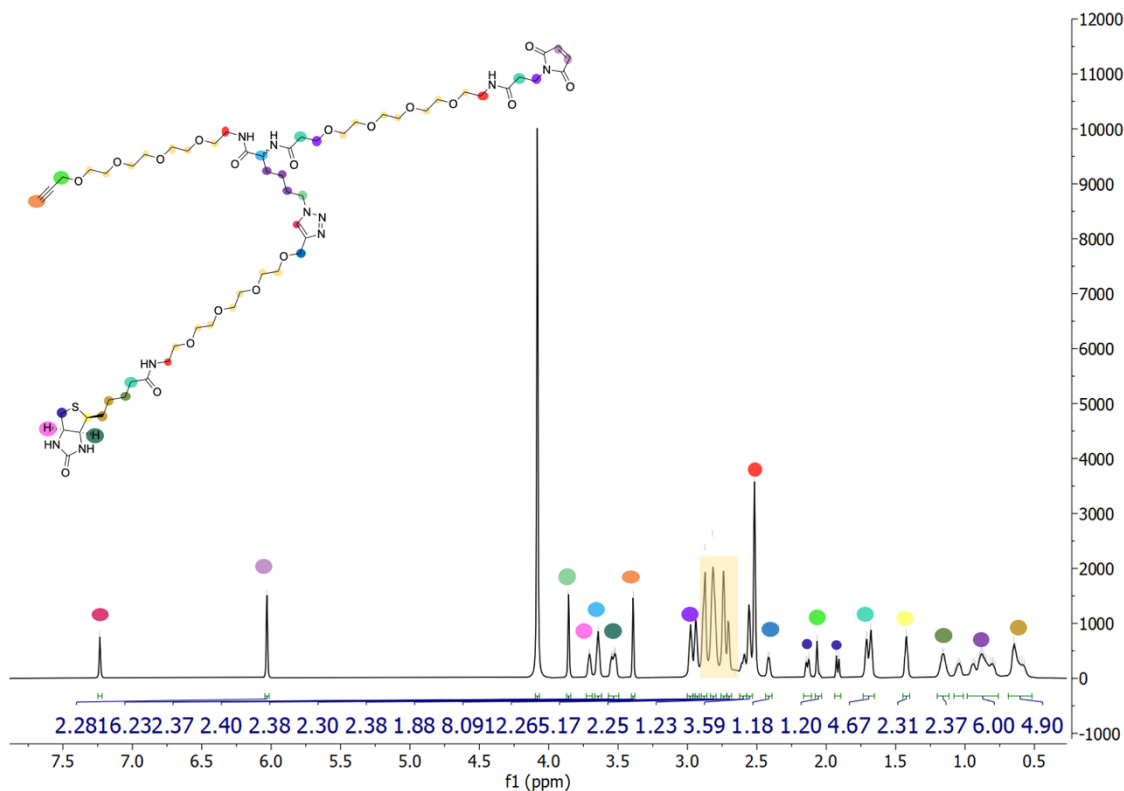


Figure 30: LC-MS analysis of compound **5** after the first (A, light blue) and the second purification procedure (B, dark blue) via preparative HPLC.

Figure 30 shows the LC-MS spectra of the first and the second purification of compound **5**. Part A displays the impurity at a retention time of 3.5 min, with a mass of 536 m/z (see Figure 30, light orange). Although the product peak (see Figure 30, light green) represents the main signal with the desired product mass of $m/z = 1242$ $[M+H]^+$, another purification attempt had to be conducted, which is shown in part B of Figure 30. After this second procedure, the contaminant peak disappeared in the LC spectrum (see light orange box), leaving the green product peak as the only signal visible in the spectrum. Also, in this chromatogram the expected product masses of $m/z = 1242$ $[M+H]^+$ and $m/z = 1264$ $[M+Na]^+$ appear in the ESI⁺ mass spectrum that product **5** remains intact despite multiple HPLC purification, albeit with lower yield. For further improvement in the future, optimization of the HPLC purification method for better separation is required, e.g. using a lower slope solvent gradient, as well as the reduction of applied material per run to prevent overloading of the column. The targeted linker molecule, compound **5** was further analyzed with 1D- and 2D-NMR.

3.1.5 Characterization of trifunctional linker molecule

To make sure that the previous described synthesis yielded the desired product, NMR studies were performed at 700 MHz in deuterated MeOH (MeOD). The following figures show the results of the ^1H , ^{13}C , ^1H - ^{15}N -HMBC and COSY NMR spectra of the trifunctional linker.



From Figure 31 it can be inferred that the trifunctional linker contains a maleimide functionality, since a new signal representing two protons appears at 6.1 ppm (purple dot) of the spectrum. The characteristic signals derived from a biotin functionality stay present compared to the previous spectra (see Figure 27), even though the signals differ in about 0.5 – 0.75 ppm in their shifts, which could have been caused by the fact that the spectra were measured at different magnetic fields strengths (300 MHz vs. 700 MHz). The important alkyne functionality remains present through a significant singlet at 3.4 ppm (orange dot), which may lead to the assumption that the propargyl group is still intact. The characteristic signal of the PEG chains appears now in a broad quartet splitting from 2.6-2.8 ppm (yellow box) like it was expected.

Since the product contains different chiral centers and thus magnetically unequal protons, it is possible to assign and differentiate the couplings caused by these atoms by measuring a COSY NMR spectrum.

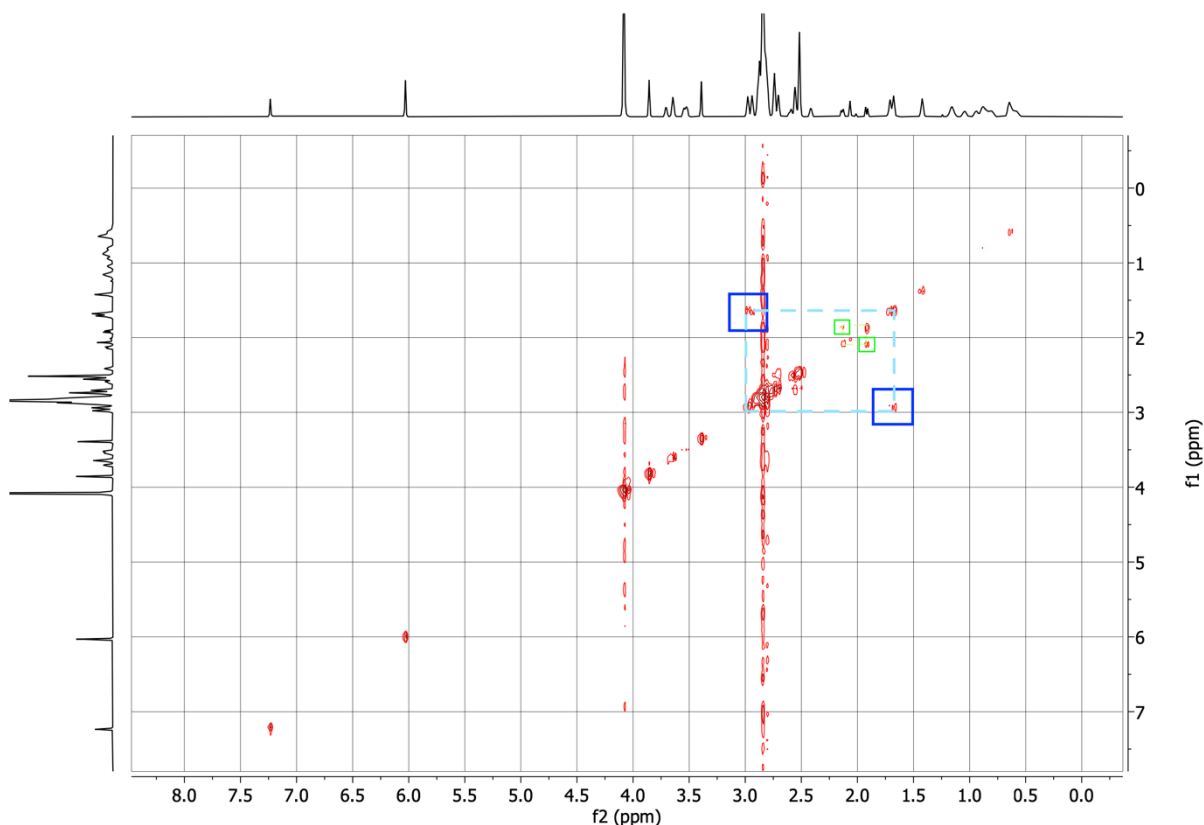


Figure 32: COSY NMR spectrum of trifunctional linker **5**. Measured at 700 MHz in MeOD.

Figure 32 shows the 2D-coupling patterns in the COSY spectrum of compound **5**. Besides the diagonal axis of coupling signals along the identical protons, two H-H couplings appear to be present in the molecule. The blue box in Figure 32 shows one of them. These signals characterize the proton coupling between a peak at 3 ppm and a peak at 1.5 ppm in the proton spectrum and, according to its integrals value, can be assigned to the protons in α - and β -position of the carbonyls in molecule **5** as shown in Figure 31 (turquoise and light purple). The second proton coupling is marked by the green box in Figure 32. These signals can be assigned to two protons at the same carbon atom, since the peaks are not differing that much in their shifts as the signals in the blue box do. As they are shifted to the high field, the protons are most likely located on an aliphatic carbon atom. The signals are assigned to the two protons in α -position to the thioether biotin, which are located next to a chiral carbon atom at the two condensed biotin cycles (dark purple in Figure 31). Since the molecule contains several nitrogen atoms, a characterization of the near molecular environment through ^1H - ^{15}N -HMBC NMR was carried out as shown in the following figure.

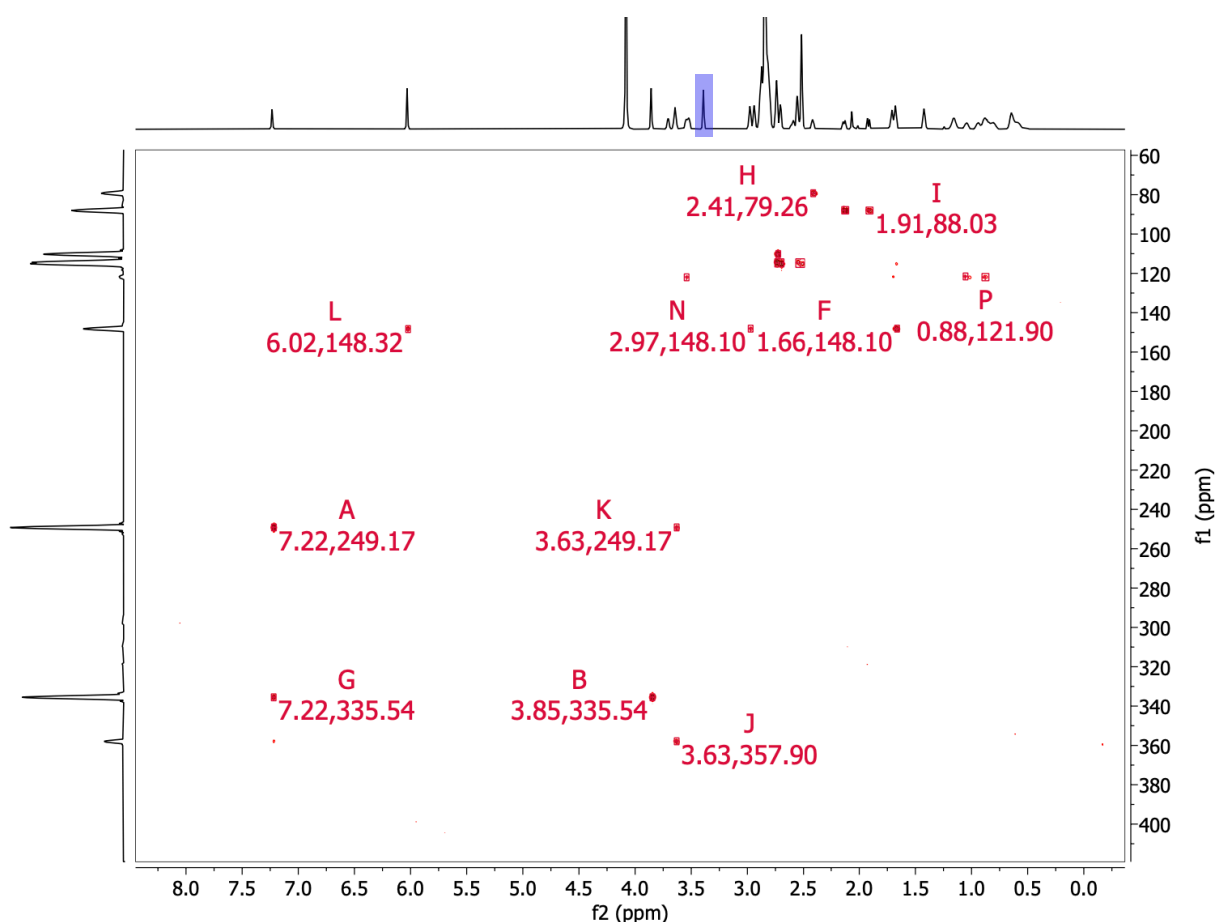


Figure 33: ^1H - ^{15}N -HMBC NMR spectrum of compound **5**. Measured at 700 MHz in MeOD.

Figure 33 shows hydrogen atoms that possess a nitrogen atom in their vicinity. The horizontal axis represents the hydrogen, whereas the vertical axis shows the shifts of the ^{15}N atoms. Since the trifunctional linker (compound **5**) contains ten different nitrogen atoms, many coupling signals appear in the high field. Most of the signals are due to the presence of nitrogen atoms in close vicinity to aliphatic hydrogen atoms, due to the racemic linker backbone, the amides in the PEG units and the aliphatic chain from the biotin moiety. A significant characteristic for the assignment of hydrogen atoms is the presence of the propargyl signal at 3.30 ppm (see Figure 33 highlighted in blue) which is not coupling with any of the nitrogen atoms, substantiating the presence of the PEG-4 alkyne. Another characteristic pattern is the coupling derived from the triazole, represented by the signals A, B, G and K in Figure 33. The signals A and G show coupling of two nitrogen atoms with one single hydrogen atom which is shifted to the low field at 7.22 ppm and can be assigned to the hydrogen bound to C5-position of the triazole. The signals K and B arise from the coupling of triazole nitrogen with neighboring aliphatic hydrogen atoms, as it is the case for the triazole heterocycle in compound **5**.

The maleimide functionality can be assigned as well, as signal L, which shows a single coupling of the low field shifted sp^2 -hybridized hydrogen atoms with one nitrogen (148 ppm and at the same time, with two other aliphatic hydrogen atoms (signals N and F). All these signals give evidence, that the obtained product has the desired structure of compound **5**. For further characterization, a ^{13}C NMR spectrum was measured, as shown in the following figure.

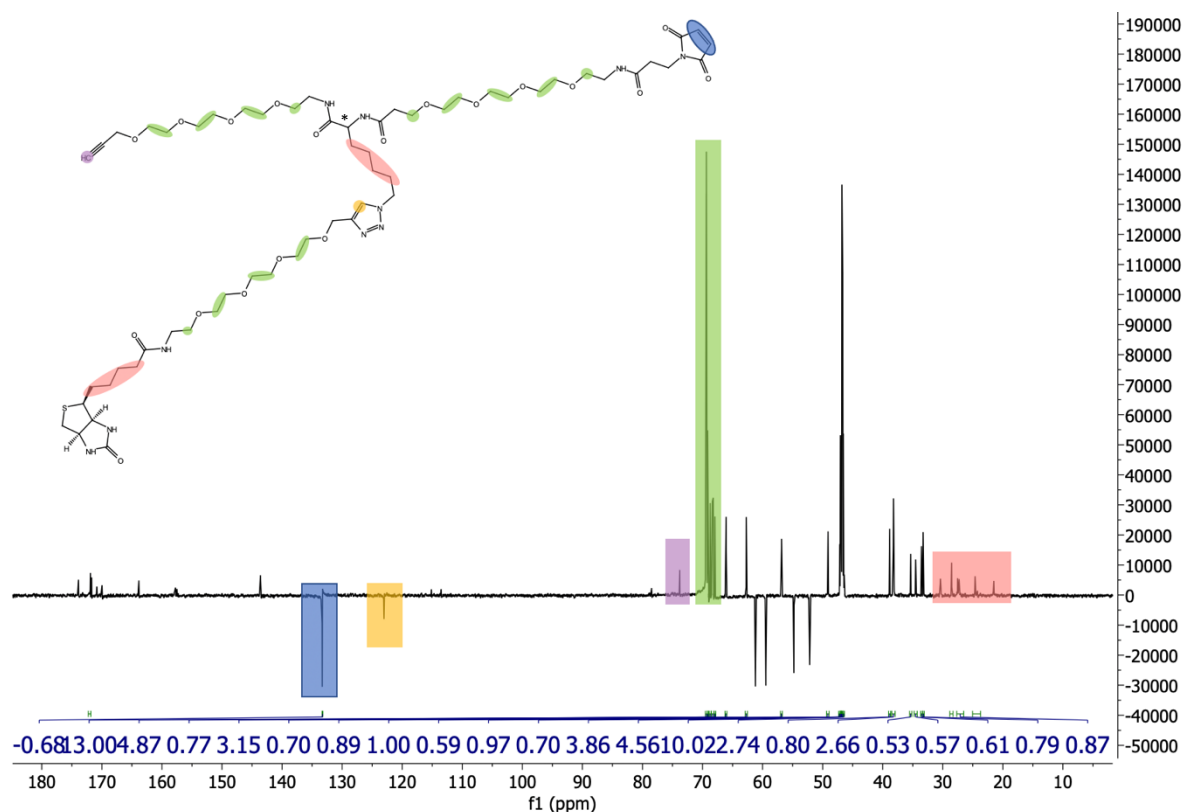


Figure 34: ^{13}C NMR spectrum of compound **5**. Measured at 176 MHz in MeOD.

As it can be seen in Figure 34, the ^{13}C NMR spectrum shows the expected signals of the desired functionalities for bioconjugation reactions. One of these is the low field shifted signal at about 135 ppm, which can be assigned to carbon atoms of the maleimide (see Figure 34, highlighted in blue). The carbon atoms of the connecting PEG-chains can be found in the main peak of the spectrum, highlighted in green. The slightly low field shifted and small peak underlaid in purple at 73 ppm can be assigned to the propargyl residue of the linker. Since only one alkyne group can be found in compound **5**, the signal was expected to be weak. Another characteristic signal in the NMR spectrum is the signal of the triazoles 5-position, which is due to its inclusion into an extremely electron poor heterocycle strongly shifted to the low field and therefore can be associated with the peak at 123 ppm, which is highlighted in yellow. Lastly, the aliphatic carbon atoms of the linker backbone and the biotin unit are expected to be

shifted to the high field, since no electron demanding groups surround them. Therefore, the signals between 20 and 30 ppm (highlighted in pink) can be seen as a proof that also these moieties are part of the product.

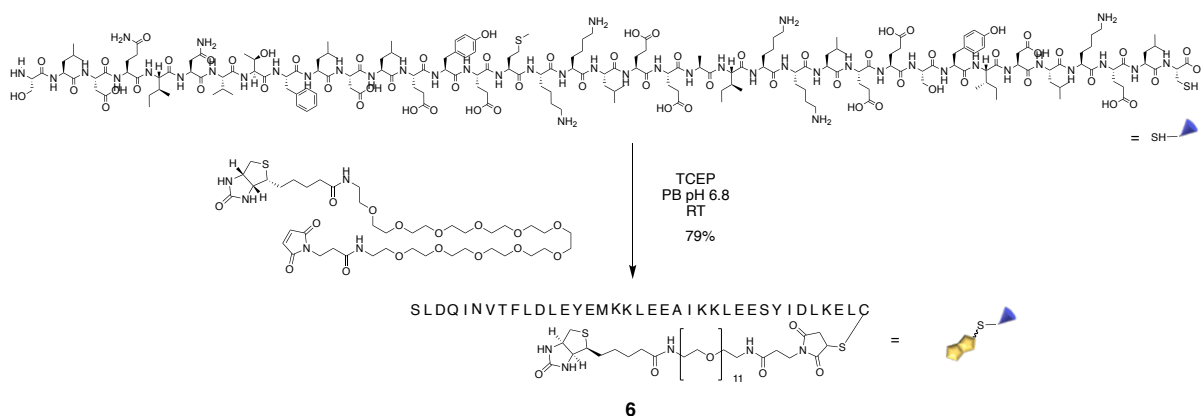
The final compound is then used subsequently for reaction with cysteine-containing antiviral peptides through its maleimide function on the one side as well as photoinitiated through a thiol-yne click reaction or an azide-alkyne click reaction on the other side.

3.2 Conjugation of antiviral peptides to biotinylated linker molecules

To enable strong and noncovalent assembly of the antiviral peptides to streptavidin or neutravidin, it is necessary to introduce a biotin moiety to the bioactive molecules. This can be done via different covalent chemical approaches, such as Michael addition or cycloadditions, as discussed in chapter 1.3.2 This section describes the peptide conjugations to different biotinylated linker molecules for eventual supramolecular multimerizations. First, a bifunctional linker (Scheme 15) was used to biotinylate the respective antiviral peptide, EK1 or VIRIP to evaluate and compare the effects of bioconjugation and assembly on avidin/streptavidin platforms on their respective activities *in vitro*. Thereafter, the synthesized trifunctional linker (compound 5) was used to covalently attach two different antiviral peptides.

3.2.1 Conjugation of EK1 peptide to bifunctional Biotin-PEG11-maleimide linker

As it was described in chapter 1.2.1, the EK1 peptide was found to work as a fusion inhibitor against SARS-CoV and MERS-CoV viruses^[8]. To investigate the effect of multimerization on its antiviral activity *in vitro*, it was necessary to introduce a biotin unit to the peptide for the assembly on streptavidin or neutravidin. Since the EK1 peptide used during this work contained a single cysteine residue, it seemed a versatile approach to use this thiol for chemoselectively modify the peptide. Therefore, a commercially available maleimide PEG-11 biotin linker was used. The performed reaction is shown in the equation below.



Scheme 15: Reaction equation for the conjugation reaction of antiviral peptide EK1 to a biotin PEG-11 maleimide linker via its thiol functionality.

From Scheme 15 it can be inferred, that the pH value of the reaction medium had to be buffered to a neutral to slightly acidic pH to avoid side reactions which can lead to a loss of chemoselectivity, such as amine additions to the maleimide functionality, as it was discussed in section 1.3.2.1. To the reaction mixture of EK1 and biotin-PEG11-maleimide was added tris(2-carboxyethyl) phosphine (TCEP) to reduce possible thiol bridges formed between two cysteines derived from EK1.

The crude product was purified by preparative HPLC, yielding in 79% of modified peptide. To prove the purity of compound **6**, LC-MS analysis was performed, of which result is shown in Figure 35.

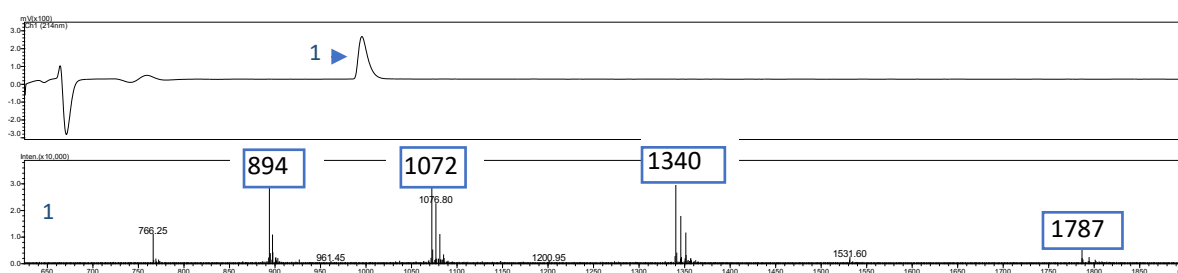


*Figure 35: LC-MS analysis of purified compound **6**. Since the modified peptide's molecular mass is above the detection range, only multiple times charged species can be detected in the mass spectrum.*

As it can be seen in the LC, the product appears to be pure since only the product peak is visible in the chromatogram. The isolated compound was detected as multiply charged species since the m/z limit of the single quadrupole detector is 2000. The framed detected masses in the MS spectrum in Figure 35 clearly show the expected mass peaks for multiple times charged molecules. The mass signals can be assigned to the charged species in the order of m/z = 1787 [M+3H⁺], m/z = 1340 [M+4H⁺], m/z 1072 [M+5H⁺] and m/z = 894 [M+6H⁺].

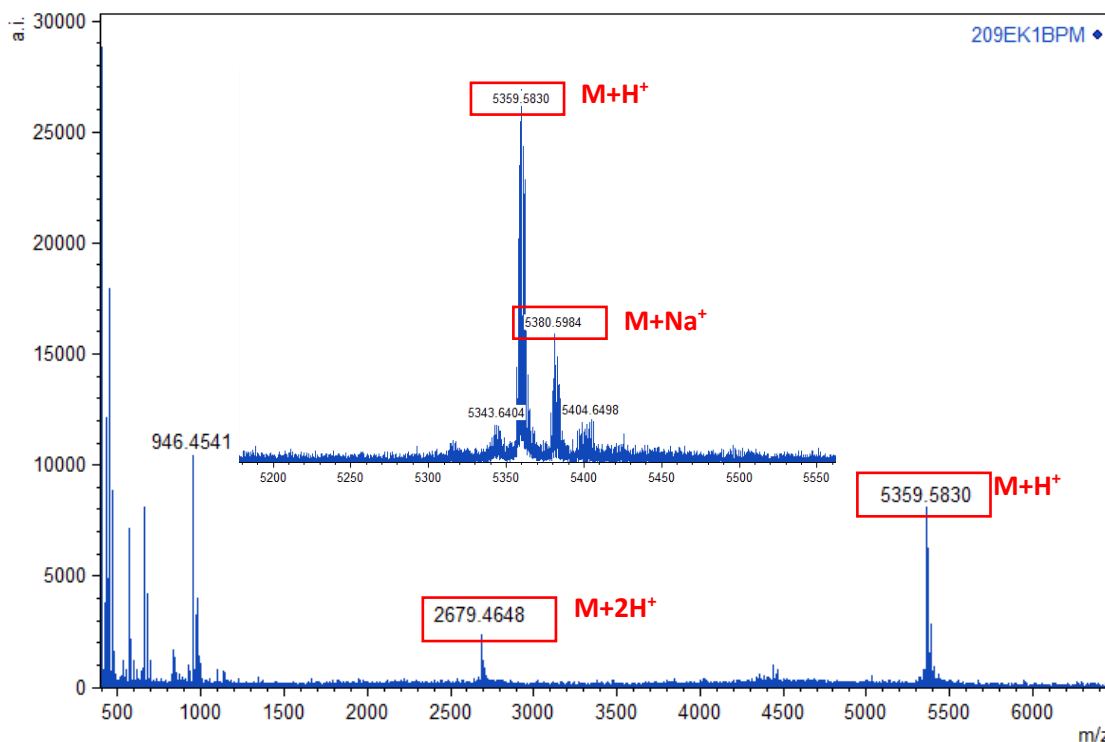
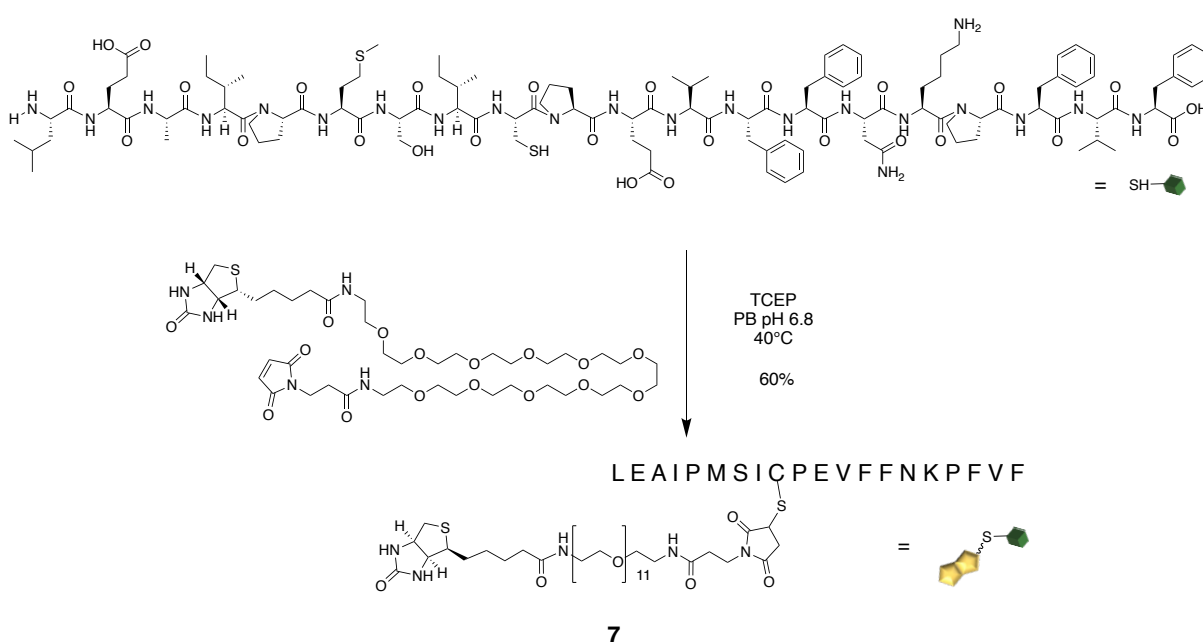


Figure 36: MALDI mass spectrum of isolated compound **6**. Measurement was performed using CHCA as a matrix.

For further confirmation of the expected mass, a MALDI measurement was performed, shown in Figure 36. The MALDI spectrum obtained using a α -cyano-4-hydroxycinnamic acid (CHCA) as matrix shows the monocharged molecule mass peak at $m/z = 5360$ [$M+H^+$] and the doubly charged molecule mass peak at $m/z = 2679$ [$M+2H^+$]. In the close up of the main peak in Figure 36 the sodium adduct at $m/z = 5381$ [$M+Na^+$] is also visible. All these data give evidence, that the coupling of EK1 to the pegylated biotin maleimide was successful and the modified peptide could be used for supramolecular multimerization on streptavidin.

3.2.2 Conjugation of VIRIP to bifunctional Biotin-PEG11-maleimide linker

Since VIRIP is a literature known entry inhibitor against HIV, it is of great interest to investigate the effect of multimerization of this peptide concerning its antiviral activity *in vitro*^[17]. As already discussed in the previous section, an assembly of this bioactive molecule requires a biotin unit which then can undergo noncovalent interaction with an ALP's biotin binding pocket. For this modification, biotin PEG-11 maleimide was used again, since VIRIP contains a single cysteine residue as well, which makes it an attractive functionality for bioconjugation reactions. The performed synthesis is shown in Scheme 16.



Scheme 16: Reaction equation of the synthesis of compound 7, the coupling of VIRIP to biotin PEG-11 maleimide.

Again, it was necessary to control the pH of the reaction mixture by using buffered solvents, such as phosphate buffer at a pH of 6.8. The afterwards obtained mixture was purified by semi-preparative HPLC, resulting in 60% yield, which was significantly lower than the yield of the bioconjugation reaction between EK1 and the biotin-PEG11-linker. One reason for the decrease could have been the poor solubility of VIRIP, which impeded the preparation of the reaction mixture and made higher reaction temperatures necessary.

To investigate the purity of the isolated product 7, LC-MS analysis was performed, its results are shown in the following figure.

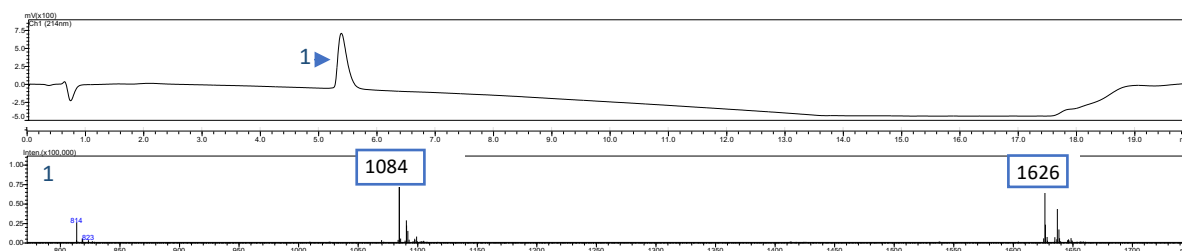


Figure 37: LC-MS analysis of the isolated compound **7**. Since the modified peptide's molecular mass is above the detection range, only multiple times charged species can be detected in the mass spectrum.

Since the expected product mass is above the ESI-MS detection range, only multiple charged species can be used to identify the product fraction. From the LC in Figure 37, only one peak appears during the analysis, indicating that the product should be pure. The corresponding mass peaks that were detected for the peak with a retention time of 5.4 min, show two characteristic signals that can be assigned to the doubly and triply charged molecule **7** with $m/z = 1626 [M+2H^+]$ and $m/z = 1084 [M+3H^+]$.

To ensure that the product fraction contains the expected molecule with a molecular mass of 3251 g/mol, MALDI mass analysis was performed. The obtained mass spectrum is shown in Figure 38.

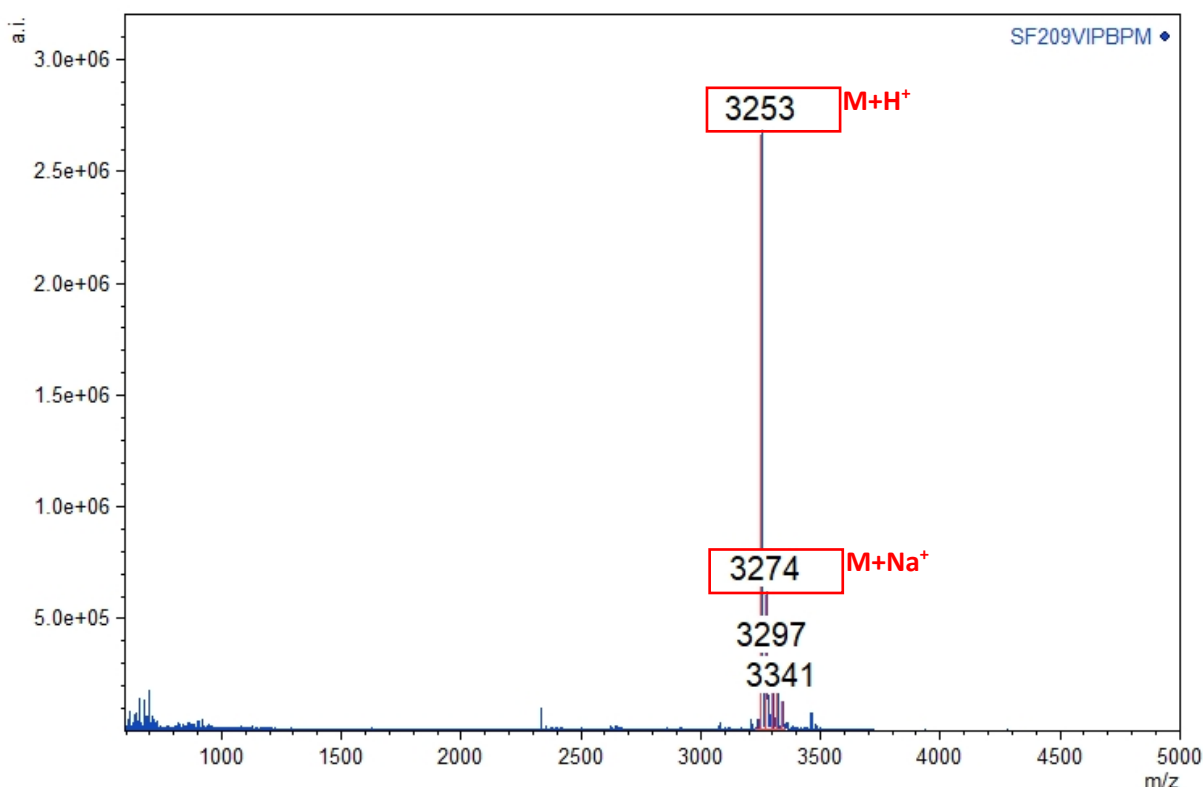


Figure 38: MALDI mass spectrum of the isolated compound **7**. Measurement was performed using a sinapic acid matrix.

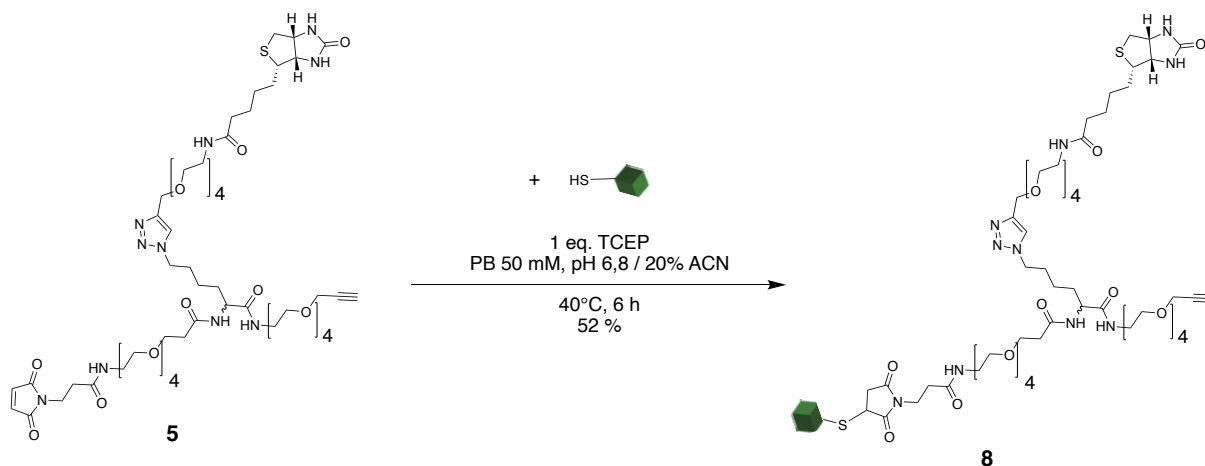
In Figure 38, it can be seen, that the isolated compound shows the expected mass at $m/z = 3253 [M+H^+]$. In addition to that, several cationic adducts of the product become visible as well, such as the sodium adduct at $m/z = 3274 [M+Na^+]$.

These data give evidence, that the coupling of VIRIP to biotin PEG-11 maleimide was successful and the obtained molecule can be used for the assembly of VIRIP to an ALP.

3.2.3 Conjugation of VIRIP to trifunctional Biotin-PEG-maleimide-alkyne linker

After both of the discussed antiviral peptides were successfully coupled to a biotin linker, the conjugation of both VIRIP and EK1 on one trifunctional linker with biotin for the assembly of a pan virus inhibitor.

Therefore, the previously synthesized linker molecule (compound **5**, see section 3.1) was used. The conducted synthesis is given in Scheme 17. First, VIRIP was conjugated via the reaction of the cysteine with the maleimide.



Scheme 17: Bioconjugation reaction equation of VIRIP with trifunctional linker via maleimide-thiol Michael-addition.

The reaction procedure was adapted from the previous bioconjugation reactions^[34], with modification of the solvent, using PB 50 mM at pH 6.8 with 20% acetonitrile to solubilize the relatively hydrophobic VIRIP. The reaction was again performed at RT and after removal of the solvent via lyophilization purified via semi-preparative HPLC. After isolation of the product, its yield was determined to be 52%. This yield appears to be lower than the one of the previous thiol-maleimide reactions. One reason for the lower yield of material in this reaction could be the increased steric demand of the linker molecule in combination with the cysteine being at an internal position within the peptide's amino acid sequence of the VIRIP peptide. This makes it less accessible for the nucleophilic maleimide. Nevertheless, the desired product was gained in this

reaction, as the LC-MS and MALDI analysis have shown. The solvent composition as well as the reaction time, could possibly be optimized to improve the reaction yield. Since the expected product mass is out of the ESI-MS detection range, only multiple charged species can be used to identify the products molecular weight. The highest

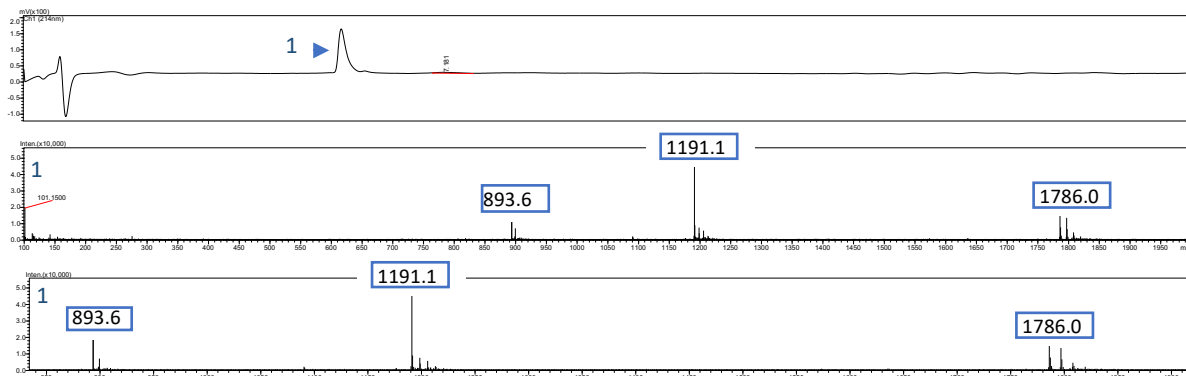


Figure 39: LC-MS analysis of purified compound 8. Since the expected product mass is higher than the ESI-MS detection range, only multiple charged product species can be detected.

mass was detected at 1786 m/z which fits to the twice charged expected molecular mass of the product $[M+2H^+]$. The triply and quadruply charged species can be assigned to $m/z = 1191 [M+3H^+]$ and $m/z = 894 [M+4H^+]$. Since no other peaks appear in the LC, the isolated product was pure and had the expected product mass.

To make sure, that the obtained substance has the calculated product mass as a single charged ionized species, MALDI analysis was performed, using a CHCA matrix. The results of this analysis are shown in Figure 40.

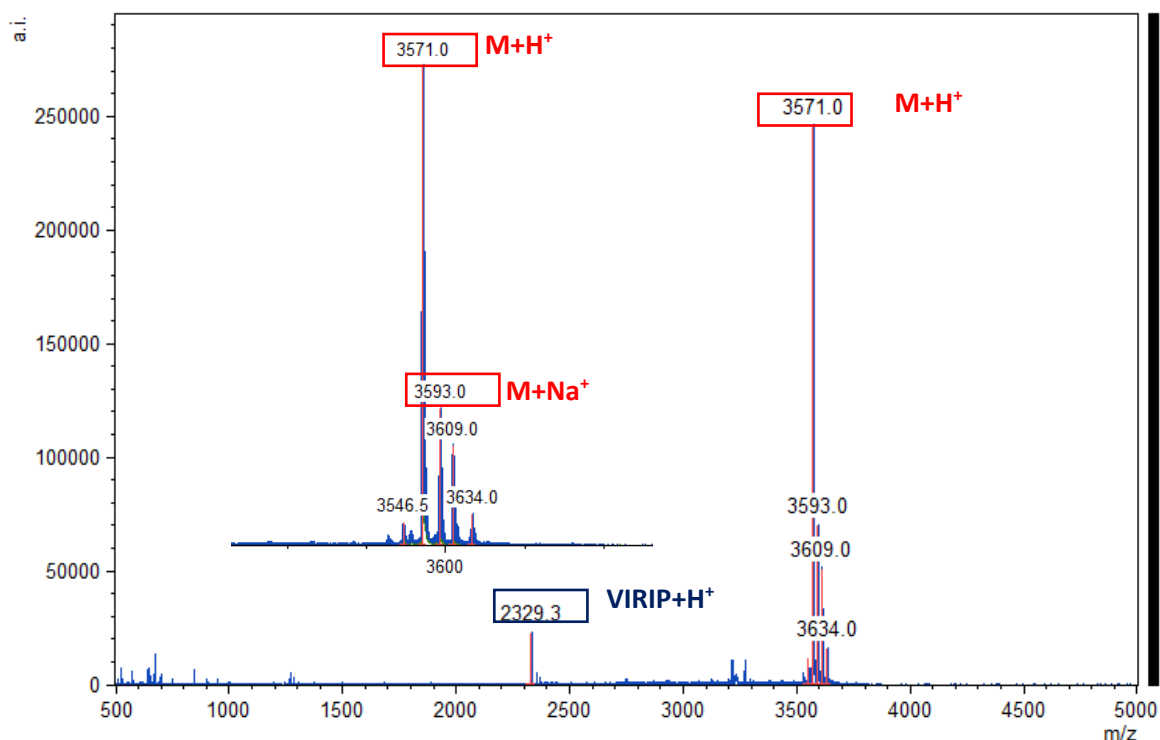
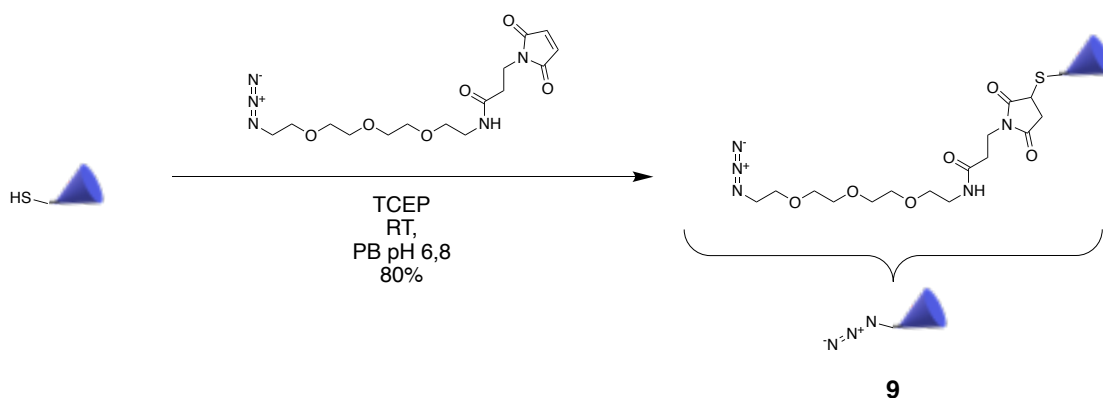


Figure 40: MALDI mass analysis of purified compound **8**. Measurement was performed by sample preparation with a CHCA matrix.

As it can be seen in the spectrum, the isolated substance has the desired molecular weight with $m/z = 3571$ [$M+H^+$]. A close up of the spectrum in Figure 40 shows some other characteristic cationic adducts such as the sodium adduct at $m/z = 3593$ [$M+Na^+$]. Besides the expected masses displayed by the main peak, another signal appears in the spectrum at $m/z = 2329$. This mass fits to the molecular weight of unmodified VIRIP but taking into account the LC-MS spectrum of the product fraction, this could be due to the ionization process which could have cause the ionized product to undergo a retro Michael addition. Consequently, this leads to the fragmentation of the desired molecule into a linker molecule and unmodified peptide. Putting together the analytics, the product is pure and will be usable for further conjugation reactions with other bioactive molecules.

3.2.4 Azide-alkyne cycloaddition of EK1 to biotinylated VIRIP linker construct

For the connection of VIRIP and EK1 on the trifunctional biotin linker, it was chosen to use an azide alkyne cycloaddition, as it promised to be conductible under physiological pH and relatively mild conditions. Therefore, the previously synthesized construct **8** containing VIRIP and an alkyne functionality was used. As the performance of this [3+2] cycloaddition requires an azide functionality, it was necessary to introduce this to the EK1 peptide in advance. The reaction equation of the procedure is shown in Scheme 18.



Scheme 18: Reaction equation of the azide functionalization of EK1.

The reaction was performed with an excess of eight equivalents of azide PEG3 maleimide to enable almost quantitative yield, since unmodified EK1 could not be separated from the modified product via preparative HPLC. As a result, the reaction was monitored via MALDI measurements and afterwards purified by size exclusion chromatography using Sephadex G-10 swollen in MilliQ water to separate the peptide compounds from the remaining linker molecule. LC-MS studies were performed to check the isolated peptide for its purity. The resulting spectra are shown below.

As Figure 41 shows, the LC spectrum displays one peak, with corresponding masses

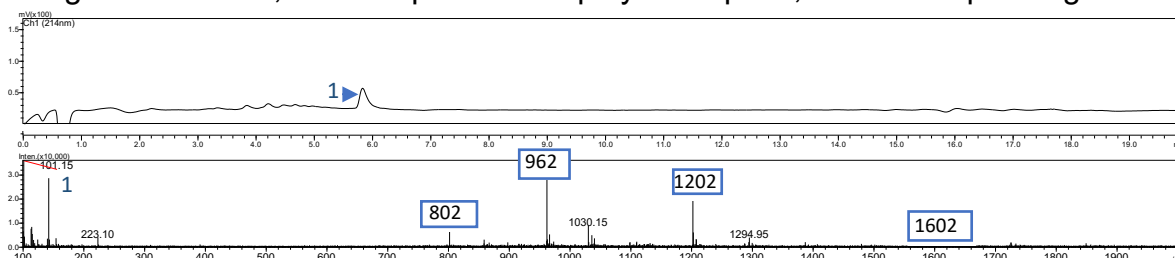


Figure 41: LC-MS spectrum of purified compound **9**. Since the product's molecular mass lays outside the ESI-MS detection range, only multiple times charged species can be detected.

that can be assigned to the expected masses of multiple charged product species. Even though the baseline of the LC spectrum appears to be uneven, no other mass peaks were detected in the ESI spectrum, which leads to the conclusion that the rough

baseline was not caused by contaminants from the product. The mass peaks shown in the ESI-MS spectrum fit to the multiple charged product molecules as $m/z = 1602 [M+3H^+]$, $m/z = 1202 [M+4H^+]$, $m/z = 962 [M+5H^+]$ and $m/z = 802 [M+6H^+]$. To check the degree of labeling of EK1 with maleimide PEG3 azide and to prove the expected molecular weight, MALDI mass analysis was performed using a CHCA matrix.

As it can be taken from Figure 42, the modified EK1 shows a higher peak intensity as

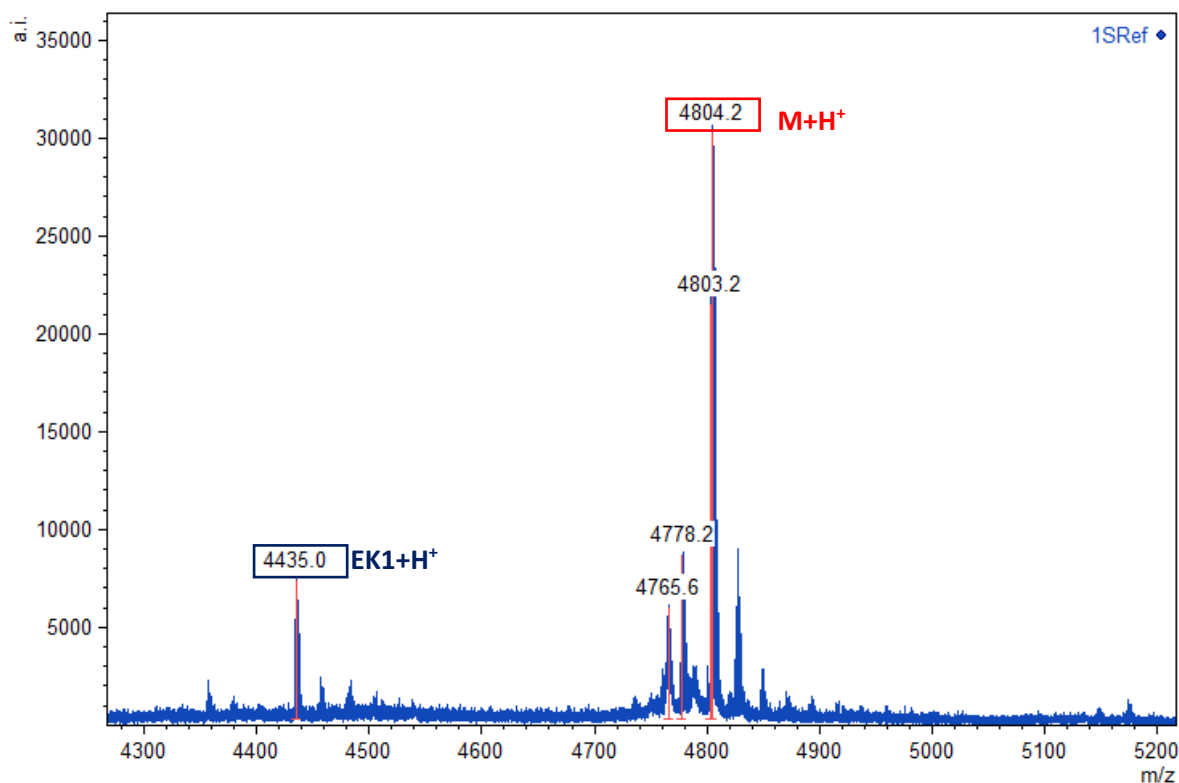
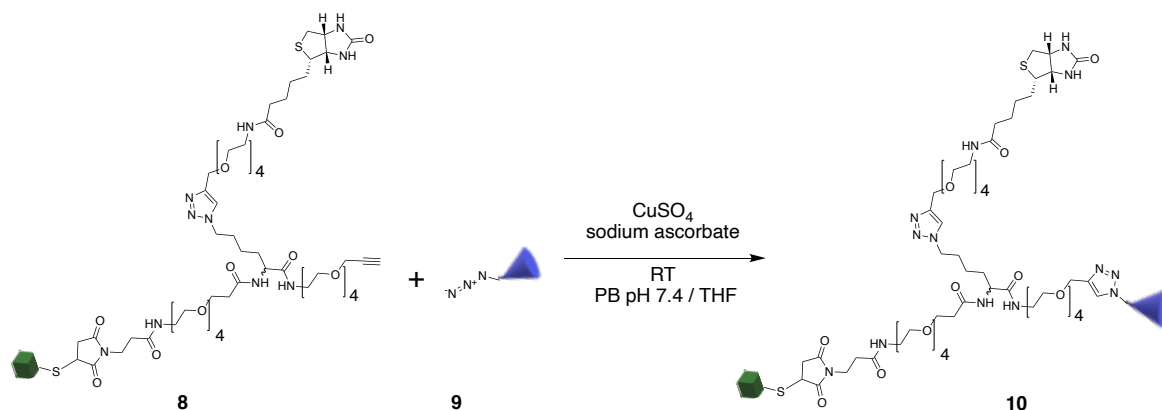


Figure 42: MALDI mass analysis of purified compound **9**. Spectrum was obtained by using a CHCA matrix.

the unmodified peptide, showing that the reaction was successful, although full conversion was not attained. The main peak in the spectrum can be assigned to $m/z = 4804 [M+H^+]$, whereas native EK1 can be found at $m/z = 4435 [EK1+H^+]$. According to the peak intensity relations of compound **9** and EK1, the yield of the reaction was calculated to be 80% of the theoretical amount of material. Taking into account the previously discussed analytical results, the product is sufficiently pure for further bioconjugation reactions, since unmodified EK1 will not interfere with the following azide alkyne cycloaddition.

As a next step, it was attempted to incorporate the modified EK1 (compound **9**) to the biotinylated VIRIP-trifunctional linker construct via a copper catalyzed Huisgen reaction. The reaction conditions from section 3.1.1 were adapted for this reaction^[59], except the used solvents, since this conjugation contains peptide components which have to be prevented from aggregation. The following reaction equation describes the performed synthesis.



Scheme 19: Reaction equation for the copper catalyzed Huisgen reaction to conjugate EK1 azide to VIRIP biotin trifunctional linker via its alkyne functionality.

The reaction was conducted under argon atmosphere to prevent the copper(I) species generated *in situ* from being oxidized. With 0.5 equivalents of copper catalyst, the reaction was allowed to proceed for 48 h before being lyophilized and analyzed via MALDI TOF mass analysis. The result of the measurement is shown in Figure 43. Only traces of the desired product could be detected in the mass spectrum (see close up Figure 43) besides the starting material peaks appearing to be the main signals. This can be explained by several reasons. One explanation for the low intensity of the desired product in the MALDI spectrum could be that the compounds molecular weight differs in a significant manner from the starting materials, making it less likely to be desorbed and ionized under the given experiment conditions of the mass analysis. This would require further optimization of selection of the matrix of the analyzed sample or variation of the laser intensity.

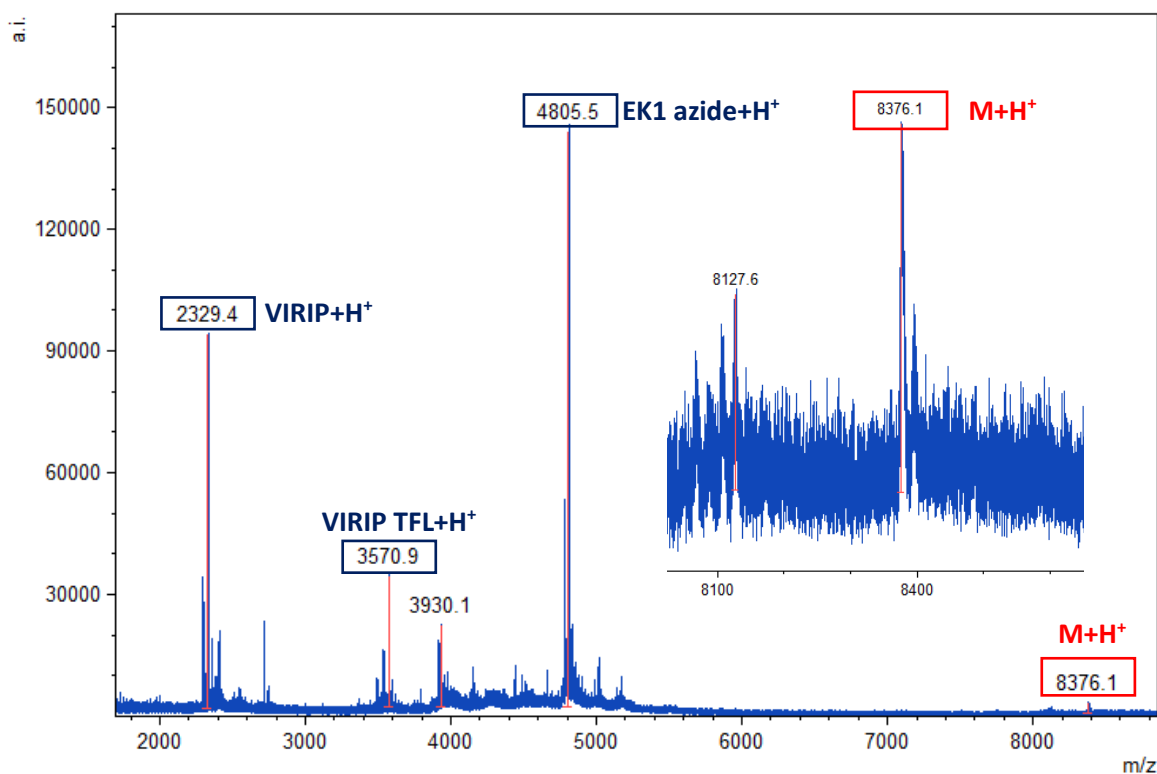


Figure 43: MALDI mass analysis of reaction mixture for the synthesis of compound **10**. Measurement was performed using SA as a matrix.

Another likely reason for the low product signal intensity, could be that the reaction did not work well because of inappropriate conditions, such as reaction temperature, solvent composition or steric hindrance due to the bulky peptide structures insulating the functional groups from their reaction partners. This possible explanation is underlined by the appearance of additional mass signals in the MALDI spectrum highlighted in blue, which lead to the assumption that fragmentation of the starting materials occurred instead of the desired conjugation. Therefore, it would be important to perform additional test reactions for investigation of possible systematic errors of the reaction, such as used equivalents of catalyst. Although some amount of compound **10** seemed to be formed, the overall yield is too low for assemblies to supramolecular platforms. Further optimization of the reaction conditions is required. For example, the azide alkyne cycloadditions can be tested with less steric demanding peptides to exclude steric hindrance from being the reason for the low product yield. In addition to that an approach could be to change the order of the conjugation. Specially, the azide-alkyne cycloaddition can be first conducted before EK1 is conjugated to the maleimide, to reduce the number of bulky groups during the cycloaddition.

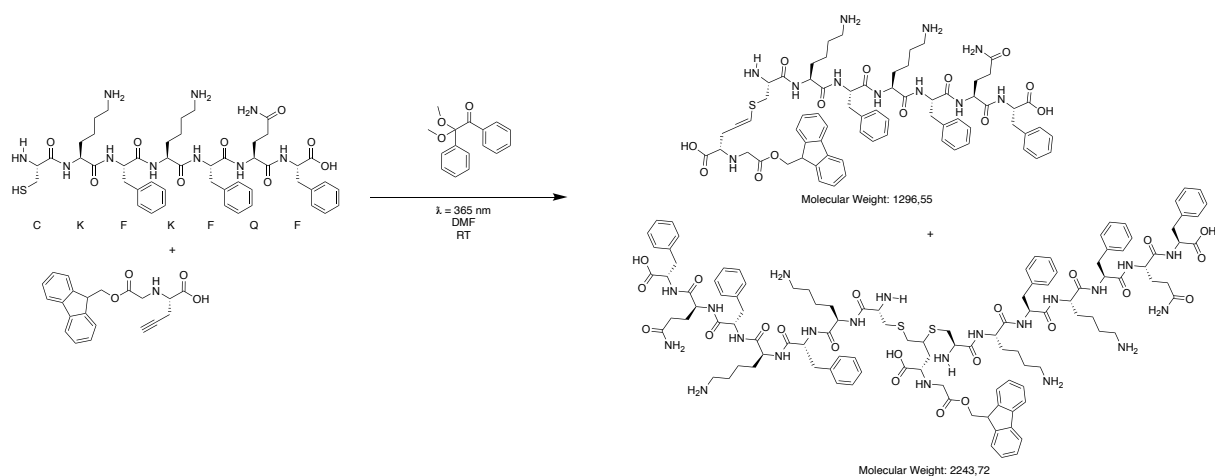
In addition, as the MALDI spectrum also shows free VIRIP being present in the product mixture, it can be assumed that the maleimide bonding of the starting material was

labile and cycloaddition occurred between the free trifunctional linker and EK1 azide. To avoid this fragmentation, the maleimide structure could be hydrolyzed in advance to prevent the VIRIP linker construct from undergoing a retro Michael addition.

3.2.5 Reaction screening for thiol-yne reaction versus thiol-maleimide reaction with test peptides

To investigate the possibility of directly linking a thiol containing antiviral peptide to the trifunctional linker construct via a photoinitiated thiol-yne click reaction as described in chapter 1.3.2, it was necessary to develop an efficient reaction system. Therefore, some test reactions were performed, including cysteine containing small peptides and different kinds of alkynes.

At first, one alkyne component, which did not possess any other thiol reactive functionalities was tested for its reaction with a simple seven amino acid peptide CKFKFQF, to investigate the distribution of mono- and double addition of thiols on one alkyne. The general equation for the performed test reaction is shown below.



Scheme 20: Reaction equation for thiol-yne test reaction using Fmoc-L-propargylglycine and test peptide CKFKFQF.

As shown in Scheme 20, the mentioned test peptide was reacted with Fmoc-L-propargylglycine as an alkyne component and DMPA as a photoinitiator with light irradiation at 365 nm. The reaction was carried out at room temperature in DMF as solvent. After irradiation was completed after 20 min, MALDI mass analysis was performed to measure the formation of mono addition product (MW = 1297 g/mol) and double addition product (MW = 2244 g/mol).

The result of the measurement is shown in Figure 44.

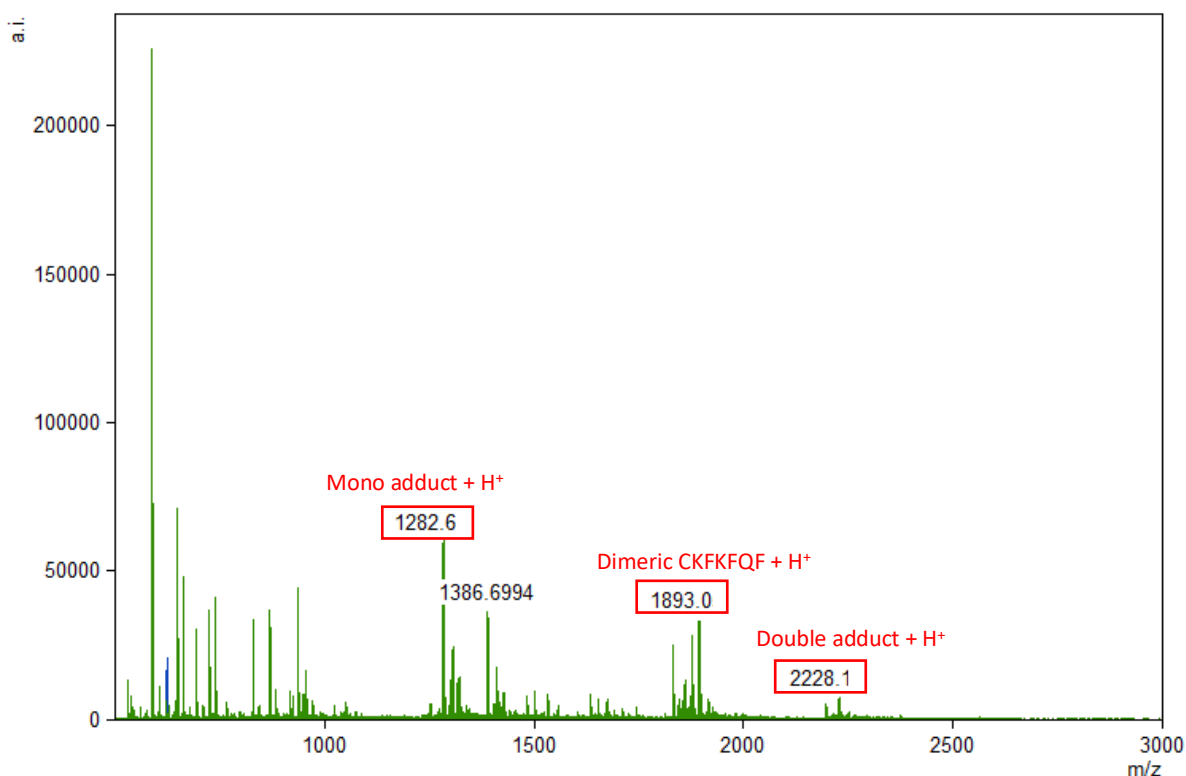
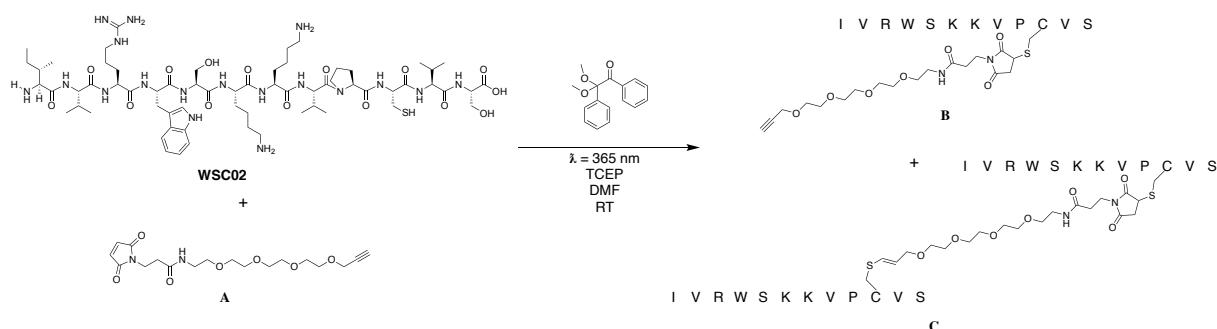


Figure 44: MALDI analysis of the test reaction shown in scheme. The spectrum was obtained by preparation of the sample with CHCA as a matrix.

With respect to the expected product masses taken from Scheme 20, the three significant mass signals highlighted in red in Figure 44 can be assigned to their corresponding molecules. At first, the main peak in the spectrum showing a mass of $m/z = 1283$ $[M+H^+]$ corresponds to the expected molecular weight of the mono addition product of Fmoc-L-propargylglycine, leading to the assumption, that under the given conditions this modification is favorable.

The second highlighted peak displays a molecular weight of $m/z = 1893$ $[M+H^+]$. Since this signal does not fit to one of the expected reaction products, but to a dimeric form of CKFKFQF, it can be assumed that the test peptide formed disulfide bridges during the reaction, preventing it from reacting with Fmoc-L-propargylglycine. The smallest noticeable peak in the MALDI spectrum represents a molecular weight of $m/z = 2228$ $[M+H^+]$. This signal can be assigned to two CKFKFQF molecules added to one Fmoc-L-propargylglycine. Since this signal only shows minor intensity, it appears that under the reaction conditions mainly mono addition occurs on the alkyne functionality. This could be due to the steric demand of the thiol containing molecule, making the photoinitiated thiol-yne reaction attractive for further bioconjugation reactions.

Even though the reaction pictured in Scheme 20 can be claimed to have been successful, it was important to investigate the influence of other functionalities' presence. Therefore, another alkyne was chosen which in addition to its propargyl group contained a maleimide functionality, as it appears to be the case for the synthesized trifunctional linker. In addition to that, it was thought to be interesting to check the influence of more steric demanding thiol moieties, in this case it was the virus entry inhibitor peptide WSC02 (see section 1.2.1). The chosen reaction conditions are shown below.



Scheme 21: Reaction equation for thiol-yne test reaction between maleimide-PEG4-alkyne and WSC02.

In this reaction, reagent **A** was used to check the influence of radical species on formed thiol-maleimide adducts. **WSC02** was used in an excess of three equivalents and reduced with TCEP in advance. Afterwards maleimide alkyne (reagent **A**) was added to the mixture and maleimide addition was allowed to proceed in the dark for one hour. Thereafter, photoinitiator DMPA was added, and the solution was irradiated with light at 365 nm for one hour. To identify the products formed, MALDI mass spectrometry was performed. The results of the analysis are shown in Figure 46. It can be seen, that mainly mono adduct (product **B**, $M = 1784 \text{ g/mol}$) was formed, shown at $m/z = 1784 [M+H^+]$. The expected double adduct (product **C**, $M = 3186 \text{ g/mol}$) appears only as a low intensity signal at $m/z = 3186 [M+H^+]$, which leads to the assumption that only small amounts of the desired product was formed. Besides the modified versions of WSC02 it can be seen that significant amounts of native WSC02 remained, shown by the peaks at $m/z = 1402 [M+H^+]$ representing the monomeric peptide and $m/z = 2802 [M+H^+]$ which can be assigned to dimeric WSC02, possibly formed by a thiol bridge.

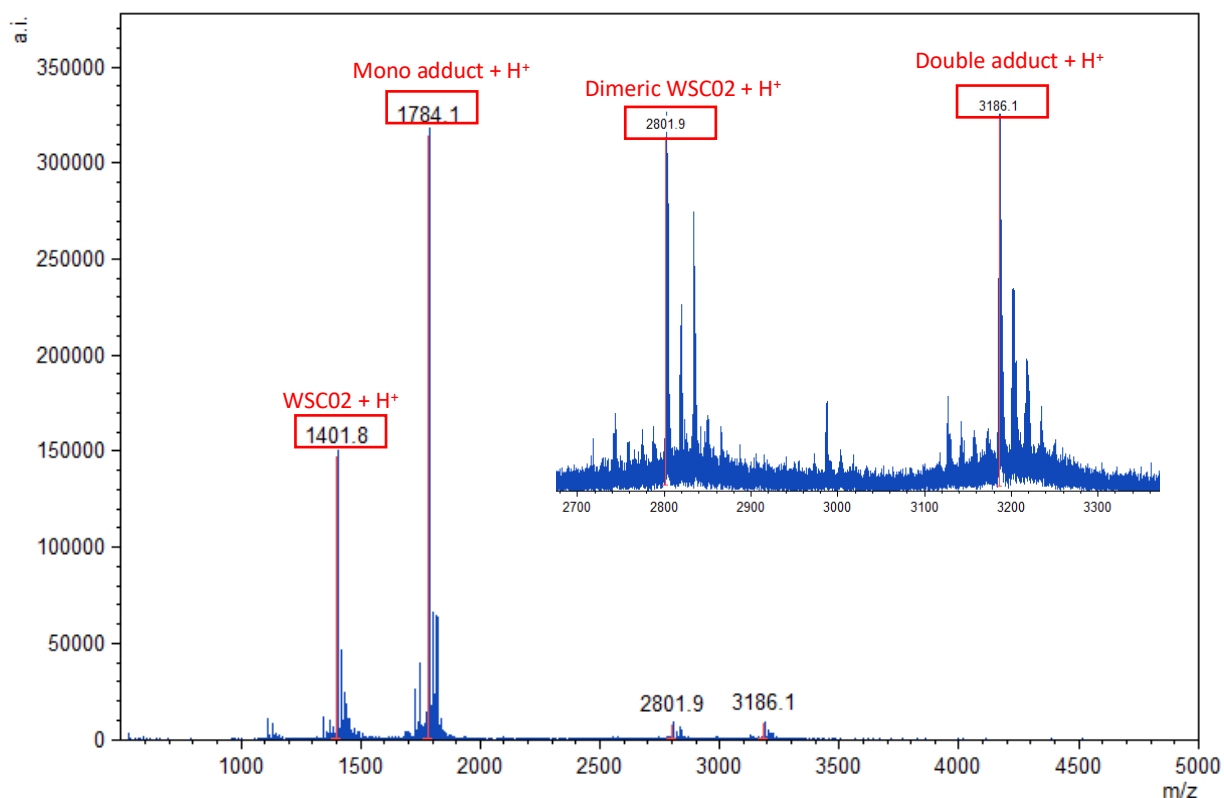
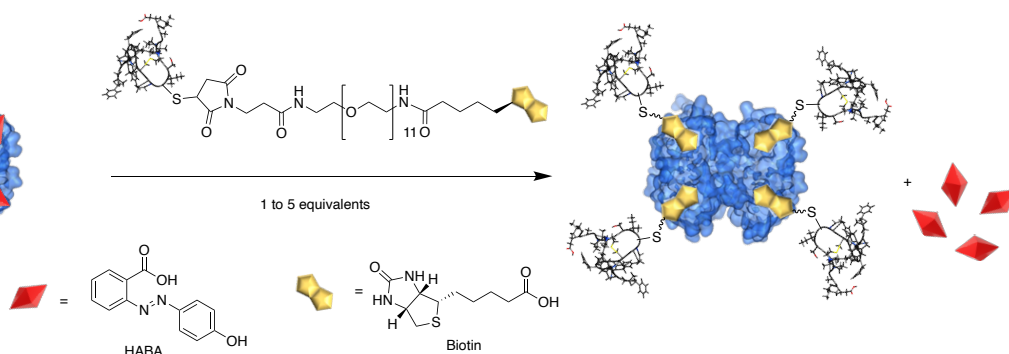


Figure 46: MALDI mass spectrum of thiol maleimide versus thiol alkyne test reaction using antiviral peptide WSC02. Measurement was performed using CHCA as a matrix.

Since only low yields of the expected double addition product was formed, the question remains, which functional groups reacted with WSC02 under formation of the mono adduct. It can be expected, that before the addition of the photoinitiator and the irradiation with light, the only possible reaction between maleimide alkyne and the thiol in cysteine is through at the maleimide, making it most likely for the formation of a mono addition product. But taking into account the following harsh conditions of the photoreaction, a possible reason for the low product yield could also be the maleimide thiol bonding undergoing a retro Michael addition, causing the fragmentation of the monoadduct. In this case, the success of the photoreaction is inconclusive. Therefore, it would be very important to characterize the formed products via NMR studies concerning the formed bonds between WSC02 and maleimide alkyne. For further improvement of the reaction leading to higher yields of the double addition product, different solvent compositions, light irradiation times and reactant concentrations could be optimized. Alternatively, a different photoinitiator can be applied. For example, switching from the really reactive and carbon radical forming DMPA to milder radical initiators, such as phosphones. Nevertheless, the reaction system proposed is a promising strategy for bioconjugation reactions, even though it requires further optimization.

3.3 Assembly of biotinylated peptides to streptavidin

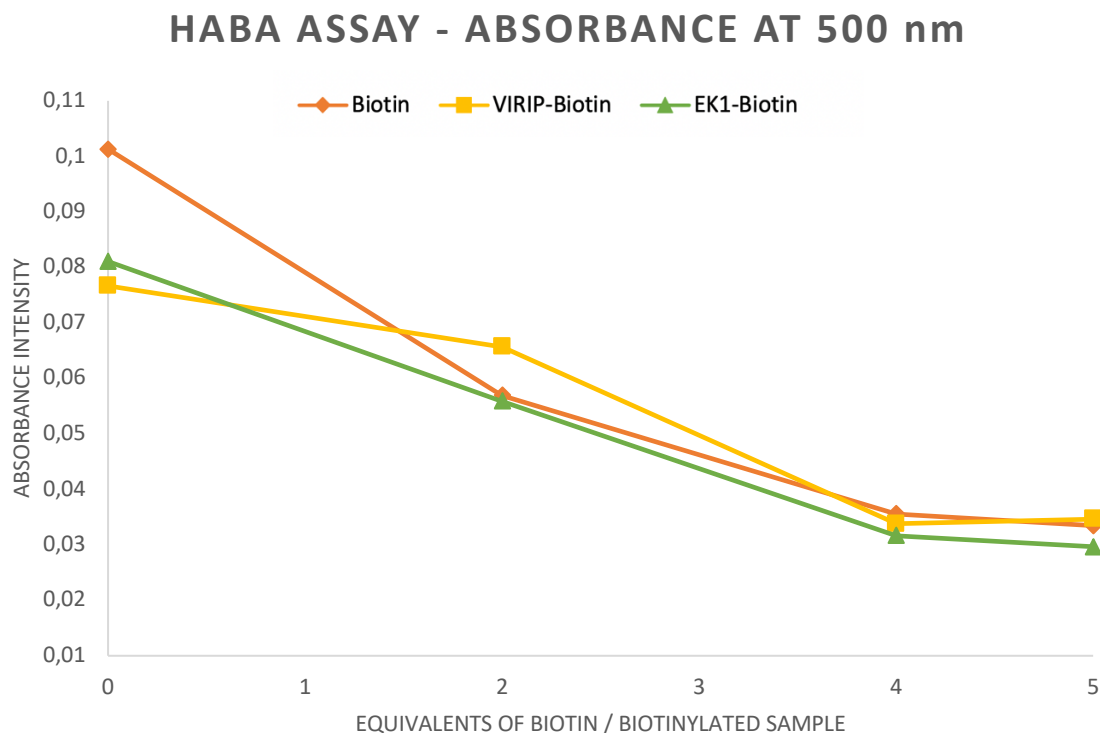
As it was discussed in chapter 3.2.1 and 3.2.1 (see page 39) the antiviral peptides EK1 and VIRIP were successfully conjugated to a biotin unit and therefore are able to be assembled on avidin-like proteins such as neutravidin and streptavidin. Since the modification of native biotin with bulky biomolecules potentially lower the molecules binding affinity to streptavidin or neutravidin, it is necessary to investigate the number of equivalents that are needed to saturate all four binding pockets of the protein with biotinylated peptide. This value can be determined by an HABA assay. HABA (2-[(4'-hydroxyphenyl)-azo] benzoic acid) is a ligand of avidin and ALPs which binds to the protein with a significantly lower affinity than biotin does ($K_D = 4 \times 10^{-4} \text{ M}$), thus is displaced from the binding pocket if the native ligand biotin is present^[34]. Since the complex of an ALP with HABA characteristically absorbs light at 500 nm wavelength, the absorption of sample solutions at 500 nm should decrease by the addition of more equivalents of biotin or biotinylated sample. When the necessary amounts of biotinylated material to saturate the ALP is reached, further biotin addition does not lead to decrease of the light absorption at 500 nm. A schematic drawing of the process is shown in Scheme 22. This assay was used to investigate the required equivalents of biotinylated EK1 and VIRIP for their assembly to streptavidin.



Scheme 22: General equation for the substitution reaction between biotin and HABA on an avidin like protein.

To a defined amount of streptavidin was added each a saturated solution of HABA in MilliQ water. Afterwards, one to five equivalents of the respective biotinylated peptides (EK1, VIRIP) were added to each well of a transparent microplate. After incubation for ten mins, the absorbance of each sample at 500 nm was measured in a plate reader. The results of the absorbance values were plotted against the corresponding equivalents of biotin sample added to each streptavidin mixture. An absorption curve of each sample line in dependence of the number of biotin equivalents was thus

obtained. The results of the performed HABA assays for EK1-PEG11-biotin and VIRIP-PEG11-biotin are shown in the following graph.



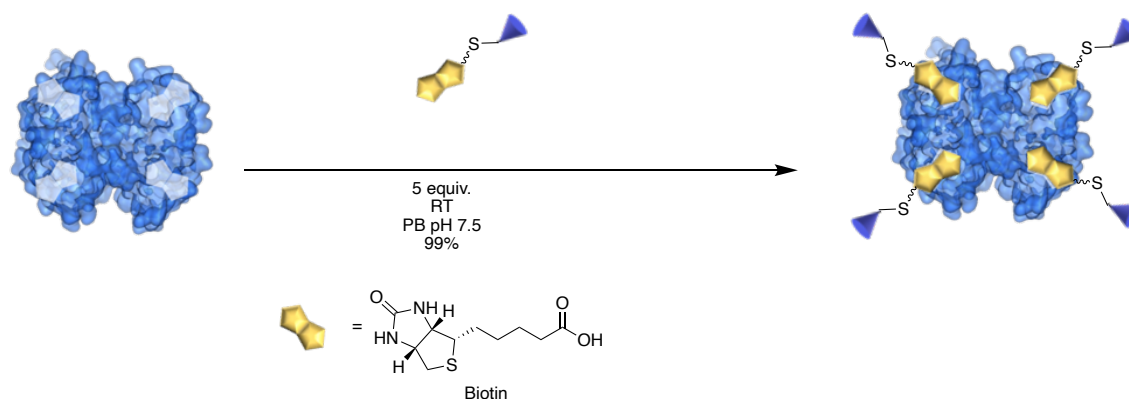
Graph 1: Results of the absorbance measurements of the HABA assay for determination of saturation equivalents for biotinylated EK1 and biotinylated VIRIP in relation to native biotin on streptavidin. Measurements were performed using a transparent 384 well plate. Absorbance was measured at 500 nm in a Tecan plate reader.

As can be seen from Graph 1, both biotinylated peptides show a similar trend compared to the native biotin standard line. All three curves show their absorbance minimum at about four mole equivalents of biotin there is no significant decrease with the addition of more biotin. Therefore, it can be assumed that the functionalized peptides have a similar binding affinity to streptavidin as unmodified biotin and assemblies of these bifunctional constructs will require four equivalents to saturate all binding pockets of ALPs.

3.3.1 Assembly of biotinylated EK1 to Streptavidin

As mentioned above, supramolecular multimerization of EK1 on streptavidin will require four equivalents of the peptide, showing that the steric demand of the heavy peptide does not significantly influence the binding affinity of the biotin moiety. This could have been caused by the spacing PEG chain that separates the amino acid sequence of the conjugate from the essential ALP binding unit.

To investigate the effect of multimerization on the antiviral activity of EK1 alone, the previously bioconjugated peptide was assembled to streptavidin. The following reaction scheme depicts the performed reaction.



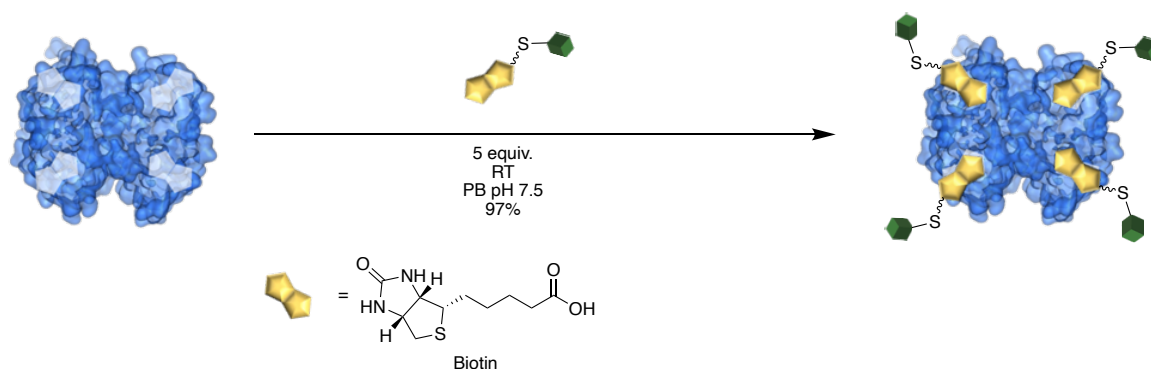
Scheme 23: Reaction equation of supramolecular multimerization of biotinylated EK1 peptide on streptavidin.

To prevent the dissolved protein from aggregating during the reaction procedure, the assembly was conducted in buffered solution using 50 mM PB at physiological pH 7.4. After being mixed for one hour at room temperature, the reaction mixture was purified by ultrafiltration using 10 kDa molecular weight cut off centrifugation tubes. With this procedure, it was possible to remove excess peptide which was not bound to streptavidin. After being washed with ultrapure water and resuspended in PB, the protein concentration was determined by nanodrop absorption measurement at 280 nm in relation to a streptavidin standard curve, making it possible to calculate the overall yield of the reaction being 99% of the theoretical amount of material. This leads to the assumption, that the purification of the crude assembly mixture did not cause any significant loss of material, making it a suitable procedure for further ALP purifications.

To check on the products purity and potential shifts in tetrameric mass of the non-denatured peptide protein conjugate, SDS PAGE was performed using silver staining for band visualization. The results of the analysis are discussed in chapter 3.3.3 (see page 59).

3.3.2 Assembly of biotinylated VIRIP to streptavidin

After successfully multimerizing EK1 on streptavidin, it was also important to reproduce perform the same procedure for the assembly of VIRIP on streptavidin to enable sufficient comparison of the tetramerization influence on the peptide's antiviral activity. The chosen reaction conditions are the same as for the previously shown peptide assembly and can be seen in Scheme 24.



Scheme 24: Reaction equation for the saturation of streptavidin with biotinylated VIRIP.

The reaction was performed in buffered solution under physiological pH to avoid protein aggregation as mentioned in the previous section. Since the HABA assay with biotinylated VIRIP has shown a similar binding affinity to streptavidin-like native biotin (see Graph 1), five equivalents of functionalized peptide were used to ensure a complete saturation of the biotin binding protein.

The reaction was performed at room temperature over a period of one hour. After completion of the assembly, the reaction mixture was purified by ultracentrifugation to separate modified streptavidin from potential unbound peptide. The concentration of the protein obtained in buffered solution was determined by absorbance measurements at 280 nm in relation to a streptavidin standard line, as discussed in section 3.3.1. Via this process, it was possible to calculate the overall yield of the reaction being 97%. This result leads to the assumption that the chosen process enables a high recovery of the deployed material and therefore is a suitable procedure for further multimerizations of biotinylated species on ALPs.

To investigate the composition of the obtained protein concerning its total mass and intact structure as tetramer, SDS PAGE was performed using silver stain for visualization of protein/peptide bands. The results of the analysis are discussed in the following chapter.

3.3.3 Characterization of multimerized peptides on streptavidin via SDS PAGE

To analyze the previously synthesized protein hybrids concerning their tetrameric structure and potential shifts in mass or bands of unbound peptide, SDS PAGE was performed. Each protein hybrid and one sample of native streptavidin was applied to the gel once in native form and once after denaturization with dithiothreitol (DTT). After completion of the electrophoresis the protein and peptide bands were stained with

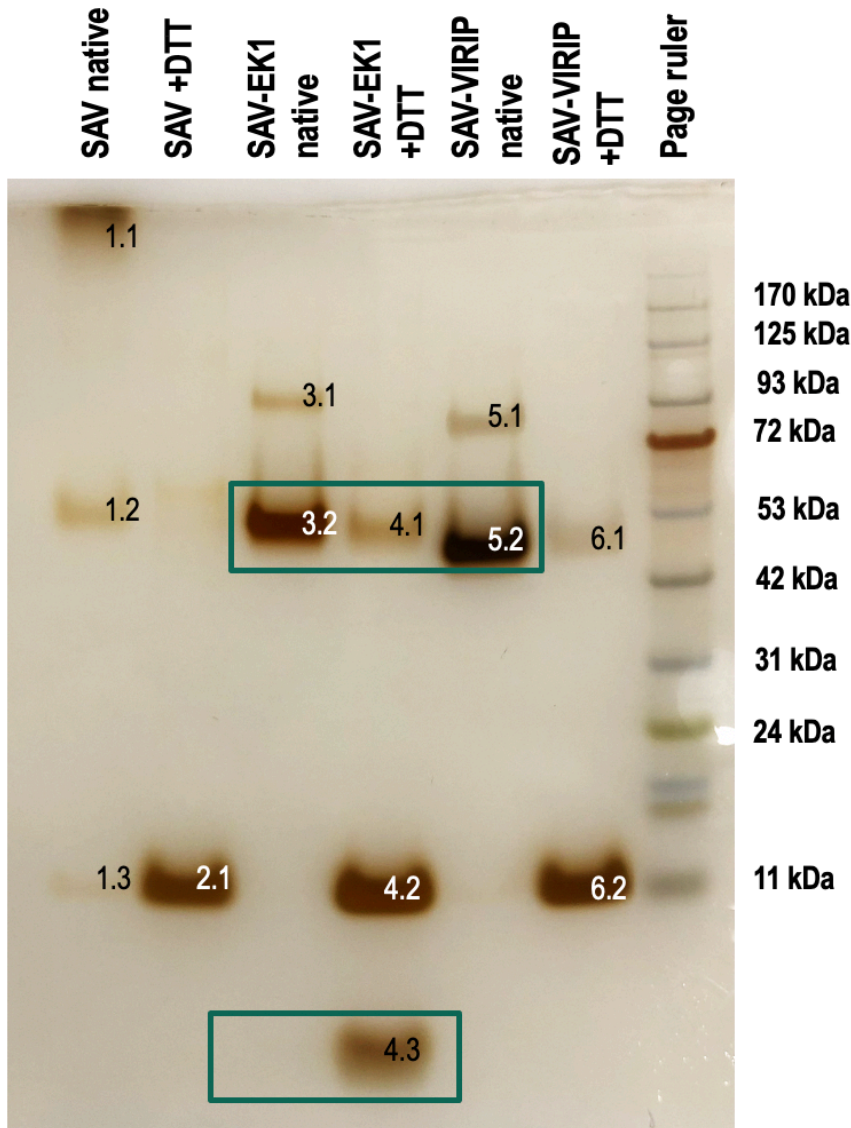


Figure 47: Silver stained SDS PAGE gel of different streptavidin (SAV) peptide hybrids in comparison to native streptavidin, each under native and denaturated conditions with DTT. Electrophoresis was run at 120 V in MES running buffer.

silver staining and analyzed. The result of the described process is shown in Figure 47.

As it can be taken from the picture on the left, it was possible to stain several characteristic bands for the different streptavidin hybrids. At first, it can be seen, that the reference traces of native streptavidin, on the left of the figure shows contaminants or more likely SAV aggregates at higher molecular weight (band 1.1). This could have been caused by the storage of the sample in ultrapure H₂O which does not have any

buffering capacity. Nevertheless, band 1.2 represents the expected molecular weight of the tetrameric SAV in reference to the page ruler at about 53 kDa. Even though the first trace sample was not prepared under denaturizing conditions with DTT, another band 1.3 appears on the lower molecular weight scale and can be assigned to the characteristic molecular weight of the streptavidin monomer at about 13 kDa. This

band is reflected as the only significant in trace two (band 2.1) in which the denatured sample of native SAV was run, which supports the assumption that the bands 1.3 and 2.1 show a monomer of SAV. In comparison to that, the analyzed peptide conjugates of SAV were expected to show a higher molecular weight as the reference, since four equivalents of biotinylated peptides were assembled to them. Considering the third trace shown in Figure 47, in which the non-denatured SAV-EK1 hybrid was applied, protein aggregates (or contaminations) were observed at around 90 kDa (band 3.1). As already discussed, this could have been caused by the non-buffering conditions of the sample solution and is expected to disappear under denaturing conditions. This is apparent from the fourth trace of the gel, which is not showing such bands. Although band 3.1 is present, it only shows low intensity compared to the other main band 3.1, which is shifted to around 53 kDa of the page ruler and thus is expected to be related to the tetrameric form of the hybrid. Since the mentioned stained protein is running in parallel to the native SAV (band 1.2) the expected mass shift to higher molecular weight could not be detected, which could have been due to the low resolution of the method and the increased thickness of the band 3.2 compared to 1.2.

Trace four shows the denatured sample of SAV-EK1. It can be taken from Figure 47, that not all of the tetrameric proteins could be denatured, since band 4.1 runs in parallel to 3.2, representing tetrameric protein hybrid. Nevertheless, the expected mass of monomeric SAV at about 13 kDa can be seen as the main band 4.2, running in parallel to the monomer of native SAV (band 2.1). The last band shown in this trace (4.3) is localized below the lowest page ruler mass at 11 kDa and therefore can be expected to own a molecular weight of about 4 kDa. This characteristic band can be assigned to the biotinylated EK1 peptide, which proves the presence of it in the purified protein sample.

It is important to mention, that trace three does not show any low molecular weight bands, which means, that biotinylated EK1 most likely is assembled to SAV, not being freely present in the sample solution, so DTT addition is required to liberate the peptide from SAV. This shows, that the SAV-EK1 hybrid is free from unbound EK1 (see lower green box in Figure 47).

The last two traces on the left of the page ruler are showing the applied samples of SAV-VIRIP hybrid. It becomes clear to see, that the non-denatured sample shows a band of higher molecular weight aggregates as well (band 5.1), like discussed for the

other traces, but these impurities disappear when going to the denaturized sample. Band 5.2 runs significantly lower than the band 3.2, approximately at around 50 kDa, indicating, that the VIRIP assembly owns the expected mass shift that was expected for the tetrameric protein in comparison to SAV-EK1, since VIRIP has a lower molecular weight than EK1. The shift between the masses is highlighted by the upper green box in Figure 47. Switching to the denatured sample of VRIP-SAV, it can be seen that the tetrameric protein has almost disappeared, making the denaturization with DTT appear to have been successful. Only a slight amount of tetrameric SAV can be seen (band 6.1), whereas the most likely monomeric form of streptavidin can be assigned to the main band 6.2, running in parallel with the previously discussed bands 2.1 and 4.2. It stands out, that in contrast to trace four, no free peptide could be detected. This is most likely due to the fact, that VIRIP is significantly smaller than EK1 and cannot be detected by silver stain. In addition to that, it also could have been that VIRIP was running out of the gel during electrophoresis or washed out during staining process. Nevertheless, further investigations have to be done to ensure that VIRIP is definitely bound to streptavidin, even though the bounding has been proven by HABA assay (see Graph 1).

Taking into account the previously discussed analysis of the multimerization of biotinylated peptides to streptavidin, it can be said, that the assemblies were successful and the SAV-EK1 construct is pure, since no free peptide could be detected in the native sample.

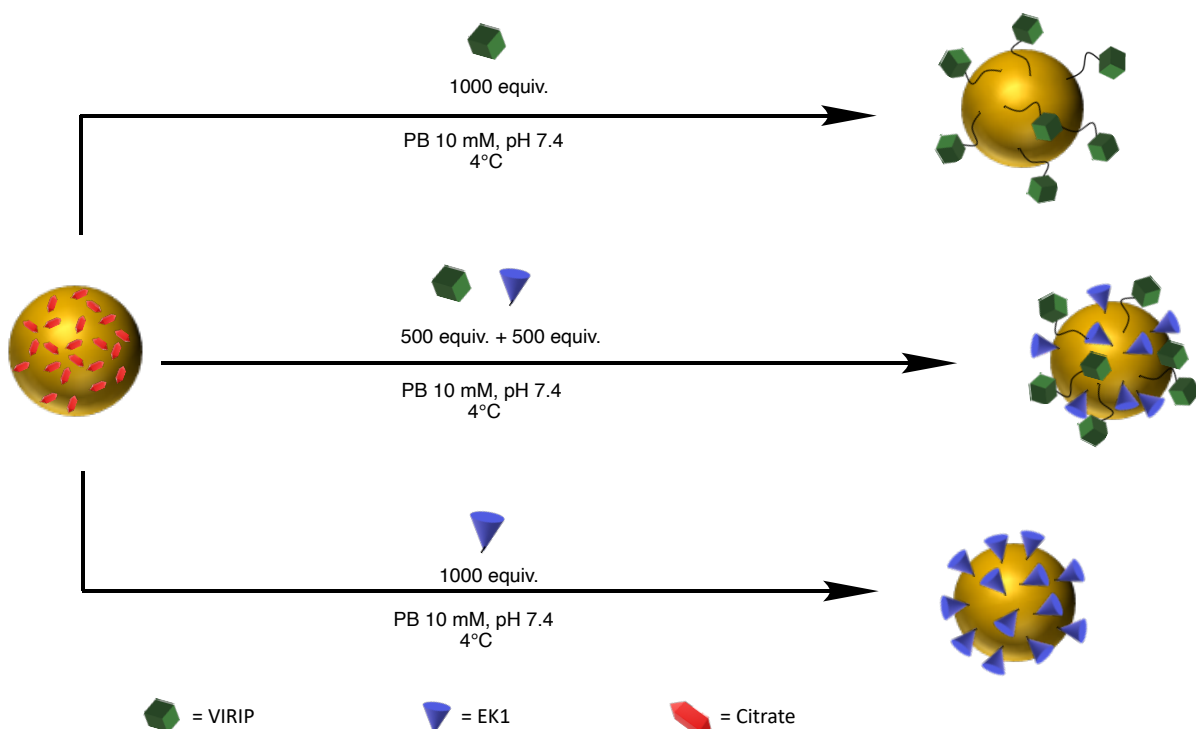
To investigate the antiviral activity of the constructs, samples of each protein solution were sent to collaboration partners at the institute for virology in the university medical center in Ulm. If *in vitro* cell culture studies will show promising results concerning the antiviral potential of the protein hybrids, it will be tried to assemble the biotinylated peptides to neutravidin (see section 1.3.1).

3.4 Assembly of antiviral peptides to citrate stabilized gold nanoparticles

To compare the biotin/streptavidin system for peptide assemblies with another multimerization platform gold nanoparticles (GNP) with an average diameter of 5 nm were chosen. As described in chapter 1.2.2, gold nanoparticles are able to undergo ligand exchange reactions in which a formerly stabilizing ligand on the surface of the particle is replaced by a thiol containing molecule under formation of a very stable sulfur-gold bond^[21]. This principle was used for the coating of gold nanoparticles with the already mentioned antiviral peptides EK1 and VIRIP, since both of them contain a thiol residue in form of a cysteine. After the coating and characterization of the particles, as described in this chapter, the nano constructs will be investigated for their antiviral activity against SARS-CoV-2 and HIV *in vitro* by collaboration partners at the department for virology at the university medical center in Ulm.

3.4.1 Assembly of EK1 and VIRIP to 5 nm gold nanoparticles

The GNPs used in this work were commercially available and shipped suspended in citrate buffer to stabilize the particles. To compare the multimerization effect of both peptides, EK1 and VIRIP were each assembled to GNPs alone and in a stoichiometric



Scheme 25: General reaction equation of the performed ligand exchange reaction of citrate stabilized gold nanoparticles (diameter 5 nm) with antiviral peptides VIRIP and EK1.

mixture together. The general reaction scheme of the performed ligand exchange reactions is shown in Scheme 25.

The coating of GNPs was performed after a protocol of *Budhadev et al. (2020)*^[60] with slight modifications. To prevent the coated nanoparticles from aggregation, it was necessary to buffer the reaction solution at a pH above the isoelectric point of the peptides which is around 4 for VIRIP and EK1 according to the manufacturer analysis protocol. Since the presence of concentrated salts could interfere the reaction, phosphate buffer with 10 mM molarity at a pH of 7.4 was chosen. In advance of the actual reaction procedure, gold nanoparticles were spun down in ultracentrifugation tubes to remove excess of citrate buffer and resuspended in PB in which the defined amount of peptides were dissolved. To prevent aggregations of the suspended particles, the reaction was carried out at 4 °C overnight. Afterwards the nanoparticles were purified via ultracentrifugation and resuspended in 10 mM PB at pH 7.4 and stored at 4 °C.

To determine the number of peptides per particle, the concentration of the peptide solutions before the reaction and after the purification was determined in the excess solution of the purification via Nanodrop absorption measurements at 214 nm. On the basis of this analysis, it was calculated, that on every particle 100 to 200 peptides could be assembled. To further characterize the particles, SDS PAGE, agarose gel, UV-vis spectra, TEM imaging and DLS studies were performed.

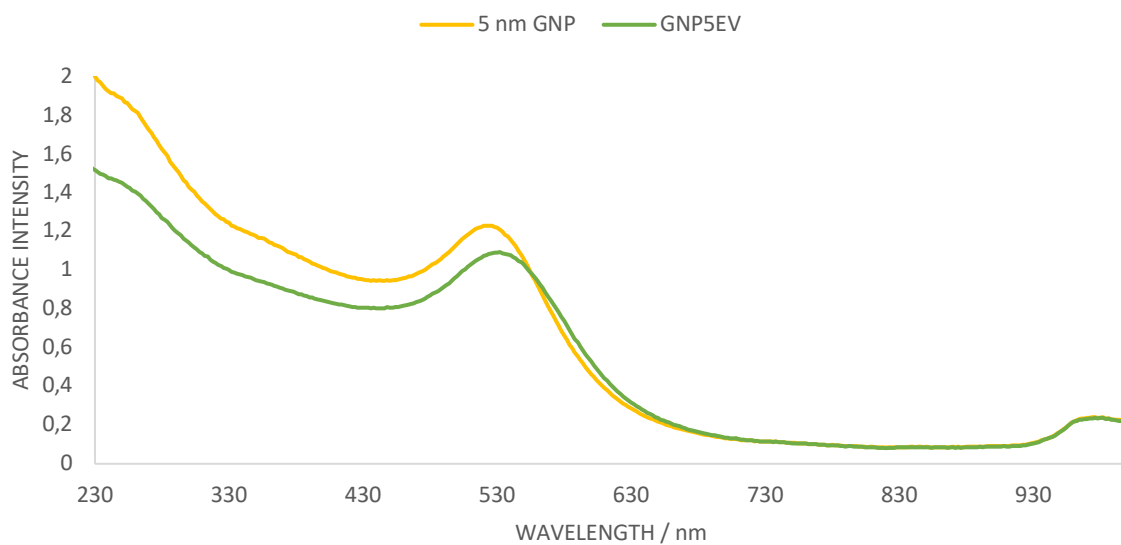
3.4.2 Characterization of peptide coated gold nanoparticles

To analyze the characteristics of the previously obtained gold nanoparticles it was necessary to perform different measurements. As many coated particles show a different surface charge status than the starting material, one could consider measuring zeta potential of the peptide coated GNPs synthesized in this work, but EK1 and VIRIP show an isoelectric point that is similar to the one of the stabilizing ligand citrate, making the method unsuitable for GNP characterization. Since in literature many nanoparticles are characterized via absorbance measurements, UV-vis spectra were obtained, as shown in Graph 2.

Graph 2 shows the results of the measured UV-vis spectra with the example of GNPs that were coated with VIRIP and EK1 in stoichiometric mixture. As it can be seen in the graph, that compared to the untreated gold nanoparticles only small differences in the absorbance spectrum occur. The absorbance maximum of the peptide coated

particles between 400 and 500 nm is only slightly shifted to longer wavelengths, which could be an evidence for a slight shift of the GNPs surface plasmon resonance, but do not show additional bands, as it could have been expected. This may be caused by the fact, that the nanoparticles themselves absorb in significantly higher intensity than the peptides, thus they cover the characteristic peptide absorbances, for example at 254 nm for aromatic amino acid residues.

ABSORBANCE SPECTRUM GOLD NANOPARTICLE VS. PEPTIDE COATED PARTICLE

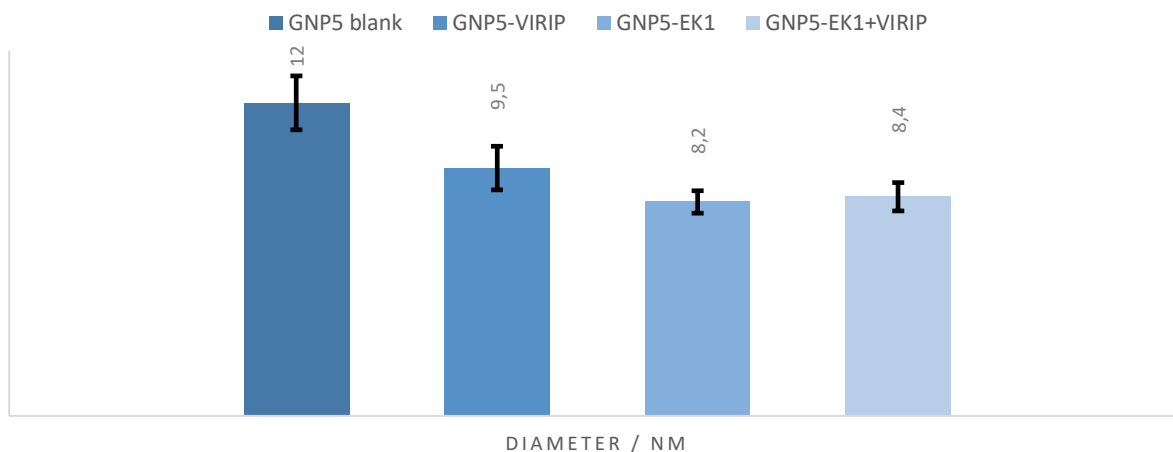


Graph 2: Results of the UV-vis measurement of EK1 and VIRIP coated gold nanoparticle in comparison to citrate stabilized GNP. Spectra were measured in a Tecan spark plate reader.

Thus, further analysis was required. As a next method, the obtained GNPs were characterized via DLS measurements, to determine a potential change in hydrodynamic radius of the particles. The following Graph 3 shows the results of the measurement.

Taking into account the significantly greater size of the used peptides in comparison to the stabilizing citrate ligands, it was expected that by coating GNPs with peptides, the particle's hydrodynamic radius would significantly increase. When analyzing the results of the DLS measurements shown in Graph 3, the reverse effect was observed: The modified GNPs show a decrease in diameter compared to the citrate stabilized blank gold nanoparticles. A plausible explanation is due to the different ligand-GNP interaction involved. Whereas the citrate interaction with GNPs is more of an

DLS MEASUREMENTS OF MODIFIED GNPs



Graph 3: Multi angle DLS measurement results of peptide coated GNPs in comparison to unmodified GNPs. Measurements were performed by Christine Rosenauer.

electrostatic or ionic manner, the peptides built up more covalent sulphur gold interaction, causing the particle coating shell to become denser and therefore lowering the hydrodynamic radius. Another explanation for the diameter decrease could have been, that most likely more citrate ligands were stabilizing the GNP than peptides do

after the exchange reaction. A greater count of citrates on the particle could have increased the repulsion between the single molecules, as a result a more voluminous shell around the particle was formed. Lastly, citrate molecules are much more soluble in water than VIRIP and EK1 are, thus they will complex more water molecules in a three-dimensional hydration sheath.

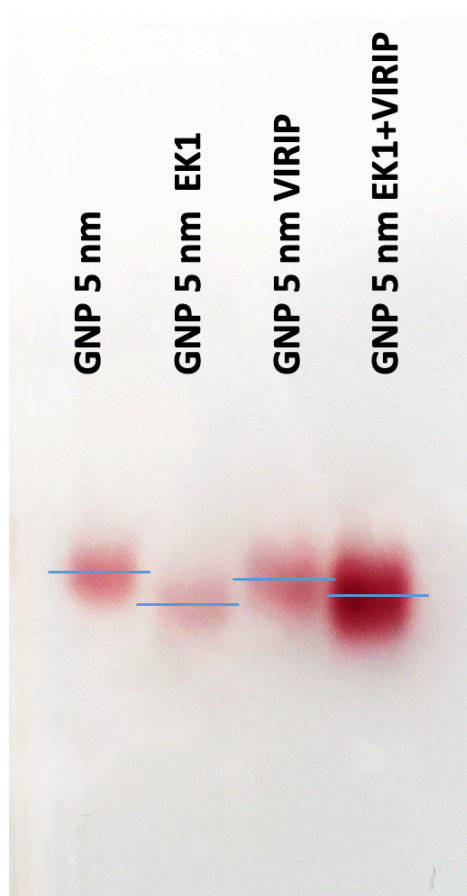


Figure 48: Results of the agarose gel electrophoresis of different GNP samples. Electrophoresis was performed using an 0.7% agarose gel in TAE running buffer at 50 V.

To further corroborate the successful coating of the GNPs with peptides, they were characterized via agarose gel electrophoresis to check on potential shifts in gel localization. Figure 48 shows the results of the separation. The figure clearly shows a shift between the different GNP samples. Whereas the EK1 containing GNPs are running below the citrate stabilized GNPs, the VIRIP coated particles are only slightly shifted below the reference and the combination of both peptides on one particle is centered between the two other peptide GNP bands. It is important to mention, that the band of

the GNPs coated with both peptides is much more intense compared to the other ones. This leads to the assumption that the applied number of particles was higher than the other ones and therefore appears broaden in the gel. While it gives a hint of the success of the assembly, the analysis should be repeated where the applied amount of sample to the other sample traces should be adapted. Since it has been found that EK1 can be detected in an SDS PAGE via silver staining (see section 3.3.3, page 59), this electrophoresis was suggested to enable the proof of peptides being attached to the particles. Figure 49 shows the result of an SDS PAGE of EK1 alone, EK1 mixed with GNPs one the one trace freshly mixed and on the other purified and GNPs alone. As it can be seen on the left side of Figure 49, the unstained gel shows traces of gold nanoparticles where they have been applied to the gel. It is important to mention, that traces which include gold nanoparticles and peptide show GNP bands that are blurry

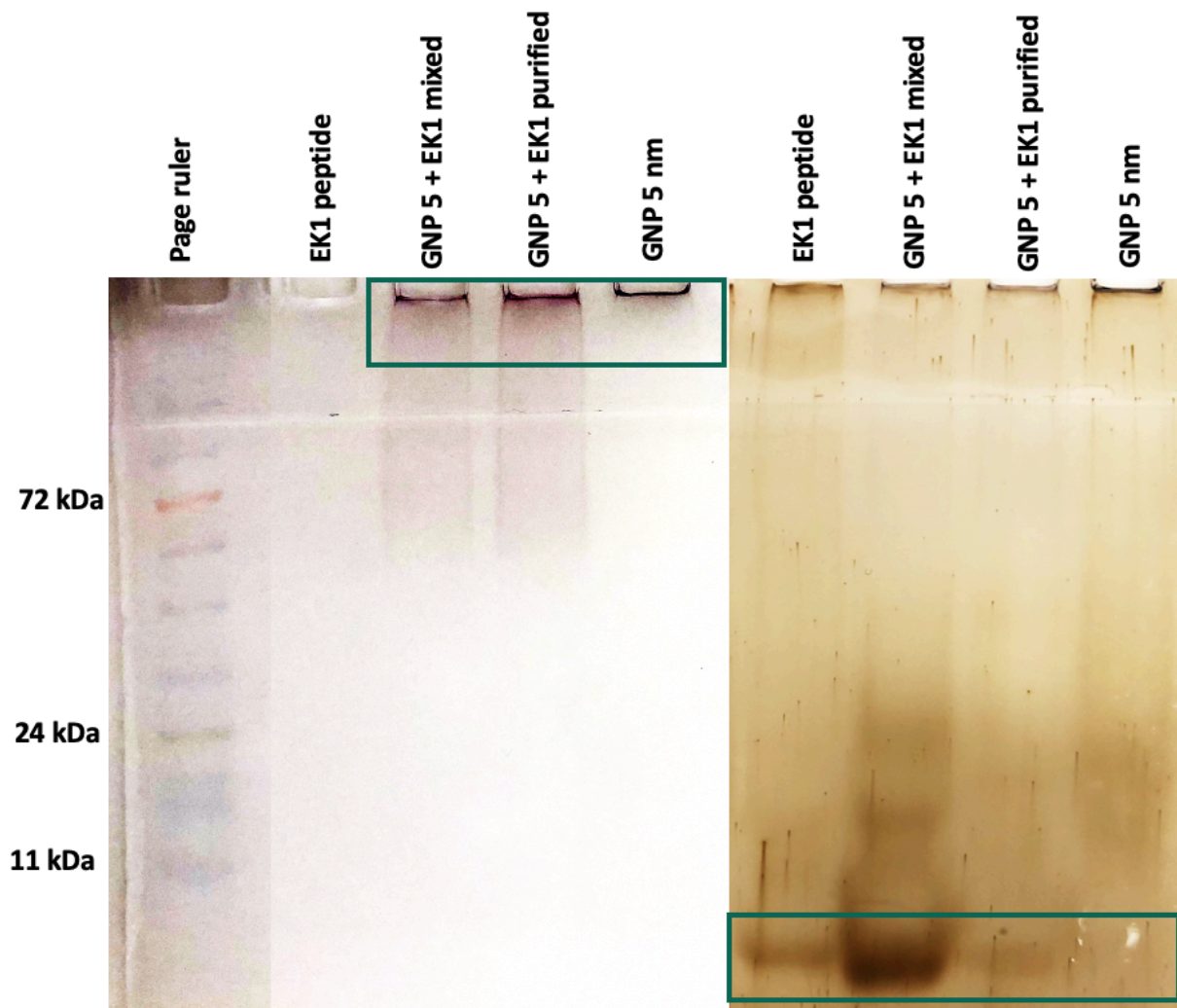


Figure 49: SDS PAGE analysis of EK1 coated GNPs. Purified EK1-GNP was monitored in comparison to freshly mixed GNP with EK1 and EK1 respectively GNP alone. Electrophoresis was performed in MES running buffer at 130 V. After capturing the unstained gel (left side), EK1 was visualized with silver stain to investigate its presence on the particles (right side).

running into the gel whereas unmodified GNPs stick on top of the gel. This could be explained by the covalent attachment of peptides, which are dragging the fairly bigger gold nanoparticles with them into the gel. In contrast to that, the stabilizing citrate on the blank GNPs are not covalently bound to the particle, therefore will most likely run out of the gel with the solvent front and will be washed out during staining process.

The silver-stained picture of the gel on the right side of Figure 49 was expected to show EK1 peptide below the lowest marker band at 11 kDa. This appears to be the case for every trace that included the peptide. It becomes clear to see, that the trace on which the fresh peptide GNP mixture was applied includes large excess of EK1, displayed by the intense band running in parallel to the EK1 reference on the left of it. In comparison to the discussed band, the trace of the purified EK1-GNP does not show such a significant band at the height of EK1, which leads to the assumption that excess peptide could be successfully removed from the mixture. Nevertheless, a characteristic EK1 band can be observed in the trace. This could on the one hand be caused by peptide which has been previously bound to GNPs but has been cleaved off during electrophoresis for example by SDS, for which the missing bands of EK1 in the higher molecular weight range on the GNPs dragged into the gel gives evidence. On the other hand, the EK1 band could also have been caused by traces of unbound peptide in the solution, which was not possible to remove, but this appears unlikely, since a high MWCO was used for ultracentrifugation and several washing steps were performed. Since the detection range of silver stain is about 5 ng of material and GNPs own a significantly higher molecular weight, it is also possible that peptide bound to the GNPs was below the staining detection range. The presence of unbound EK1 in the purified solution remains unclear and has to be further investigated.

In combination with the observations made on the agarose gel, the assembly of the peptides to GNPs was successful, which was shown by the different shifts of the particles in the agarose gel and different electrophoretic behavior of the particles compared to unmodified gold nanoparticles in the SDS gel.

To investigate potential differences in shape of the particles, TEM imaging was performed. For the measurements, samples of the particles were rebuffered in ultrapure water and transferred onto a standard copper grid without plasma coating. To investigate the possibility of visualizing a peptide corona on the particles, the sample which included GNPs with EK1 was stained with uranyl acetate. The results of the microscopy studies are shown in the following figure.

From Figure 50, it is that almost all samples showed aggregation during the preparation procedure, which could be caused by the hydrophobic surface of the grid on which the hydrophilic samples were transferred. Only the sample of the VIRIP

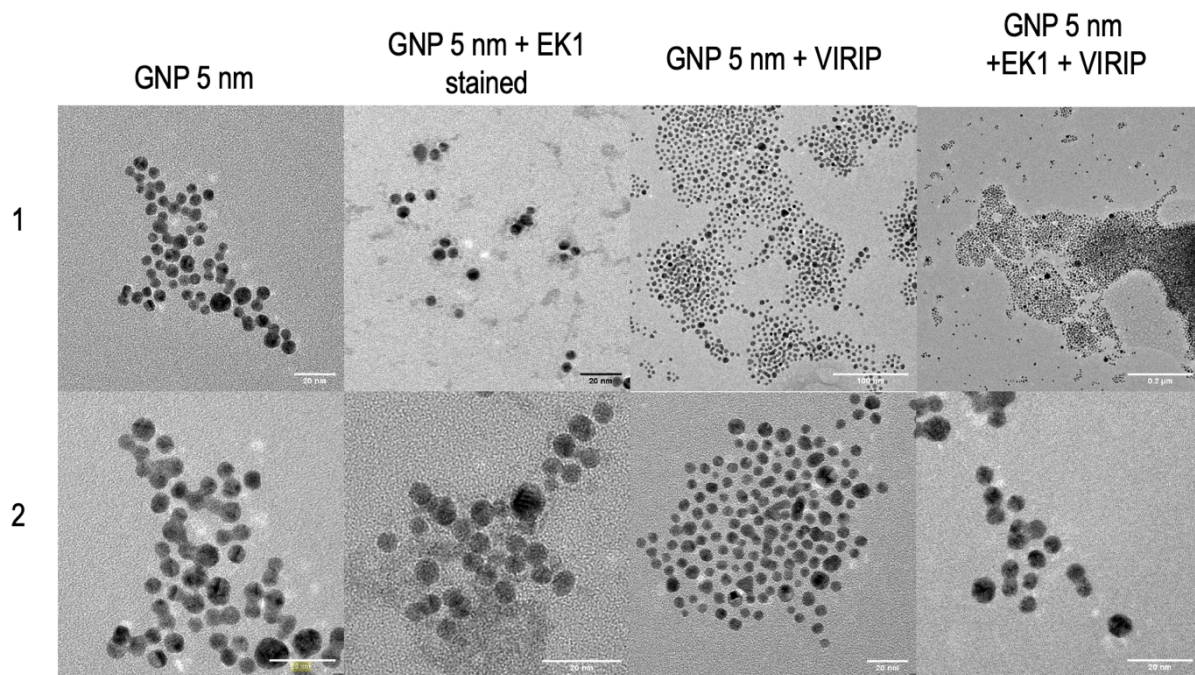


Figure 50: TEM images of the different peptide coated gold nanoparticles in comparison to unmodified GNPs. The sample of GNP coated with EK1 was stained with uranyl acetate. All samples were measured on an uncoated copper grid. Measurement was performed by Jiaxu Liang.

coated GNPs shows less aggregation which implies that that since VIRIP contains many hydrophobic amino acids, it prevents the particles from aggregating on the grid. Nevertheless, if the measurements should be repeated the usage of a plasma coated grid would be necessary to prevent aggregation of the samples.

Besides the discussed aggregation behavior, it can be seen that the shape of the particles remains unchanged compared to the uncoated nanoparticles. Despite attempts to stain one of the samples with uranyl acetate, no peptide corona was observed. This is due the high contrast of the gold nanoparticles, which will suppress the weak peptides signal. To further prove the presence of peptides on the gold nanoparticles surface future studies could investigate the fluorescence quenching effect of GNPs in combination with fluorescent labeled peptides.

Summarizing the GNP preparation and characterizations discussed in this chapter, there is evidence for a successful coating of gold nanoparticles with a diameter of 5 nm with the antiviral peptides EK1 and VIRIP. Nevertheless, further characterization methods could be tested, such as surface plasmon resonance, to improve the understanding of the obtained nanostructures.

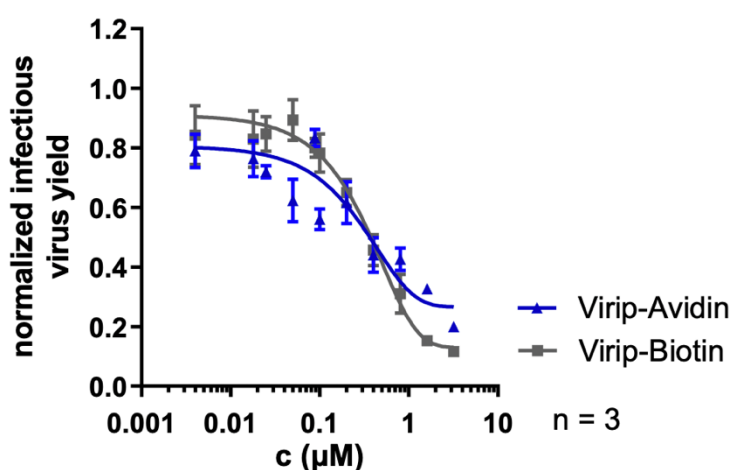
To investigate the antiviral activity of different peptide coated gold nanoparticles, samples of the nanoplatforms described in this chapter were sent to collaboration partners at the department of virology at the university medical center in Ulm.

3.5 *In vitro* studies on antiviral activity of multimerized antiviral peptides

The peptide nanoplateforms prepared and discussed in chapter 3.3 and 3.4 were further investigated for their antiviral activity against SARS-CoV-2 and HIV infectivity, in collaboration with the group of Prof. Dr. Frank Kirchhoff at the university medical center in Ulm. To date, the results for *in vitro* testing of EK1 functionalized streptavidin and VIRIP functionalized avidin hybrids are obtained and will be discussed in this chapter. All experiments in this chapter were performed by Fabian Zech, PhD student in the group of Prof. Dr. Kirchhoff and all of the following data were shown with permission from the collaboration partner.

3.5.1 Antiviral activity of streptavidin-based peptide constructs

To investigate the effect of biotinylation of EK1 and VIRIP and their multimerization of avidin-like proteins on their antiviral activity, Calu3 cells for SARS-CoV2 respectively TZM-bl reporter cells for HIV were used, since Calu3 is a lung carcinoma cell line which expresses the SARS-coreceptor ACE2^[61] and TZM-bl reporter cells express the HIV-coreceptors CXCR4 and CCR5^[62]. The cultured cells were treated with the respective protein hybrid or a negative control in different concentrations. Afterwards, the cells were infected with HIV or SARS-CoV-2. After two days of incubation, cells were harvested and characterized concerning their viral infection rate via flow cytometry analysis (SARS-CoV-2) or β -Galactosidase assay (HIV).



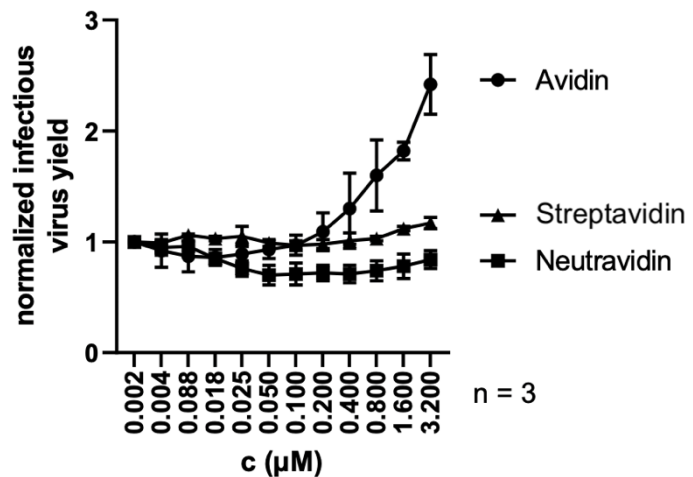
Graph 4: Normalized HIV infection rate of TZM-bl cells under treatment of either biotinylated VIRIP or biotinylated VIRIP multimerized on avidin in dependence of the used substance concentration of antiviral peptide in μM . Biotinylated VIRIP and corresponding avidin hybrids were synthesized by Astrid Heck, experiment and measurement was performed by Fabian Zech as part of his PhD thesis.

For biotinylated VIRIP, the effect of multimerization on different avidin-like proteins concerning the peptide's antiviral activity against HIV was investigated.

Previous studies with VIRIP being assembled on avidin showed an increased HIV infectivity of the protein construct in comparison with non-conjugated, biotinylated VIRIP, as shown in Graph 4.

The results lead to the assumption, that the avidin platform had an influence on the virus blocking efficiency, thus the investigation of the influence avidin like proteins have on viral infectivity appeared to be necessary. This was performed by comparison of avidin, streptavidin and neutravidin concerning their influence on HIV infectivity without being modified with any functional peptide in a dose dependent manner.

The results of this experiment are shown in Graph 5. As it can be obtained from the experimental results, only avidin shows a significant influence on HIV infectivity in the *in vitro* model. Streptavidin and neutravidin do not show an impact on the viral reproduction up to concentrations above 3 μM , whereas avidin is able to increase the virus yield up to two to three times of the normalized

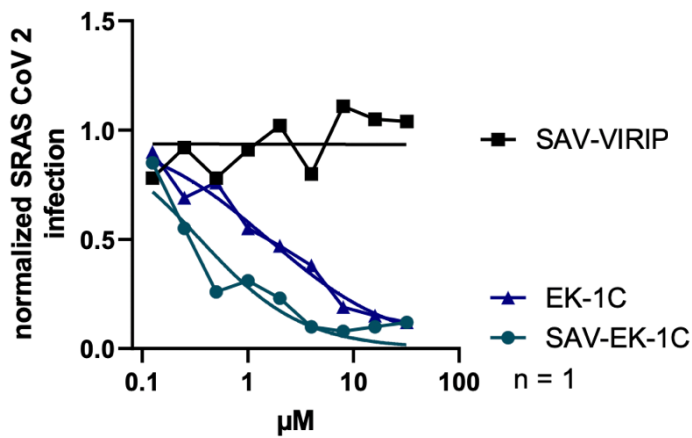


Graph 5: Normalized HIV infection rate of cultured TZM-bl cells under treatment of either avidin, streptavidin or neutravidin in dependence of the used substance concentration of protein in μM . Experiment and measurement was performed by Fabian Zech as part of his PhD thesis.

value. One reason for this difference compared to other ALPs could be the glycosylation pattern of avidin, that is differing from the one of streptavidin, which is expressed in bacteria or neutravidin, which is not glycosylated at all. Taking into account the sample size of three measurements and the low standard deviation, it can be concluded, that streptavidin or neutravidin should be used as multimerization platforms for antiviral peptides to enable the highest antiviral activity, as it was done in this project.

For tetramerized EK1 on streptavidin, which was synthesized and described in this thesis, the results of the infectivity studies are shown in Graph 6. The concentrations of applied peptide (-hybrid) refers to the overall concentration of antiviral peptide, which means that the respective protein concentration is only 25% as high as the given concentration on the horizontal axis. Both EK1-containing samples lower the infection rate of the treated cells in a dose dependent manner, whereas the negative control, represented by VIRIP functionalized streptavidin does not have any influence on the SARS-CoV-2 infection rate. From the regression curves of the EK1 containing

samples, it can be seen that EK1 which was biotinylated and assembled on streptavidin shows a similar antiviral effect compared to the unmodified peptide and



Graph 6: Normalized SARS-CoV-2 infection of Calu3 cells under treatment of either unmodified EK1C, EK1C multimerized on streptavidin or streptavidin carrying VIRIP as a negative control in dependence of the used substance amount of antiviral peptide in µM. Experiment and measurement was performed by Fabian Zech as part of his PhD thesis.

therefore proves the preserved bioactivity, which makes the multimerization approach on avidin-like proteins a promising tool for enhanced antiviral treatment. As this is a quick screening with one experiment (n = 1) per concentration, statistical analysis is not possible. Nevertheless, the assembly of four copies of EK1 on

streptavidin appears to have a multivalency effect and the initial results appear promising. Therefore, it is essential to repeat the experiment to ensure reproducibility and at the same time, the serum stability should also be investigated to determine if the half-life of the peptides can be improved using the nanoplatform approach developed in this thesis.

4. Conclusion and outlook

The overall goal of the described work was the development of multivalent nanoplatforms, which were functionalized with antiviral peptides to allow treatment and diagnosis of diseases that are caused by HIV and SARS-CoV-2 infections.

As a first multimerization platform the system of avidin-like proteins, *i.e.* streptavidin, was investigated. To allow the assembly of antiviral peptides on the protein, it was necessary to introduce a biotin functionality to the bioactive molecule. A trifunctional linker molecule was synthesized in four steps to enable the conjugation of two different antiviral peptides on one biotin unit and allows subsequent assembly of four equivalents of each bioactive molecule on one streptavidin. The final molecule contained a biotin unit and two thiol reactive moieties: with a maleimide on the one side and an alkyne group on the other side. Notably, the alkyne group is also able to react in cycloadditions.

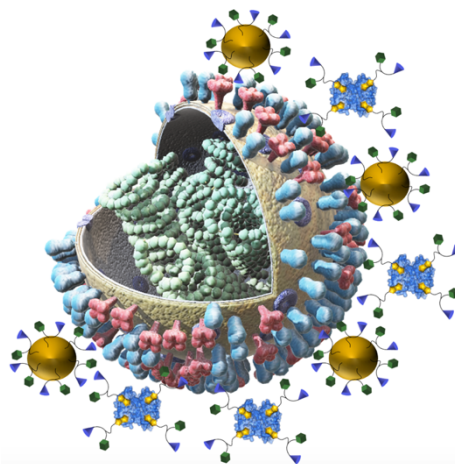


Figure 51: Schematic drawing of potential interactions between peptide coated gold nanoparticles and peptides multimerized on avidin-like proteins with a targeted virus, such as SARS-CoV-2.

As a next step, the chosen antiviral peptides were successfully conjugated to bivalent biotin linker molecules in a thiol-selective Michael addition to allow the investigation of each peptide on streptavidin alone. Furthermore, the same peptides were conjugated to the previously gained trifunctional linker molecule in a chemo-selective approach. The first conjugation step of one peptide on the maleimide group was successful with moderate to good yield of product. The second peptide conjugation reaction was realized by azide-alkyne cycloaddition on the propargyl group but with low yield. Further optimization of this reaction step is required. To investigate the possibility of directly conjugating the second peptide to the linker construct via a photoinitiated thiol-yne click reaction, test reactions of short thiol containing peptides with different alkynes were performed. The results of this investigation showed that the proposed synthetic approach is viable, but will need further optimizations, mainly in the reduction of steric hindrance. In conclusion, the developed system shows great potential for the trifunctional merge of different bioactive moieties.

The biotinylated peptides were tested afterwards for their binding properties to streptavidin, to exclude the potential reduction in multimerization efficiency. All tested biotinylated samples have shown similar binding properties in comparison to the native ligand biotin. As a result, biotinylated antiviral peptides were successfully assembled on streptavidin and characterized via SDS PAGE. The purified protein hybrids were investigated for antiviral activity *in vitro*. EK1 multimerized on streptavidin shows similar antiviral activity compared to the unmodified peptide and a multivalency effect, making it a promising approach for further studies for the assembly of two different antiviral peptides on one avidin-like protein. In addition to that, neutravidin can also be used as a multimerization platform, as it has no significant influence on the host cell infectivity in contrast to avidin.

The second multimerization platform was citrate stabilized gold nanoparticles with a diameter of five nanometers, which were able to undergo ligand exchange reaction in the presence of thiol-containing ligands. With this approach, it was possible to coat the particles with two different antiviral peptides, which contained a cysteine residue for sulphur-gold interactions. Each peptide was multimerized on the particle alone and in stoichiometric mixture with the respectively other peptide. The obtained peptide-Au hybrid nanoplatfoms were characterized via different gel electrophoreses, DLS, UV-vis and TEM measurements. The purified peptide-coated gold nanoparticles were sent to collaboration partners for investigation of antiviral activity *in vitro*.

Overall, two supramolecular platforms were functionalized with two different antiviral peptides against HIV and SARS-CoV-2 and successfully characterized in this thesis. Preliminary results of *in vitro* testing demonstrated that multimerization of antiviral peptides is a promising tool for potential combinatory treatment of viral infections and the optimization of these systems holds great potential for targeted inhibition of HIV and SARS-CoV-2.

5.Experimental Section

5.1 Instruments and Materials

Unless otherwise stated, all chemicals and materials required for synthesis and analysis were sourced from the following commercial providers.

SIGMA-ALDRICH (Sigma-Aldrich Chemie GmbH, Taufkirchen, Germany), ALFA AESAR (Alfa Aesar GmbH & Co.KG, Karlsruhe, Germany), MERCK (Merck KGaA, Darmstadt, Germany), Roth (Carl Roth GmbH + Co. KG, Karlsruhe, Germany), SIGMA-ALDRICH (Sigma-Aldrich Chemie GmbH, Taufkirchen, Germany), Thermo Fisher (Thermo Fisher Scientific Inc., Waltham, USA), VWR-Chemicals (VWR International GmbH, Darmstadt, Germany).

High-Performance liquid chromatography (HPLC)

Semi preparative HPLC analysis and purification was performed using an Eclipse XDB-C18 column (100 Å, 4.6 x 150 mm, 5 µm ø) or a Phenomenex Jupiter® C18 column (300 Å, 4.6 x 150 mm, 5 µm ø).

Preparative HPLC analysis was performed by using a Phenomenex Kinetex® EVO C18 (100 Å, 150 x 30 mm, 5 µm ø).

Mobile phase was composed from ultrapure Millipore H₂O (solvent A) and ACN (solvent B) including 0.1% of trifluoro acetic acid.

Liquid chromatography and mass spectrometry (LC-MS)

LC-MS analysis was performed using a Shimadzu LC-MS-2020 (Shimadzu Deutschland GmbH, Duisburg, Germany) in combination with a Kinetex® EVO C18 (50 x 2.1 mm, 2.6 µm) column. Mobile phase was composed from ultrapure Millipore H₂O (solvent A) and ACN (solvent B) including 0.1% of formic acid. Sample preparation was performed by dissolving material in ultrapure water to obtain a final concentration of 50 µg/mL.

Lyophilization

For freeze drying a CHRIST Alpha 2-4 LD plus freeze dryer (Martin Christ Gefriertrocknungsanlagen GmbH, Osterode am Harz, Germany) was used. The material was frozen in liquid nitrogen in advance of the lyophilization process.

Nuclear magnetic resonance Spectroscopy (NMR)

¹H-NMR spectra were obtained from a BRUKER 300, 500 or 700 MHz spectrometer (Bruker Corporation, Billerica, USA). ¹³C-NMR- and 2D-spectra were obtained from a BRUKER 500 or 700 MHz spectrometer (Bruker Corporation, Billerica, USA). Samples were dissolved in deuterated solvents methanol (MeOD) or D₂O. Magnetic shifts of the measured samples were given in ppm, the signals coupling constants *J* were given in Hertz (Hz).

MALDI-TOF measurements

MALDI-TOF analysis was performed using a BRUKER rapifleX® MALDI-TOF (Bruker Corporation, Billerica, USA) or a Synapt (Waters corporation, Milford, USA) system. Matrix embedment was performed using CHCA or SA as matrixes.

5.2 Frequently practiced Methods

Agarose gel electrophoresis

Agarose gel electrophoresis was performed by dissolving 0.7% agarose in TAE buffer. Solutions were loaded to an agarose-mold for solidification. Afterwards the gel was transferred to an agarose gel electrophoresis tank, covered with 1x TAE buffer and loaded with glycerol mixed samples. Electrophoresis was performed at 50 V with ice pack cooling.

HABA – Assay

To determine the required equivalents biotinylated peptides for SAV saturation, 2-((4'-hydroxyphenyl)-azo) benzoic acid (HABA) was used. One equivalent of streptavidin was mixed each with one to five equiv. of biotin units to a final concentration of 1 mg/mL in phosphate buffer (50 mM, pH 7.4).

Triplets of each sample (48 μ L) were introduced to a flat-bottomed transparent 384-well plate (UV-star®, Greiner Bio-one GmbH, Frickenhausen, Germany). Afterwards 8 μ l of a saturated HABA solution in ultrapure Millipore water was added to each well. Sample absorbance was measured at 500 nm in a Tecan Spark 20M microplate reader (Tecan Trading AG, Männedorf, Switzerland).

Polyacrylamide gel electrophoresis (PAGE)

Polyacrylamide gel electrophoresis (PAGE) was performed using 10% SDS separating gels topped with 6% SDS stacking gels. Gel compositions for two gels are listed below.

Table 1: Composition chart of SDS PAGE gels. Recipe yields two gels.

| Component | 10% separating gel | 6 % stacking gel |
|-------------------------|--------------------|------------------|
| MilliQ H ₂ O | 10 ml | 6 ml |
| Acrylamide (40%) | 5 ml | 1.5 ml |
| Bis-tris buffer pH 6.5 | 5 ml | 2.5 ml |
| 10% SDS | 200 μ l | 60 μ l |
| 10% APS | 100 μ l | 50 μ l |
| TEMED | 10 μ l | 5 μ l |

The separation gel was composed as listed above and introduced into a gel mold (Bio-Rad Laboratory Inc., Hercules, USA), and covered with isopropanol for even polymerization. After 20 min, isopropanol was removed and stacking gel solution was composed as listed above. The stacking solution was layered above the separation gel, sample pockets were introduced by adding a 10 to 15 pocket comb to the stacking and the gel was left for polymerization.

SDS PAGE samples were prepared with 4x sample buffer (NuPage, Thermo Fisher Scientific Inc., Waltham, USA) and 6 μ l of 1M DTT solution in ultrapure water if denaturing conditions were required. DTT containing samples were denatured for 10 min at 95°C in a heating block. Previously obtained SDS gels were transferred into a PAGE tank and covered with 1 x MES running buffer (NuPage, Thermo Fisher Scientific Inc., Waltham, USA). After removal of the comb, samples and page ruler were loaded onto the stacking gel and electrophoresis was performed at 130 V for about 1 h.

Band visualization was performed using silver staining (Pierce™ silver stain kit, Thermo Scientific Inc., Waltham, USA) according to the manufacturer protocol.

Determination of protein or gold nanoparticle concentrations

Protein concentration determination was performed via a standard line of the respective protein or GNP of known concentration. 2 μ L of each standard solution and the sample solution of which concentration had to be determined were transferred onto the detection surface of a NanoDrop spectrophotometer (NanoDrop 2000c, Thermo Fisher Scientific Inc., Waltham, USA) and the absorption of each sample was measured at 280 nm (for proteins) or 520 nm (for GNPs).

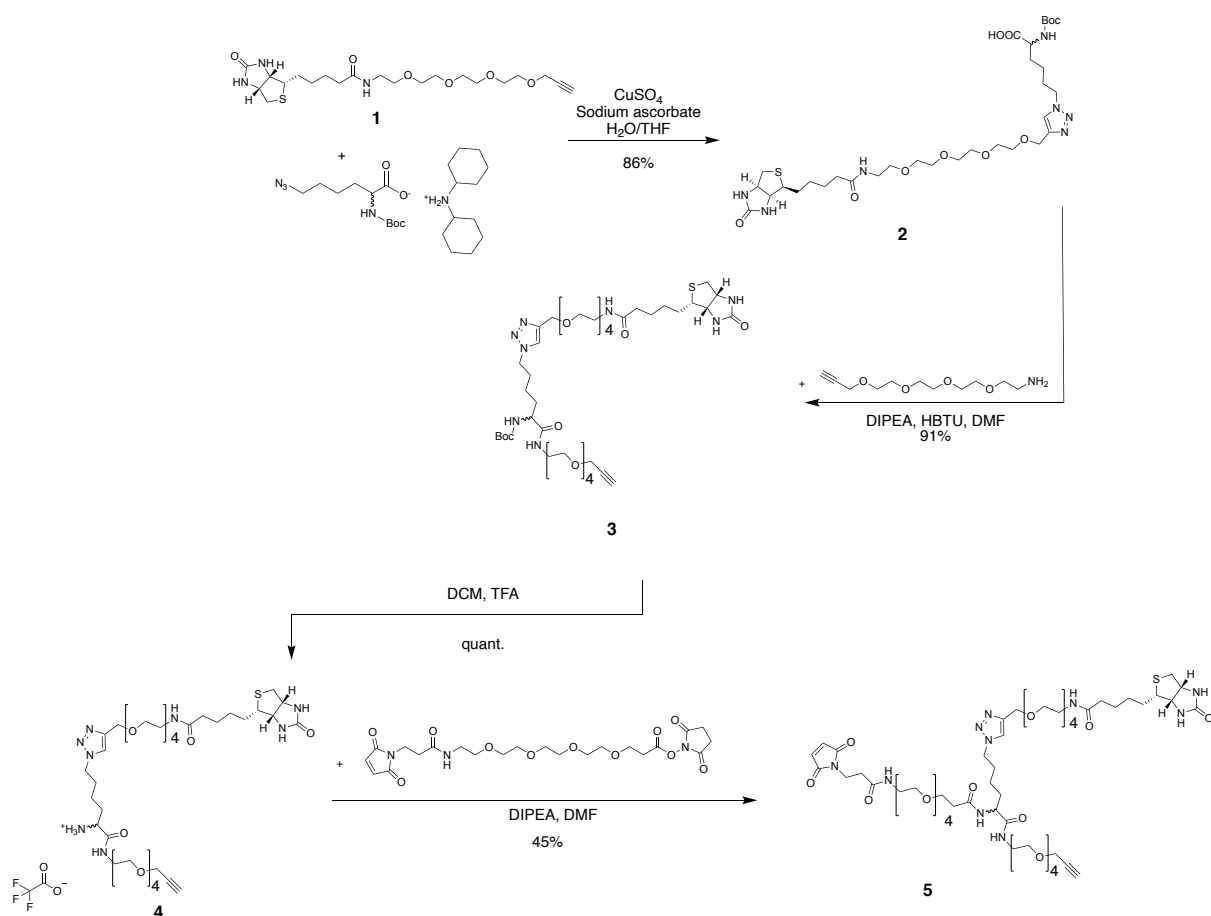
Size exclusion chromatography (SEC)

SEC was performed using Sephadex® G-10 (GE Healthcare, Buckinghamshire, United Kingdom) suspended in ultrapure water in disposable columns (5 mL) after swelling at RT for 24 h. Samples were applied on top of the column and eluted with ultrapure water. Fractions were collected in 5 mL vials and freeze dried.

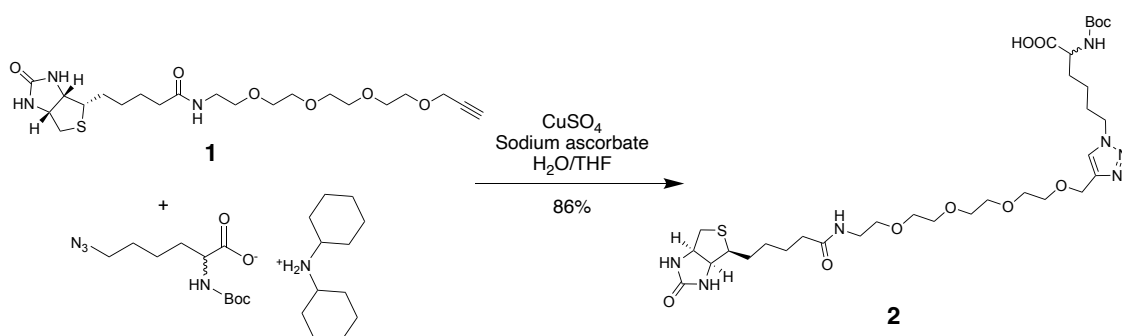
Ultrafiltration

Ultrafiltration was performed by the usage of Vivaspin® ultrafiltration tubes 500 μ l (Sartorius AG, Göttingen, Germany) or Vivaspin™ ultrafiltration tubes 6 mL (GE Healthcare Life Sciences, Buckinghamshire, GB) with a MWCO of 10 kDa or 100 kDa. Centrifugation was performed at 4 000 G for 5-10 min.

5.3 Synthesis of trifunctional linker



5.3.1 Synthesis of 2-((tert-butoxycarbonyl) amino)-6-(4-(15-oxo-19-((3aS,4S,6aR)-2-oxohexahydro-1H-thieno[3,4-d]imidazol-4-yl)-2,5,8,11-tetraoxa-14-azanonadecyl)-1H-1,2,3-triazol-1-yl) hexanoic acid (2)



The reaction was performed after a protocol of *Wang et al.* (2016)^[59]. **1** (400 mg, 1 equiv.) and *N*-*boc*-azidolysine (485 mg, 1.2 equiv.) were dissolved in 10 mL of $\text{H}_2\text{O}/\text{THF}$ 1:1. Copper sulfate (14 mg, 0.1 equiv.) and sodium ascorbate (175 mg, 1 equiv.) were dissolved in 10 mL of $\text{H}_2\text{O}/\text{THF}$ 1:1 and added stepwise to the solution. The reaction mixture stirred at RT and under argon atmosphere for 40 h. Copper sulfate was removed by precipitation as basic copper carbonate by adding saturated

NaHCO₃ solution to the mixture and filtration. The obtained copper free solution was freeze dried yielding in 552 mg (86%) of pure product **2** with respect to remaining dicyclohexyl amine and ascorbate.

¹H NMR (300 MHz, Methanol-d₄) δ 8.03 (s, 1H), 5.51 (s, 1H), 4.66 (s, 2H), 4.56 – 4.39 (m, 3H), 4.32 (dd, J = 8.0, 4.5 Hz, 1H), 4.20 (d, J = 2.6 Hz, 1H), 4.13 – 3.94 (m, 1H), 3.65 (t, J = 7.6 Hz, 18H), 3.55 (t, J = 5.5 Hz, 3H), 3.36 (t, J = 5.5 Hz, 4H), 3.28 – 3.07 (m, 2H), 3.02 – 2.83 (m, 2H), 2.72 (d, J = 12.7 Hz, 1H), 2.23 (t, J = 7.3 Hz, 2H), 1.96 (t, J = 8.0 Hz, 3H), 1.82 – 1.47 (m, 9H), 1.45 (s, 9H).

¹³C NMR (75 MHz, Methanol-d₄) δ 176.16, 166.10, 145.81, 125.24, 71.55, 71.27, 70.86, 70.58, 70.12, 64.90, 63.41, 61.68, 59.06, 57.01, 54.85, 54.65, 52.65, 52.61, 52.53, 51.32, 41.07, 40.39, 36.74, 32.19, 30.80, 29.77, 29.51, 28.76, 26.87, 25.48, 23.92.

5.3.2 Synthesis of tert-butyl (17-oxo-22-(4-(15-oxo-19-((3a*S*,4*S*,6a*R*)-2-oxohexahydro-1*H*-thieno[3,4-*d*]imidazol-4-yl)-2,5,8,11-tetraoxa-14-azanonadecyl)-1*H*-1,2,3-triazol-1-yl)-4,7,10,13-tetraoxa-16-azadocos-1-yn-18-yl)carbamate (**3**)



The reaction was performed after a protocol of *Mackiewicz et al.* (2014)^[63] with slight modifications.

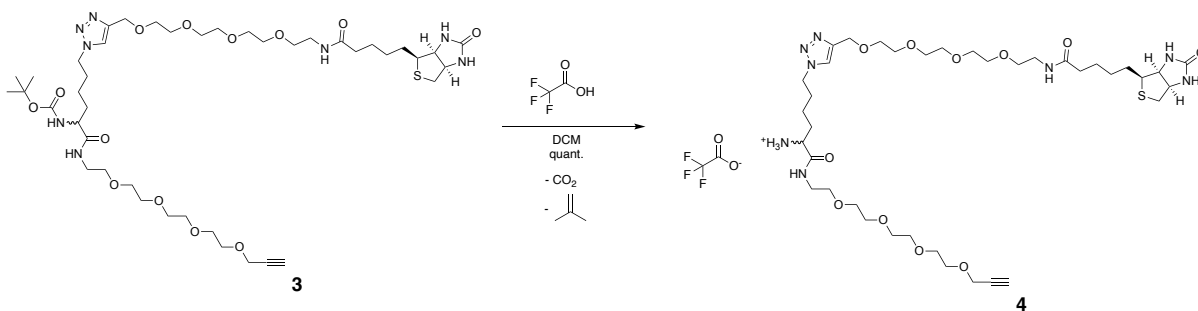
Compound **2** (500 mg, 1 equiv.) was dissolved in 40 mL of peptide grade DMF under argon atmosphere. DIPEA (124 mg, 1.4 equiv.), HBTU (364 mg, 1.4 equiv.) and propargyl-PEG4-amine (158 mg, 1 equiv.) were dissolved in 3 mL of peptide grade DMF each and added to the biotin solution. The reaction mixture stirred at RT for 6 h. The solvents were removed under high vacuum before the crude product was dissolved in 2 mL of ACN and 15 mL of water and freeze dried. The crude product was purified by preparative HPLC starting with 10% of ACN + 0.1% TFA in H₂O + 0.1% TFA over a period of 2 min, increasing to 100% ACN within 18 min, holding 100% ACN for 2 min and afterwards lowering back to 10% ACN until minute 20, holding the level until

min 22. The product fraction was freeze dried yielding in 591 mg (91%) of compound **3**.

¹H NMR (300 MHz, Methanol-d₄) δ 7.91 (s, 1H), 5.39 (s, 1H), 4.55 (s, 2H), 4.40 (dd, J = 7.8, 4.9 Hz, 1H), 4.33 (t, J = 7.1 Hz, 2H), 4.21 (dd, J = 7.9, 4.5 Hz, 1H), 4.08 (d, J = 2.4 Hz, 2H), 3.90 (s, 1H), 3.57 (d, J = 3.1 Hz, 8H), 3.54 (s, 11H), 3.52 – 3.39 (m, 8H), 3.27 (dd, J = 10.0, 5.3 Hz, 7H), 3.11 (dt, J = 9.6, 5.2 Hz, 1H), 2.83 (dd, J = 12.8, 5.0 Hz, 1H), 2.75 (t, J = 2.4 Hz, 1H), 2.60 (d, J = 12.7 Hz, 1H), 2.11 (t, J = 7.3 Hz, 2H), 1.83 (q, J = 7.3 Hz, 2H), 1.68 – 1.43 (m, 6H), 1.37 (d, J = 7.2 Hz, 2H), 1.34 (s, 9H), 1.31 (s, 1H).

¹³C NMR (75 MHz, Methanol-d₄) δ 125.23, 75.99, 71.57, 71.37, 71.28, 70.90, 70.58, 70.13, 64.93, 63.41, 61.67, 59.05, 57.01, 41.05, 40.39, 30.85, 29.77, 29.51, 28.75, 26.86.

5.3.3 Synthesis of 17-oxo-22-(4-(15-oxo-19-((3a*S*,4*S*,6a*R*)-2-oxohexahydro-1*H*-thieno[3,4-*d*]imidazol-4-yl)-2,5,8,11-tetraoxa-14-azanonadecyl)-1*H*-1,2,3-triazol-1-yl)-4,7,10,13-tetraoxa-16-azadocos-1-yn-18-amine (**4**)



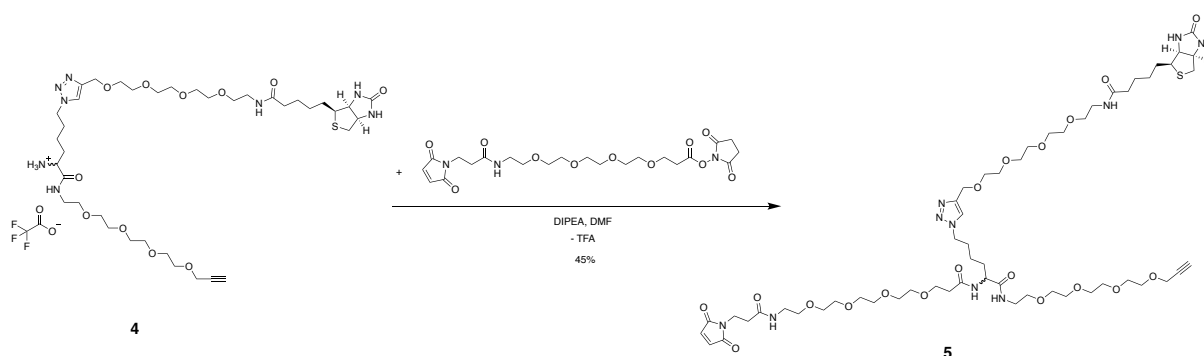
The reaction was performed after a protocol of *Pokorski et al.* (2011)^[58] with slight modifications. Compound **3** (591 mg) was dissolved in 10 mL of DCM and 10 mL TFA were added. The reaction stirred overnight with frequently opening the reaction flask to allow overpressure reduction due to gas development. Solvents and acid were removed under reduced pressure and diethylether was added to remove remaining TFA from the solution, yielding in 700 mg (100%) of compound **4**.

¹H NMR (300 MHz, Methanol-d₄) δ 8.01 (s, 1H), 4.65 (s, 2H), 4.49 (dt, J = 14.4, 7.3 Hz, 3H), 4.33 (dd, J = 7.9, 4.5 Hz, 1H), 4.20 (d, J = 2.4 Hz, 2H), 3.83 (t, J = 6.5 Hz, 1H), 3.67 (d, J = 10.9 Hz, 27H), 3.59 – 3.53 (m, 3H), 3.53 – 3.45 (m, 2H), 3.45 – 3.31

(m, 8H), 3.22 (dt, J = 9.8, 5.3 Hz, 1H), 3.00 – 2.84 (m, 2H), 2.72 (d, J = 12.8 Hz, 1H), 2.23 (t, J = 7.3 Hz, 2H), 2.07 – 1.81 (m, 4H), 1.81 – 1.52 (m, 4H), 1.45 (p, J = 8.3, 7.8 Hz, 4H).

¹³C NMR (75 MHz, Methanol-d₄) δ 176.16, 169.97, 166.11, 159.94, 146.04, 125.20, 76.05, 71.56, 71.49, 71.31, 71.27, 71.19, 70.95, 70.57, 70.23, 70.12, 65.02, 63.41, 61.68, 59.05, 57.02, 54.81, 54.30, 52.61, 50.90, 41.07, 40.59, 40.38, 36.73, 32.00, 30.74, 29.76, 29.51, 26.87, 22.81.

5.3.4 Synthesis of 1-(3-(2,5-dioxo-2,5-dihydro-1H-pyrrol-1-yl) propanamido)-N-(17-oxo-22-(4-(15-oxo-19-((3a*S*,4*S*,6a*R*)-2-oxohexahydro-1H-thieno[3,4-*d*]imidazol-4-yl)-2,5,8,11-tetraoxa-14-azanonadecyl)-1H-1,2,3-triazol-1-yl)-4,7,10,13-tetraoxa-16-azadocos-1-yn-18-yl)-3,6,9,12-tetraoxapentadecan-15-amide (**5**)



The reaction was performed after a protocol of *Zettlitz et al.* (2019)^[64] with slight modifications.

Compound **4** (281 mg, 1 equiv.) was dissolved in 15 mL of dry peptide grade DMF under argon atmosphere. DIPEA (210 mg, 5.2 equiv.) was added to the solution. Maleimide-PEG₄-NHS ester (380 mg, 2.5 equiv.) was dissolved in 10 mL of dry peptide grade DMF and added dropwise to the solution of compound **4** and DIPEA. The reaction mixture stirred at RT for 6 h under argon atmosphere. The solvent was removed under reduced pressure. The remaining substance was mixed with 7 mL of water and freeze dried to remove leftover DMF. The resulting crude product was purified twice via preparative HPLC starting with 10% of ACN + 0.1% TFA in H₂O + 0.1% TFA over a period of 2 min, increasing to 50% ACN within 10 min, afterwards reaching 100% ACN within 4 min, holding 100% ACN for 2 min and afterwards lowering back to 10% ACN until minute 20, holding the level until min 22.

The product fractions were freeze dried, resulting in 163 mg (45%) of compound **5**.

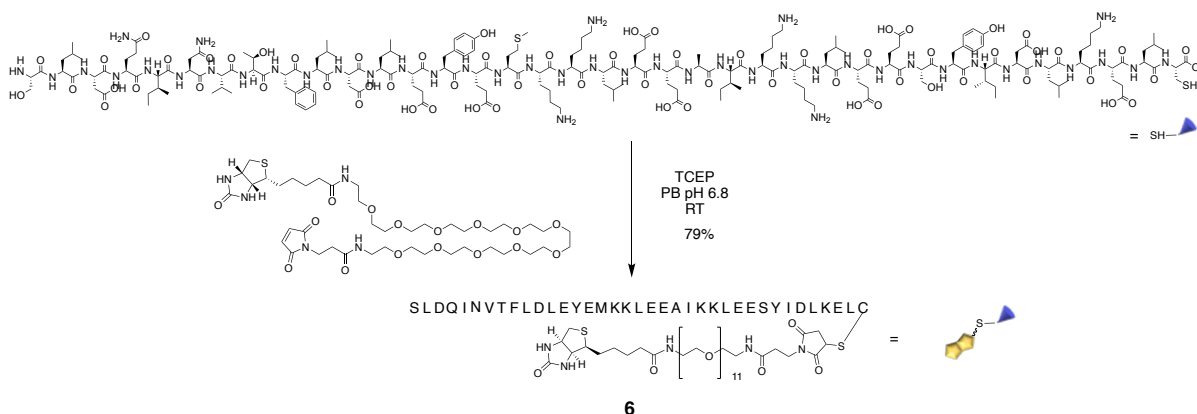
^1H NMR (700 MHz, Methanol- d_4) δ 7.23 (d, J = 3.3 Hz, 1H), 6.03 (d, J = 3.5 Hz, 2H), 4.08 (d, J = 3.4 Hz, 16H), 3.86 (d, J = 3.4 Hz, 2H), 3.71 (p, J = 4.0 Hz, 1H), 3.64 (q, J = 6.0, 5.3 Hz, 2H), 3.53 (ddt, J = 16.4, 7.7, 4.2 Hz, 2H), 3.39 (s, 2H), 3.01 – 2.66 (m, 58H), 2.60 (dd, J = 11.7, 6.4 Hz, 1H), 2.56 (q, J = 4.8 Hz, 4H), 2.42 (dt, J = 9.5, 4.7 Hz, 1H), 2.14 (dd, J = 13.0, 4.6 Hz, 1H), 2.07 (s, 1H), 1.92 (d, J = 12.6 Hz, 1H), 1.73 – 1.65 (m, 5H), 1.42 (d, J = 8.0 Hz, 2H), 1.16 (h, J = 9.0 Hz, 2H), 1.05 (tt, J = 11.2, 4.9 Hz, 1H), 0.98 – 0.76 (m, 6H), 0.69 – 0.52 (m, 5H).

^{13}C NMR (176 MHz, Methanol- d_4) δ 173.90, 171.91, 171.72, 170.84, 169.98, 163.85, 157.74, 157.51, 143.61, 133.26, 115.15, 113.53, 78.48, 73.80, 69.41, 69.36, 69.33, 69.27, 69.15, 69.10, 69.06, 69.03, 68.73, 68.48, 68.36, 68.27, 68.22, 67.93, 66.07, 62.71, 56.84, 49.11, 47.16, 47.03, 46.91, 46.79, 46.67, 46.55, 46.43, 38.84, 38.23, 38.21, 38.18, 35.34, 34.52, 33.55, 33.28, 30.40, 28.53, 27.55, 27.28, 24.63, 24.22, 21.50.

^{15}N NMR (700 MHz, Methanol- d_4) δ 7.24 – 7.20 (m), 7.24 – 7.20 (m), 6.04 – 6.00 (m), 3.87 – 3.83 (m), 3.65 – 3.61 (m), 3.65 – 3.61 (m), 3.56 – 3.52 (m), 2.99 – 2.95 (m), 2.75 – 2.70 (m), 2.76 – 2.67 (m), 2.57 – 2.49 (m), 2.43 – 2.39 (m), 2.16 – 2.09 (m), 1.94 – 1.88 (m), 1.68 – 1.64 (m), 1.07 – 1.03 (m), 0.91 – 0.85 (m).

5.4 Bioconjugation of antiviral peptides to biotinylated molecules

5.4.1 Conjugation of EK1 to maleimide-PEG11-biotin (6)



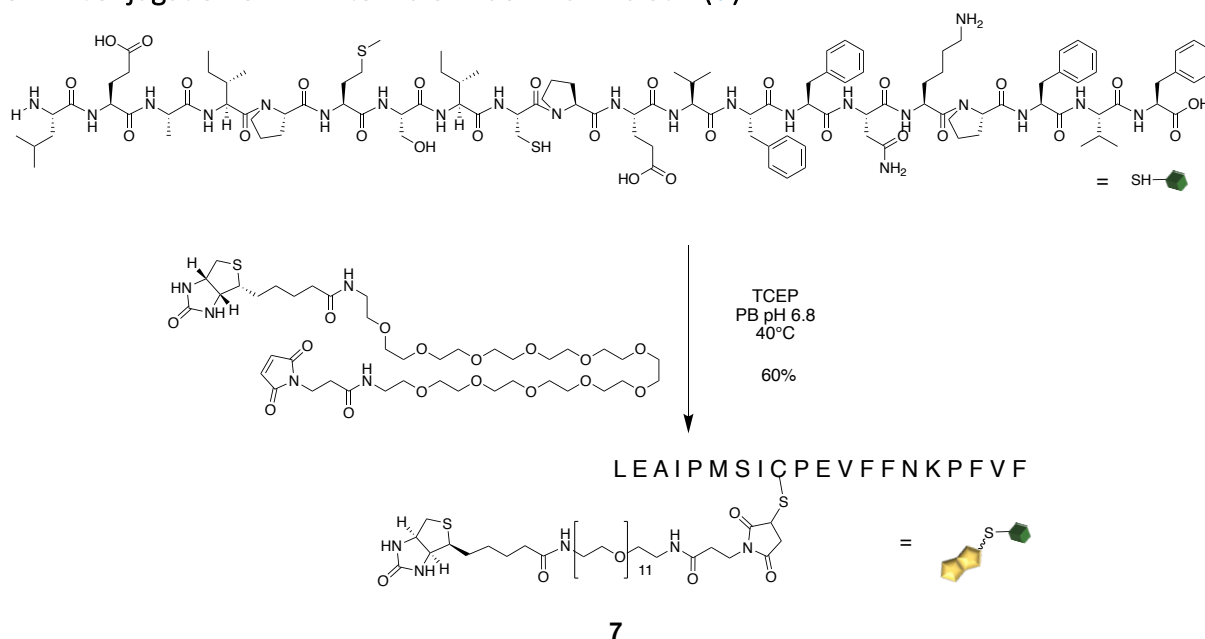
The reaction was performed after a protocol of *Heck et al.*(2019)^[34] with minimal modifications.

EK1C peptide (5.0 mg, 1 equiv.) was dissolved in 5 mL of PB (50 mM, pH 6.8). The reaction solution was heated to 40°C. TCEP (1 mg/mL in PB, 282 µg, 1 equiv.) was added and the mixture stirred at 40°C for 30 min. Maleimide-PEG11-biotin (1.56 mg, 1.5 equiv.) was dissolved in 156 µL DMF and added to the peptide solution. The mixture stirred at RT overnight. Solvents were removed through freeze drying and the crude product was purified by semi preparative HPLC starting with 5% of ACN + 0.1% TFA in H₂O + 0.1% TFA over a period of 2 min, increasing to 40% ACN within 9 min, reaching 50% ACN after 16 min, afterwards increasing to 100% within 6 min, holding it for 3 min and afterwards lowering back to 5% ACN until minute 29, holding the level until min 30.

The product fractions were freeze dried yielding in 4.8 mg (79%) of compound 6.

MALDI-TOF: $m/z = 5360$ [M+H⁺], $m/z = 2679$ [M+2H⁺]

5.4.2 Conjugation of VIRIP to maleimide-PEG11-biotin (**7**)



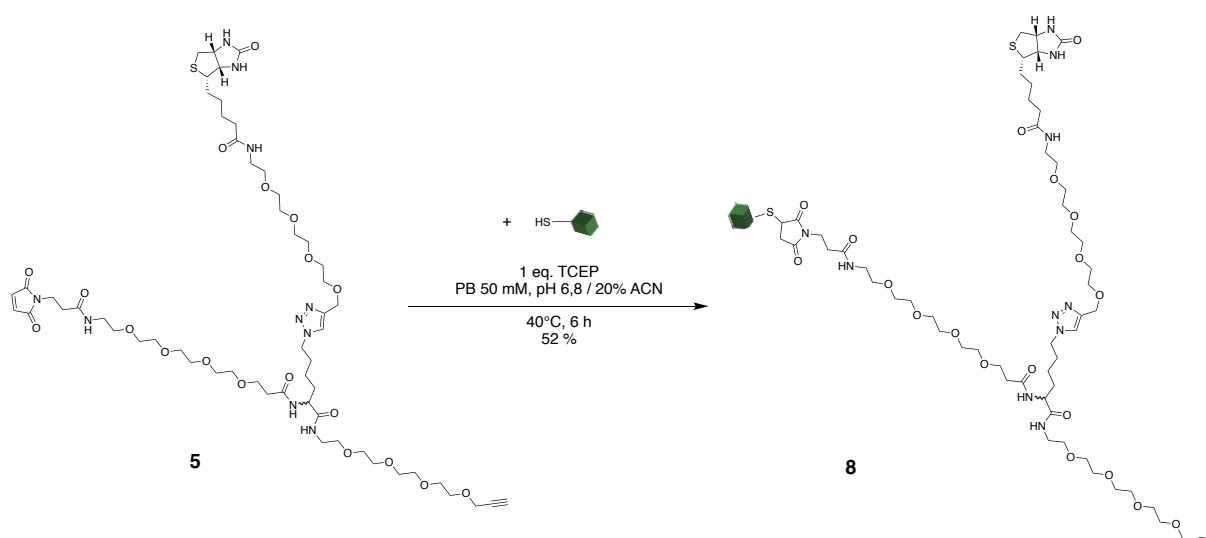
The reaction was performed after a protocol of *Heck et al.*(2019)^[34] with minimal modifications.

VIRIP peptide (5.0 mg, 1 equiv.) was dissolved in 5 mL of PB (50 mM, pH 6.8) with 20% ACN. The reaction solution was heated to 40°C. TCEP (1 mg/mL in PB, 537 µg, 1 equiv.) was added and the mixture stirred at 40°C for 1 h. Maleimide-PEG11-biotin (2.88 mg, 1.5 equiv.) was dissolved in 288 µL DMF and added to the peptide solution. The mixture stirred at 40°C overnight. Solvents were removed through freeze drying and the crude product was purified by semi preparative HPLC starting with 20% of ACN + 0.1% TFA in H₂O + 0.1% TFA over a period of 2 min, increasing to 50% ACN within 10 min, reaching 60% ACN after 25 min, afterwards increasing to 100% within 5 min, holding it for 1 min and afterwards lowering back to 20% ACN until minute 33, holding the level until min 35.

The product fractions were freeze dried yielding in 4.3 mg (60%) of compound **7**.

MALDI-TOF: $m/z = 3253$ [M+H⁺], $m/z = 3274$ [M+Na⁺]

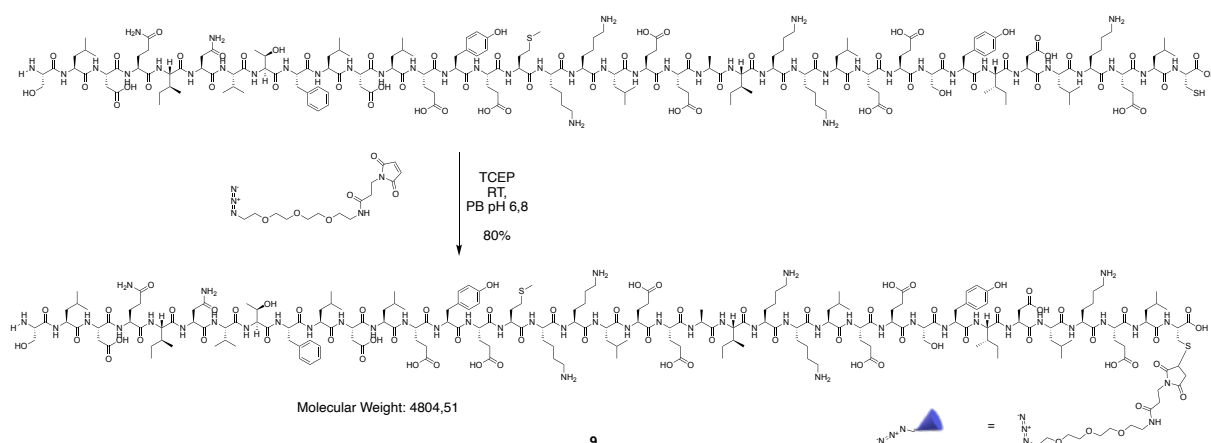
5.4.3 Conjugation of VIRIP to trifunctional biotin-PEG-maleimide-alkyne linker (**8**)



The reaction was performed after a protocol of *Heck et al.* (2019)^[34] with modifications. VIRIP peptide (10.0 mg, 1 equiv.) was dissolved in 10 mL of PB (50 mM, pH 6.8) with 20% ACN. The reaction solution was heated to 40°C. TCEP (1 mg/mL in PB, 1.23 mg, 1 equiv.) was added and the mixture stirred at 40°C for 30 min. Compound **5** (7.99 mg, 1.5 equiv.) was dissolved in 800 μ L DMF and added to the peptide solution. The mixture stirred in the dark at 40°C for 6 h. Solvents were removed through freeze drying and the crude product was purified by semi preparative HPLC starting with 10% of ACN + 0.1% TFA in H₂O + 0.1% TFA over a period of 2 min, increasing to 100% ACN within 25 min, holding 100% ACN for 1 min and afterwards lowering back to 10% ACN until minute 30, holding the level until min 32. The product fractions were freeze dried yielding in 8 mg (52%) of compound **8**.

MALDI-TOF: $m/z = 3571$ [M+H⁺], $m/z = 3593$ [M+Na⁺]

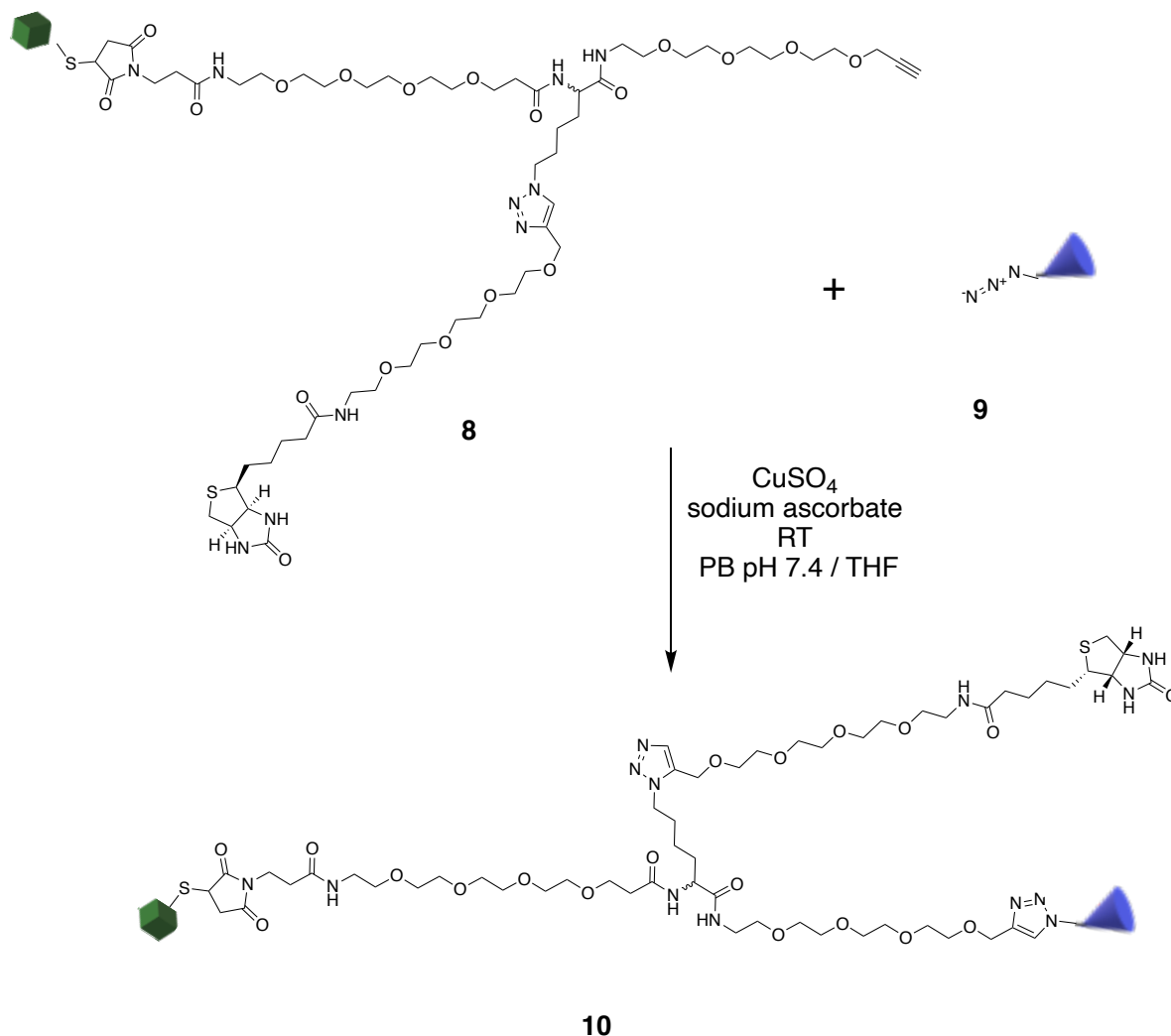
5.4.4 Conjugation of EK1 peptide to maleimide-PEG3-azide (9)



Maleimide-PEG3-azide was prepared by manufacturer's protocol in advance of the reaction. EK1C (6.0 mg, 1 equiv.) was dissolved in 2 mL of PB (50 mM, pH 6.8). TCEP (1 mg/mL in PB, 453 μ g, 1 equiv.) was added and the mixture stirred at RT for 40 min. Maleimide-PEG3-azide (approx. 8.0 mg, 15 equiv.) in 200 μ L dry DMF were added to the mixture and the reaction stirred at RT for 4 h. Solvents were removed through freeze drying. The crude product was purified from excess azide linker by size exclusion chromatography using Sephadex G-10 swollen in ultrapure Millipore water. The peptide fraction was freeze dried yielding in 6.0 mg (80%) of compound **9** containing about 20% of unmodified EK1.

MALDI-TOF: $m/z = 4804$ [M+H⁺]

5.4.4 Azide alkyne cycloaddition between EK1-azide and VIRIP on trifunctional linker (10)



The reaction was performed after a protocol of *Wang et al.* (2016)^[59].

Compound **8** (2.5 mg, 1 equiv.) and compound **9** (4.0 mg, 1.2 equiv.) were dissolved in 2 mL of PB (50 mM, pH 7.4) and 1.5 mL of THF. The solution was degassed by bubbling argon through the mixture. Copper sulfate (1 mg/mL, 60 μg , 0.5 equiv.) and sodium ascorbate (1 mg/mL, 209 μg , 1.5 equiv.) in degassed PB (50 mM, pH 7.4) were added and the reaction stirred at RT for 48 h. The solution was freeze dried. The yield of the reaction could not be determined, as only a small amount of product was obtained, which could not be isolated from the reaction mixture.

MALDI-TOF: $m/z = 8376$ $[\text{M}+\text{H}^+]$

5.5 Assembly of biotinylated peptides on streptavidin

5.5.1 Assembly of biotinylated EK1 on streptavidin

EK1-maleimide-PEG11-biotin (2.34 mg, 5 equiv.) was dissolved in 5.5 mL of PB (50 mM, pH 7.4). Streptavidin (10 mg/mL, 4.5 mg, 1 equiv.) in MilliQ water was added to the peptide solution and the mixture was shaking at RT for 1 h. The protein hybrid was purified using 6 mL Vivaspin ultrafiltration tubes with 10 kDa MWCO.

The concentration of the solution was determined as 2.13 mg/mL by Nanodrop absorption measurement at 280 nm. Yield was calculated to be 4.5 mg (99%) of protein in solution.

5.5.2 Assembly of biotinylated VIRIP on streptavidin

VIRIP-maleimide-PEG11-biotin (1.39 mg, 5 equiv.) was dissolved in 5.5 mL of PB (50 mM, pH 7.4). Streptavidin (10 mg/mL, 4.5 mg, 1 equiv.) in MilliQ water was added to the peptide solution and the mixture was shaking at RT for 1 h. The protein hybrid was purified using 6 mL Vivaspin ultrafiltration tubes with 10 kDa MWCO.

The concentration of the solution was determined as 2.86 mg/mL by Nanodrop absorption measurement at 280 nm. Yield was calculated to be 4.4 mg (97%) of protein in solution.

5.6 Assembly of peptides on 5 nm gold nanoparticles

3x3 mL of the commercially available GNP suspension in citrate buffer (3 x 5.5x10¹³ particles per mL, 3x0,274 nmol, 3x1 equiv.) were centrifuged each through a 100 kDa MWCO Vivaspin ultrafiltration tube to remove citrate buffer. The concentrated GNPs were resuspended in the respective peptide solutions: 1x EK1 (1 mg/mL in PB, 10 mM, pH 7.4, 1.2 mg, 1000 equiv.), 1x VIRIP (1 mg/mL in PB, 10 mM, pH 7.4, 0.64 mg, 1000 equiv.), 1x EK1+VIRIP (1 mg/mL in PB, 10 mM, pH 7.4, 0.60 mg + 0.32 mg, 500 equiv. + 500 equiv.). The reaction mixtures were shaking at 4°C overnight. The coated GNPs were purified by 100 kDa MWCO ultrafiltration tubes and washed 3x with 500 µL PB (10 mM, pH 7.4). The concentrates were resuspended in 1 mL of PB (10 mM, pH 7.4). Concentrations were determined by absorbance measurements at 520 nm using a Nanodrop spectrometer.

Literature

- [1] E. B. Ludmir, L. W. Enquist, *Nat. Rev. Microbiol.* **2009**, *7*, 615–615.
- [2] N. Terasaka, Y. Azuma, D. Hilvert, **n.d.**, DOI 10.1073/pnas.1800527115.
- [3] L. W. Enquist, for the E. of the J. of Virology, *J. Virol.* **2009**, *83*, 5296–5308.
- [4] F. Kirchhoff, in *Encycl. AIDS*, Springer New York, New York, NY, **2013**, pp. 1–9.
- [5] T. Tang, M. Bidon, J. A. Jaimes, G. R. Whittaker, S. Daniel, *Antiviral Res.* **2020**, *178*, 104792.
- [6] T. Cihlar, M. Fordyce, *Curr. Opin. Virol.* **2016**, *18*, 50–56.
- [7] W.-G. Forssmann, Y.-H. The, M. Stoll, K. Adermann, U. Albrecht, H.-C. Tillmann, K. Barlos, A. Busmann, A. Canales-Mayordomo, G. Giménez-Gallego, et al., *Sci. Transl. Med.* **2010**, *2*, 63re3-63re3.
- [8] S. Xia, M. Liu, C. Wang, W. Xu, Q. Lan, S. Feng, F. Qi, L. Bao, L. Du, S. Liu, et al., *Cell Res.* **2020**, *30*, 343–355.
- [9] S. C. Jordan, P. Zakowski, H. P. Tran, E. A. Smith, C. Gaultier, G. Marks, R. Zabner, H. Lowenstein, J. Oft, B. Bluen, et al., *Clin. Infect. Dis.* **2020**, DOI 10.1093/cid/ciaa812.
- [10] W.-C. Ko, J.-M. Rolain, N.-Y. Lee, P.-L. Chen, C.-T. Huang, P.-I. Lee, P.-R. Hsueh, *Int. J. Antimicrob. Agents* **2020**, *55*, 105933.
- [11] Y. Wu, D. Y. W. Ng, S. L. Kuan, T. Weil, *Biomater. Sci.* **2015**, *3*, 214–230.
- [12] L. M. Weiner, R. Surana, S. Wang, *Nat. Rev. Immunol.* **2010**, *10*, 317–327.
- [13] O. Zirafi, P. C. Hermann, J. Münch, *J. Leukoc. Biol* **2015**, *99*, 863–868.
- [14] J. Münch, L. Ständker, K. Adermann, A. Schulz, M. Schindler, R. Chinnadurai, S. Pöhlmann, C. Chaipan, T. Biet, T. Peters, et al., *Cell* **2007**, *129*, 263–275.
- [15] A. Riegger, C. Chen, O. Zirafi, N. Daiss, D. Mukherji, K. Walter, Y. Tokura, B. Stöckle, K. Kremer, F. Kirchhoff, et al., *ACS Macro Lett.* **2017**, *6*, 241–246.
- [16] D. D. Billadeau, S. Chatterjee, P. Bramati, R. Sreekumar, V. Shah, K. Hedin, R. Urrutia, *Int J Gastrointest Canc* **2006**, *37*, 110–119.
- [17] H. Jäger, *Entry Inhibitoren : Neue Formen Der HIV-Therapie*, Springer Medizin, **2008**.
- [18] H. Li, Y. Zhou, M. Zhang, H. Wang, Q. Zhao, J. Liu, *Antimicrob. Agents Chemother.* **2020**, *64*, DOI 10.1128/AAC.00483-20.
- [19] Y. Huang, C. Yang, X. Xu, W. Xu, S. Liu, *Acta Pharmacol. Sin.* **2020**, *41*, 1141–1149.
- [20] S. Xia, L. Yan, W. Xu, A. S. Agrawal, A. Algaissi, C.-T. K. Tseng, Q. Wang, L. Du, W. Tan, I. A. Wilson, et al., *Sci. Adv.* **2019**, *5*, eaav4580.
- [21] S. Akhter, M. Z. Ahmad, F. J. Ahmad, G. Storm, R. J. Kok, *Expert Opin. Drug Deliv.* **2012**, *9*, 1225–1243.
- [22] H. Yang, S.-Y. Fung, S. Xu, D. P. Sutherland, T. R. Kollmann, M. Liu, S. E. Turvey, **2015**, DOI 10.1021/nn505634h.
- [23] L. Wang, H. Zhang, L. Sun, W. Gao, Y. Xiong, A. Ma, X. Liu, L. Shen, Q. Li, H. Yang, *J. Nanobiotechnology* **2020**, *18*, 1–16.
- [24] A. M. Paul, Y. Shi, D. Acharya, J. R. Douglas, A. Cooley, J. F. Anderson, F. Huang, F. Bai, *J. Gen. Virol.* **2014**, *95*, 1712.
- [25] V. Cagno, P. Andreozzi, M. D’Alicarnasso, P. Jacob Silva, M. Mueller, M. Galloux, R. Le Goffic, S. T. Jones, M. Vallino, J. Hodek, et al., *Nat. Mater.* **2018**, *17*, 195–203.
- [26] S. Bagheri, M. Yasemi, E. Safaie-Qamsari, J. Rashidiani, M. Abkar, M. Hassani, S. A. Mirhosseini, H. Kooshki, *Artif. Cells, Nanomedicine, Biotechnol.* **2018**, *46*, 462–471.
- [27] G. Yilmaz, C. R. Becer, *Polym. Chem.* **2015**, *6*, 5503–5514.
- [28] X. Gao, J. Chen, J. Chen, B. Wu, H. Chen, X. Jiang, *Bioconjug. Chem.* **2008**, *19*, 2189–

- 2195.
- [29] S. Hoppmann, Z. Miao, S. Liu, H. Liu, G. Ren, A. Bao, Z. Cheng, *Bioconjugate Chem* **2011**, *22*, 413–421.
- [30] S. Noda, T. Matsumoto, T. Tanaka, A. Kondo, *Microb. Cell Fact.* **2015**, *14*, 5.
- [31] H.-G. Zoch, *Umweltwissenschaften und Schadstoff-forsch.* **2003**, *15*, 280–280.
- [32] “RCSB PDB - 6M9B: Wild-type streptavidin in complex with biotin solved by native SAD with data collected at 6 keV,” can be found under <https://www.rcsb.org/3d-view/6M9B>, **n.d.**
- [33] A. T. Marttila, O. H. Laitinen, K. J. Airene, T. Kulik, E. A. Bayer, M. Wilchek, M. S. Kulomaa, *FEBS Lett.* **2000**, *467*, 31–36.
- [34] A. J. Heck, T. Ostertag, L. Schnell, S. Fischer, B. K. Agrawalla, P. Winterwerber, E. Wirsching, M. Fauler, M. Frick, S. L. Kuan, et al., *Adv. Healthc. Mater.* **2019**, *8*, DOI 10.1002/adhm.201900665.
- [35] D. Y. W. Ng, J. Fahrner, Y. Wu, K. Eisele, S. L. Kuan, H. Barth, T. Weil, *Adv. Healthc. Mater.* **2013**, *2*, 1620–1629.
- [36] G. A. Orr, *J. Biol. Chem.* **1981**, *256*, 761–766.
- [37] J. D. Hirsch, L. Eslamizar, B. J. Filanoski, N. Malekzadeh, R. P. Haugland, J. M. Beechem, R. P. Haugland, *Anal. Biochem.* **2002**, *308*, 343–357.
- [38] M. P. Raphael, C. A. Rappole, L. K. Kurihara, J. A. Christodoulides, S. N. Qadri, J. M. Byers, *J. Fluoresc.* **2011**, *21*, 647–652.
- [39] D. Xu, A. J. Heck, S. L. Kuan, T. Weil, S. V Wegner, *Chem. Commun* **2020**, *56*, 9858.
- [40] L. Neutsch, B. Eggenreich, E. Herwig, M. Marchetti-Deschmann, G. Allmaier, F. Gabor, M. Wirth, *Pharm. Res.* **2014**, *31*, 819–832.
- [41] P. Ochtrop, C. P. R. Hackenberger, *Curr. Opin. Chem. Biol.* **2020**, *58*, 28–36.
- [42] G. Elia, *Proteomics* **2008**, *8*, 4012–4024.
- [43] J. M. Chalker, G. J. L. Bernardes, B. G. Davis, *Acc. Chem. Res.* **2011**, *44*, 730–741.
- [44] M. H. Stenzel, *ACS Macro Lett.* **2013**, *2*, 14–18.
- [45] S. M. Deneke, B. L. Fanburg, <https://doi.org/10.1152/ajplung.1989.257.4.L163> **1989**, DOI 10.1152/AJPLUNG.1989.257.4.L163.
- [46] T. Wang, Y. Wu, S. L. Kuan, O. Dumele, M. Lamla, D. Y. W. Ng, M. Arzt, J. Thomas, J. O. Mueller, C. Barner-Kowollik, et al., *Chem. - A Eur. J.* **2015**, *21*, 228–238.
- [47] B. H. Northrop, S. H. Frayne, U. Choudhary, *Polym. Chem.* **2015**, *6*, 3415–3430.
- [48] S. B. Gunnoo, A. Madder, *ChemBioChem* **2016**, *17*, 529–553.
- [49] S. L. Kuan, F. R. G. Bergamini, T. Weil, *Chem. Soc. Rev.* **2018**, *47*, 9069–9105.
- [50] Qian Wang, Timothy R. Chan, Robert Hilgraf, * Valery V. Fokin, * and K. Barry Sharpless, M. G. Finn*, **2003**, DOI 10.1021/JA021381E.
- [51] B. D. Fairbanks, T. F. Scott, C. J. Kloxin, K. S. Anseth, C. N. Bowman, *Macromolecules* **2009**, *42*, 211–217.
- [52] V. Hong, S. I. Presolski, C. Ma, M. â. G. Finn, *Angew. Chemie - Int. Ed.* **2009**, *48*, 9879–9883.
- [53] V. O. Rodionov, V. V. Fokin, M. G. Finn, *Angew. Chemie* **2005**, *117*, 2250–2255.
- [54] T. Kobayakawa, K. Ebihara, K. Tsuji, T. Kawada, M. Fujino, Y. Honda, N. Ohashi, T. Murakami, H. Tamamura, *Bioorg. Med. Chem.* **2020**, *28*, 115812.
- [55] R. Wang, R. Xiao, Z. Zeng, L. Xu, J. Wang, *Int. J. Nanomedicine* **2012**, *7*, 4185–98.
- [56] R. Knorr, A. Trzeciak, W. Bannwarth, D. Gillessen, *Tetrahedron Lett.* **1989**, *30*, 1927–1930.
- [57] W. Clayden, Greeves, Warren, *Organic Chemistry*, **2001**.
- [58] J. K. Pokorski, K. Breitenkamp, L. O. Liepold, S. Qazi, M. G. Finn, *J. Am. Chem. Soc.*

- 2011**, *133*, 9242–9245.
- [59] T. Wang, A. Riegger, M. Lamla, S. Wiese, P. Oeckl, M. Otto, Y. Wu, S. Fischer, H. Barth, S. L. Kuan, et al., *Chem. Sci.* **2016**, *7*, 3234–3239.
- [60] D. Budhadev, E. Poole, I. Nehlmeier, Y. Liu, J. Hooper, E. Kalverda, U. S. Akshath, N. Hondow, W. B. Turnbull, S. Pöhlmann, et al., *J. Am. Chem. Soc.* **2020**, *142*, 18022–18034.
- [61] X. Ren, J. Glende, M. Al-Falah, V. de Vries, C. Schwegmann-Wessels, X. Qu, L. Tan, T. Tschernig, H. Deng, H. Y. Naim, et al., *J. Gen. Virol.* **2006**, *87*, 1691–1695.
- [62] M. Sarzotti-Kelsoe, R. T. Bailer, E. Turk, C. Lin, M. Bilska, K. M. Greene, H. Gao, C. A. Todd, D. A. Ozaki, M. S. Seaman, et al., *J. Immunol. Methods* **2014**, *409*, 131–46.
- [63] N. Mackiewicz, J. Nicolas, N. Handké, M. Noiray, J. Mougín, C. Daveu, H. R. Lakkireddy, D. Bazile, P. Couvreur, *Chem. Mater.* **2014**, *26*, 1834–1847.
- [64] K. A. Zettlitz, C. M. Waldmann, W.-T. K. Tsai, R. Tavaré, J. Collins, J. M. Murphy, A. M. Wu, *J. Nucl. Med.* **2019**, *60*, 1467–1473.

Abbreviations

| | |
|--------------------|--|
| ACN | Acetonitrile |
| ALP | Avidin-like protein |
| Boc | <i>tert</i> -butyloxycarbonyl |
| CHCA | <i>alpha</i> -Cyano-4-hydroxycinnamic acid |
| CXCR4 | CXC-receptor 4 |
| DCM | Dichloromethane |
| DIPEA | Diisopropyl ethylamine |
| DLS | Differential light scattering |
| DMF | Dimethyl-formamide |
| DMPA | Dimethoxy phenyl acetophenone |
| DMSO | Dimethyl-sulfoxide |
| DNA | Deoxy ribonucleic acid |
| DOTA | 1,4,7,10-Tetraazacyclododecane-1,4,7,10-tetraacetic acid |
| DTT | Dithiothreitol |
| ESI-MS | Electron-spray-ionization-mass-spectrometry |
| Fmoc | Fluorenylmethoxycarbonyl |
| GNP | Gold nanoparticle |
| HABA | 2-((4'-hydroxyphenyl)-azo) benzoic acid |
| HBTU | 2-(1 <i>H</i> -Benzotriazol-1-yl)-1,1,3,3- tetramethyluronium-hexafluoro phosphate |
| HIV | Human immunodeficiency virus |
| HPLC | High-Pressure-Liquid-Chromatography |
| HSA | Human serum albumin |
| LC-MS | Liquid-Chromatography-Mass-Spectrometry |
| MALDI-TOF | Matrix-assisted laser-desorption-ionization-Time-of-flight |
| MeOD | Methanol-D ₄ |
| MeOH | Methanol |
| MES | 2-(<i>N</i> -Morpholino) ethane sulfonic acid |
| MWCO | Molecular weight cut off |
| NaHCO ₃ | Sodium hydrogencarbonate |
| NHS | <i>N</i> -Hydroxy-succinimide |
| NMR | Nuclear-Magnetic-Resonance-Spectroscopy |

| | |
|------------|--|
| PAGE | Polyacrylamide-gel electrophoresis |
| PB | Phosphate buffer |
| PEG | Polyethylene glycol |
| PET | Positron emission tomography |
| RNA | Ribonucleic acid |
| RT | Room temperature |
| SA | Sinapinic acid |
| SARS | Severe acute respiratory syndrome |
| SAV | Streptavidin |
| SDS | Sodium dodecyl-sulfate |
| SEC | Size exclusion chromatography |
| TAE-Buffer | TRIS-acetate-EDTA-buffer |
| TCEP | Tris(2-carboxyethyl) phosphine (hydrochloride) |
| TEM | Transmission electron microscopy |
| TFA | Trifluoro acetic acid |
| TIC | Total ion count |
| VIRIP | Virus inhibiting peptide |

List of figures

| | |
|---|----|
| <i>Figure 1: replication mechanism of HIV. Source:[4].</i> | 1 |
| <i>Figure 2: Fusion and replication mechanism of SARS-CoV-2. Source:[5].</i> | 2 |
| <i>Figure 3: Approved antiviral drugs against HIV and AIDS since 1986. Source: [6].</i> | 3 |
| <i>Figure 4: The molecular structure of Stavudine and Nevirapine.</i> | 4 |
| <i>Figure 5: Fusion mechanism of the HI virus with host cell membrane and interfering points of entry inhibitors. Adapted from source [13].</i> | 6 |
| <i>Figure 6: Molecular structure of CXCR4 antagonist WSC02^[15].</i> | 7 |
| <i>Figure 7: Molecular structure of fusion protein inhibitor VIRIP^[14].</i> | 7 |
| <i>Figure 8:a) Structure of SARS-CoV-2 spike protein, b) Interaction between S1 subdomain of the virus with host cells ACE2 receptor, c) Fusion mechanism of SARS-CoV-2 with host cell membrane via its spike protein. Source: ^[19].</i> | 8 |
| <i>Figure 9: Model of interaction between EK1 (green) in complex with the HR1 domain of SARS-CoV. Source: ^[20].</i> | 8 |
| <i>Figure 10: Molecular structure of the EK1 peptide containing 37 amino acids^[20].</i> | 9 |
| <i>Figure 11: Varieties of possible surface modifications of gold nanoparticles either A.: noncovalently or B.: covalently via thiol-gold-bonds. Source: ^[21].</i> | 9 |
| <i>Figure 12: TEM images of herpes simplex viruses type 2 (HSV-2) treated with 3-mercaptopropanesulfonate coated gold nanoparticles for 90 min. Source: ^[25].</i> | 10 |
| <i>Figure 13: Effects of near infrared light irradiation of gold nanostructures. Source: ^[21].</i> | 11 |
| <i>Figure 14: Formation of lectin-carbohydrate-conjugates through glyconanoparticles. Source: ^[27].</i> | 12 |
| <i>Figure 15: Different functionalities united on one HSA molecule to provide tumor targeting through an HER2 Affinity body and a cancer treatment through chelator DOTA in complex with a radioactive nuclide. Source: ^[29].</i> | 13 |
| <i>Figure 16: Ribbon diagram of tetrameric witt type streptavidin in complex with four Biotin molecules. Source: RCSB protein data bank, entry 6M9B. Source: ^[32].</i> | 13 |

| | |
|--|----|
| Figure 17: Combination of different biotinylated targeting identities on one avidin to inhibit Rho activity in neutrophils. Source: [34]. | 14 |
| Figure 18: Molecular structures of biotin and 2-iminobiotin. | 14 |
| Figure 19: Possible tags and their reaction in order to chemoselectively modify proteins or peptides. Source:[43]. | 17 |
| Figure 20: Molecular structure of DMPA. | 20 |
| Figure 21: General idea of dimerization/functionalization of different biomolecules through click chemistry with PEG chain spacing units. | 22 |
| Figure 22: Envisioned molecular structure of the trifunctional linker molecule for chemo selective bioconjugation reactions. | 23 |
| Figure 23: Model of potential inhibition of SARS-CoV-2 virus by peptide coated gold nanoparticles and streptavidin/ neutravidin conjugates. | 25 |
| Figure 24: LC-MS analysis of the filtrated compound 2 . Peak 1 in the upper TIC spectrum represents the desired product. The lower ESI ⁺ mass spectrum shows the integrated mass peaks from peak 1 in the TIC spectrum. | 27 |
| Figure 25: ¹ H-NMR spectrum of purified compound 2 . Measured at 300 MHz in MeOD. | 28 |
| Figure 26: LC-MS spectrum of the purified product 3 . Peak 1 represents the product, peak 2 represents the boc-deprotected form of the product, that probably formed during HPLC purification under acidic conditions (0,1 vol% TFA). For clarity, only m/z from 800 to 1020 is shown here. Full MS is available in appendix 18. | 29 |
| Figure 27: ¹ H-NMR spectrum of purified compound 3 . Measured at 300 MHz in MeOD. | 30 |
| Figure 28: LC-MS spectrum of deprotected product 3 after removal of the solvent and excess TFA. | 31 |
| Figure 29: ¹ H-NMR spectrum of compound 4 . Measured at 300 MHz in MeOD. | 32 |
| Figure 30: LC-MS analysis of compound 5 after the first (A, light blue) and the second purification procedure (B, dark blue) via preparative HPLC. | 34 |
| Figure 31: ¹ H NMR spectrum of the trifunctional linker molecule 5 . Measured at 700 MHz in MeOD. | 35 |
| Figure 32: COSY NMR spectrum of trifunctional linker 5 . Measured at 700 MHz in MeOD. | 36 |
| Figure 33: ¹ H- ¹⁵ N-HMBC NMR spectrum of compound 5 . Measured at 700 MHz in MeOD. | 37 |
| Figure 34: ¹³ C NMR spectrum of compound 5 . Measured at 176 MHz in MeOD. | 38 |
| Figure 35: LC-MS analysis of purified compound 6 . Since the modified peptide's molecular mass is above the detection range, only multiple times charged species can be detected in the mass spectrum. | 40 |
| Figure 36: MALDI mass spectrum of isolated compound 6 . Measurement was performed using CHCA as a matrix. | 41 |
| Figure 37: LC-MS analysis of the isolated compound 7 . Since the modified peptide's molecular mass is above the detection range, only multiple times charged species can be detected in the mass spectrum. | 43 |
| Figure 38: MALDI mass spectrum of the isolated compound 7 . Measurement was performed using a sinapic acid matrix. | 43 |
| Figure 39: LC-MS analysis of purified compound 8 . Since the expected product mass is higher than the ESI-MS detection range, only multiple charged product species can be detected. | 45 |
| Figure 40: MALDI mass analysis of purified compound 8 . Measurement was performed by sample preparation with a CHCA matrix. | 46 |
| Figure 41: LC-MS spectrum of purified compound 9 . Since the product's molecular mass lays outside the ESI-MS detection range, only multiple times charged species can be detected. | 47 |
| Figure 42: MALDI mass analysis of purified compound 9 . Spectrum was obtained by using a CHCA matrix. | 48 |
| Figure 43: MALDI mass analysis of reaction mixture for the synthesis of compound 10 . Measurement was performed using SA as a matrix. | 50 |
| Figure 44: MALDI analysis of the test reaction shown in scheme. The spectrum was obtained by preparation of the sample with CHCA as a matrix. | 52 |
| Figure 45: MALDI mass spectrometry of the finally obtained reaction mixture of WSC02 with maleimide PEG4 alkyne after irradiation with light at 365 nm for 110 min. | 52 |
| Figure 46: MALDI mass spectrum of thiol maleimide versus thiol alkyne test reaction using antiviral peptide WSC02. Measurement was performed using CHCA as a matrix. | 54 |
| Figure 47: Silver stained SDS PAGE gel of different streptavidin (SAV) peptide hybrids in comparison to native streptavidin, each under native and denaturated conditions with DTT. Electrophoresis was run at 120 V in MES running buffer. | 59 |
| Figure 48: Results of the agarose gel electrophoresis of different GNP samples. Electrophoresis was performed using an 0.7% agarose gel in TAE running buffer at 50 V. | 65 |
| Figure 49: SDS PAGE analysis of EK1 coated GNPs. Purified EK1-GNP was monitored in comparison to freshly mixed GNP with EK1 and EK1 respectively GNP alone. Electrophoresis was performed in MES running buffer at | |

| | |
|---|----|
| 130 V. After capturing the unstained gel (left side), EK1 was visualized with silver stain to investigate its presence on the particles (right side). | 66 |
| Figure 50: TEM images of the different peptide coated gold nanoparticles in comparison to unmodified GNPs. The sample of GNP coated with EK1 was stained with uranyl acetate. All samples were measured on an uncoated copper grid. Measurement was performed by Jiaxu Liang..... | 68 |
| Figure 51: Schematical drawing of potential interactions between peptide coated gold nanoparticles and peptides multimerized on avidin-like proteins with a targeted virus, such as SARS-CoV-2. | 73 |

List of schemes

| | |
|--|----|
| Scheme 1: reaction scheme for the assembly of different functionalities to one streptavidin molecule with precise stoichiometry. Source: [39] | 15 |
| Scheme 2: Overview of common thiol selective bioconjugation reactions. Source:[44]..... | 18 |
| Scheme 3: Reaction mechanism of the thiol-maleimide reaction. Adapted from source [47]..... | 19 |
| Scheme 4: Mechanism of radical initiated thiol-yne reaction. Adapted from source [51]. | 20 |
| Scheme 5: General reaction equation of copper catalyzed Huisgen reaction in bioconjugation reactions. Adapted from source [52]. | 21 |
| Scheme 6: Mechanism of the copper catalyzed [3+2] cycloaddition of azides with alkynes. Source: [53] | 21 |
| Scheme 7: General reaction scheme of supramolecular assembly of multimerized antiviral peptides to streptavidin/neutravidin..... | 24 |
| Scheme 8: General reaction scheme of ligand exchange on the surface of gold nanoparticles with antiviral peptides. | 24 |
| Scheme 9: Synthesis route performed to synthesize a trifunctional linker molecule..... | 26 |
| Scheme 10: Reaction equation of [3+2]-cycloaddition of biotin-PEG-4-alkyne and N-boc-azidolysine. | 27 |
| Scheme 11: Reaction equation of biotin-PEG-4-triazololysine with propargyl-PEG-4-amine..... | 28 |
| Scheme 12: General coupling mechanism between carboxylic acid and primary amine via HBTU as a coupling agent. Mechanism adapted from sources [57] and [58]. | 29 |
| Scheme 13: Reaction equation of the deprotection step of product 3 to yield its free amine form 4 | 31 |
| Scheme 14: Reaction equation of the NHS coupling between compound 4 and maleimide-PEG-4-NHS. | 33 |
| Scheme 15: Reaction equation for the conjugation reaction of antiviral peptide EK1 to a biotin PEG-11 maleimide linker via its thiol functionality. | 40 |
| Scheme 16: Reaction equation of the synthesis of compound 7 , the coupling of VIRIP to biotin PEG-11 maleimide..... | 42 |
| Scheme 17: Bioconjugation reaction equation of VIRIP with trifunctional linker via maleimide-thiol Michael-addition. | 44 |
| Scheme 18: Reaction equation of the azide functionalization of EK1..... | 47 |
| Scheme 19: Reaction equation for the copper catalyzed Huisgen reaction to conjugate EK1 azide to VIRIP biotin trifunctional linker via its alkyne functionality. | 49 |
| Scheme 20: Reaction equation for thiol-yne test reaction using Fmoc-L-propargylglycine and test peptide CKFKFQF. | 51 |
| Scheme 21: Reaction equation for thiol-yne test reaction between maleimide-PEG4-alkyne and WSC02. | 53 |
| Scheme 22: General equation for the substitution reaction between biotin and HABA on an avidin like protein..... | 55 |
| Scheme 23: Reaction equation of supramolecular multimerization of biotinylated EK1 peptide on streptavidin..... | 57 |
| Scheme 24: Reaction equation for the saturation of streptavidin with biotinylated VIRIP. | 58 |
| Scheme 25: General reaction equation of the performed ligand exchange reaction of citrate stabilized gold nanoparticles (diameter 5 nm) with antiviral peptides VIRIP and EK1..... | 62 |

List of graphs

| | |
|---|-----------|
| <i>Graph 1: Results of the absorbance measurements of the HABA assay for determination of saturation equivalents for biotinylated EK1 and biotinylated VIRIP in relation to native biotin on streptavidin. Measurements were performed using a transparent 384 well plate. Absorbance was measured at 500 nm in a Tecan plate reader.</i> | <i>56</i> |
| <i>Graph 2: Results of the UV-vis measurement of EK1 and VIRIP coated gold nanoparticle in comparison to citrate stabilized GNP. Spectra were measured in a Tecan spark plate reader.</i> | <i>64</i> |
| <i>Graph 3: Multi angle DLS measurement results of peptide coated GNPs in comparison to unmodified GNPs. Measurements were performed by Christine Rosenauer.</i> | <i>65</i> |
| <i>Graph 4: Normalized HIV infection rate of TZM-bl cells under treatment of either biotinylated VIRIP or biotinylated VIRIP multimerized on avidin in dependence of the used substance concentration of antiviral peptide in μM. Biotinylated VIRIP and corresponding avidin hybrids were synthesized by Astrid Heck, experiment and measurement was performed by Fabian Zech as part of his PhD thesis</i> | <i>70</i> |
| <i>Graph 5: Normalized HIV infection rate of cultured TZM-bl cells under treatment of either avidin, streptavidin or neutravidin in dependence of the used substance concentration of protein in μM. Experiment and measurement was performed by Fabian Zech as part of his PhD thesis.</i> | <i>71</i> |
| <i>Graph 6: Normalized SARS-CoV-2 infection of Calu 3 cells under treatment of either unmodified EK1C, EK1C multimerized on streptavidin or streptavidin carrying VIRIP as a negative control in dependence of the used substance amount of antiviral peptide in μM. Experiment and measurement was performed by Fabian Zech as part of his PhD thesis.</i> | <i>72</i> |

List of tables

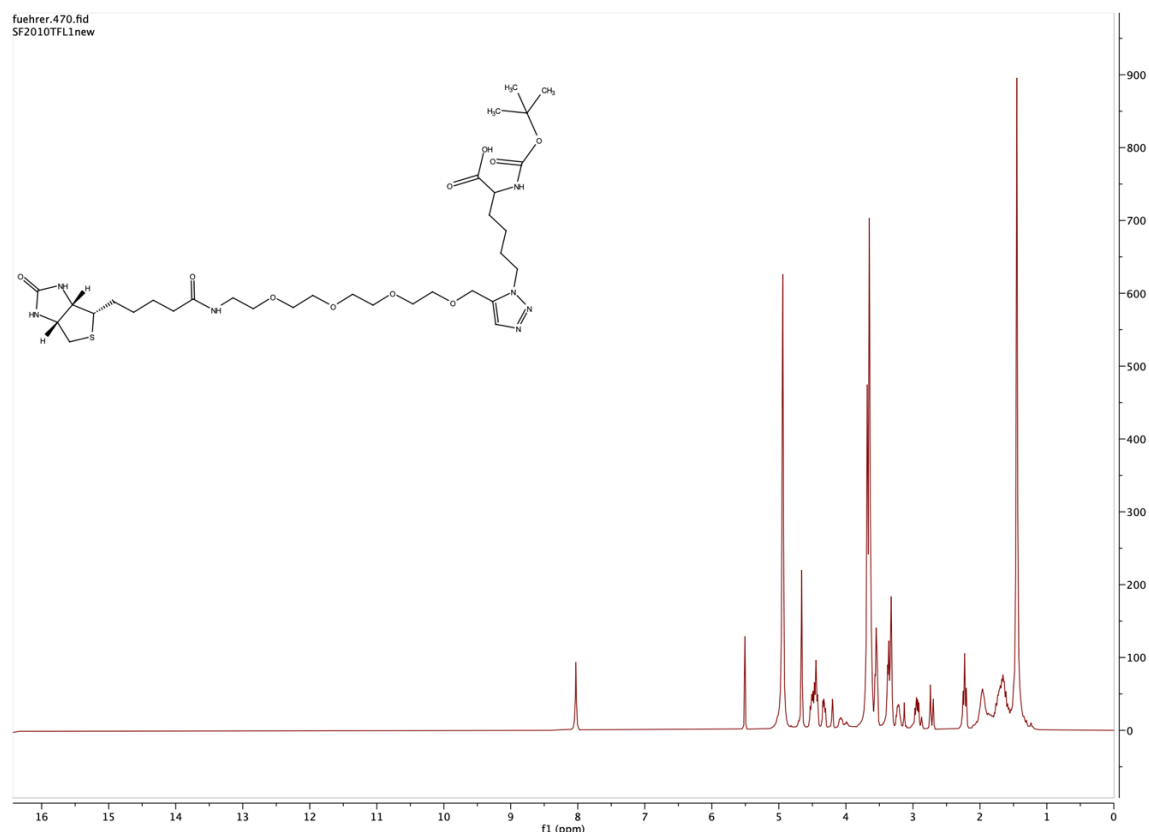
| | |
|---|-----------|
| Table 1: <i>Composition chart of SDS PAGE gels. Recipe yields two gels.</i> | <i>77</i> |
|---|-----------|

List of appendixes

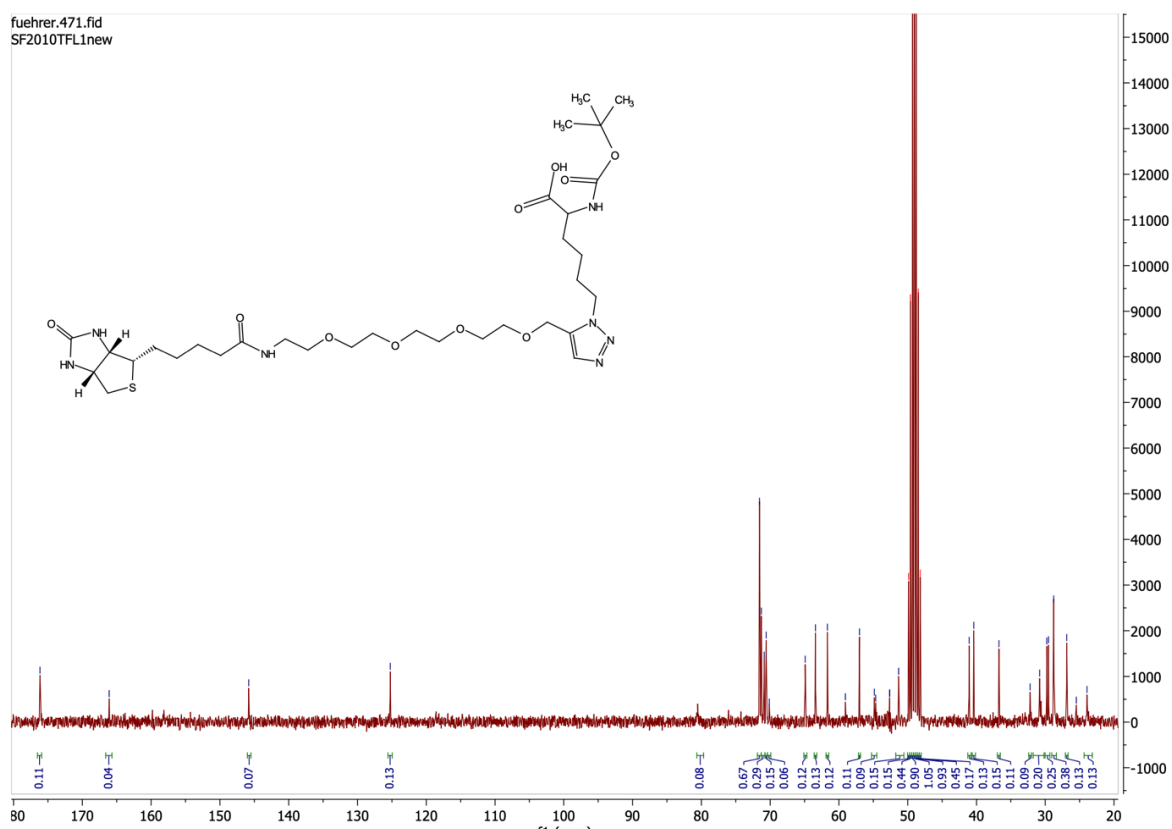
| | |
|---|------------|
| <i>Appendix 1: ^1H NMR of compound 2. Measurement conducted at 300 MHz in MeOD.</i> | <i>99</i> |
| <i>Appendix 2: ^{13}C NMR of compound 2. Measurement conducted at 300 MHz in MeOD.</i> | <i>99</i> |
| <i>Appendix 3: ^1H NMR of compound 3. Measurement conducted at 300 MHz in MeOD.</i> | <i>100</i> |
| <i>Appendix 4: ^{13}C NMR of compound 3. Measurement conducted at 300 MHz in MeOD.</i> | <i>100</i> |
| <i>Appendix 6: ^{13}C NMR of compound 4. Measurement conducted at 300 MHz in MeOD.</i> | <i>101</i> |
| <i>Appendix 5: ^1H NMR of compound 4. Measurement conducted at 300 MHz in MeOD.</i> | <i>101</i> |
| <i>Appendix 8: ^{13}C NMR of compound 5. Measurement conducted at 700 MHz in MeOD.</i> | <i>102</i> |
| <i>Appendix 7: ^1H NMR of compound 5. Measurement conducted at 700 MHz in MeOD.</i> | <i>102</i> |
| <i>Appendix 9: COSY of compound 5. Measurement conducted at 700 MHz in MeOD.</i> | <i>103</i> |
| <i>Appendix 10: ^1H-^{13}C-HMBC NMR of compound 5. Measurement conducted in MeOD at 700 MHz.</i> | <i>103</i> |
| <i>Appendix 11: ^1H-^{13}C HSQC NMR spectrum of compound 5. Measurement obtained in MeOD at 700 MHz.</i> | <i>104</i> |
| <i>Appendix 12: MALDI TOF spectrum of compound 6. Measurement was performed using SA as a matrix.</i> | <i>105</i> |
| <i>Appendix 13: MALDI TOF analysis of compound 7. Measurement was performed using CHCA as a matrix.</i> | <i>105</i> |
| <i>Appendix 14: MALDI TOF analysis of compound 8. Measurement was performed using CHCA as a matrix.</i> | <i>106</i> |
| <i>Appendix 15: MALDI TOF analysis of compound 9. Measurement was performed using CHCA as a matrix.</i> | <i>106</i> |
| <i>Appendix 16: MALDI TOF analysis of reaction mixture of compound 10. Measurement was performed using SA as a matrix.</i> | <i>107</i> |
| <i>Appendix 17: LC spectrum of LC-MS analysis of compound 2. The shown LC- chromatogram was measured at 254 nm.</i> | <i>108</i> |
| <i>Appendix 18: LC-MS analysis of compound 3. The shown LC- chromatogram was measured at 254 nm.</i> | <i>108</i> |
| <i>Appendix 19: LC spectrum of LC-MS analysis of compound 5. The shown chromatogram was measured at 214 nm.</i> | <i>108</i> |
| <i>Appendix 20: LC spectrum of LC-MS analysis of compound 4. The shown chromatogram was measured at 254 nm.</i> | <i>108</i> |

| | |
|--|-----|
| <i>Appendix 21: LC spectrum of LC-MS analysis of compound 7. The shown chromatogram was measured at 254 nm.</i> | 108 |
| <i>Appendix 22: LC spectrum of LC-MS analysis of compound 6. The shown chromatogram was measured at 254 nm.</i> | 108 |
| <i>Appendix 23: LC spectrum of LC-MS analysis of compound 8. The shown chromatogram was measured at 254 nm.</i> | 108 |
| <i>Appendix 24: LC spectrum of LC-MS analysis of compound 9. The shown chromatogram was measured at 254 nm.</i> | 108 |
| <i>Appendix 25: LC-MS analysis of the reaction mixture of compound 10. The shown chromatogram was measured at 214 nm and 254 nm.</i> | 109 |
| <i>Appendix 26: MALDI TOF analysis of streptavidin with VIRIP-PEG11-biotin. Measurement was performed using SA as a matrix.</i> | 109 |
| <i>Appendix 27: SDS PAGE of purified streptavidin protein hybrids and native streptavidin. Electrophoresis was performed at 120 V in MES running buffer. Band visualization was performed by silver staining.</i> | 110 |
| <i>Appendix 28: Visible light photography of gold nanoparticles with EK1. Once purified, once freshly mixed and once each compound alone. Electrophoresis was performed at 130 V in MES running buffer.</i> | 111 |
| <i>Appendix 29: Silver stained SDS PAGE of gold nanoparticles with EK1. Once purified, once freshly mixed and once each compound alone. Electrophoresis was performed at 130 V in MES running buffer.</i> | 111 |
| <i>Appendix 30: Visible light photography of agarose gel electrophoresis of peptide coated gold nanoparticles. Electrophoresis was performed using an 1.0% agarose gel in TAE running buffer. Electrophoresis was performed at 50 V.</i> | 112 |
| <i>Appendix 31: TEM imaging of peptide coated gold nanoparticles in comparison to untreated GNPs. EK1 coated GNP sample was stained with uranyl acetate. Measurement was performed by Jiaxu Liang.</i> | 112 |
| <i>Appendix 32: Multi angle DLS measurement data of blank GNPs. Measurement was performed in ultrapure water by Christine Rosenauer.</i> | 113 |
| <i>Appendix 33: Multi angle DLS measurement data of VIRIP coated GNPs. Measurement was performed in ultrapure water by Christine Rosenauer.</i> | 113 |
| <i>Appendix 34: Multi angle DLS measurement data of EK1 coated GNPs. Measurement was performed in ultrapure water by Christine Rosenauer.</i> | 114 |
| <i>Appendix 35: Multi angle DLS measurement data of VIRIP and EK1 coated GNPs. Measurement was performed in ultrapure water by Christine Rosenauer.</i> | 114 |
| <i>Appendix 36: Zeta potential measurement of peptide coated GNPs versus citrate stabilized GNPs. Measurement was performed in 1 M KCl solution by Astrid Heck.</i> | 115 |

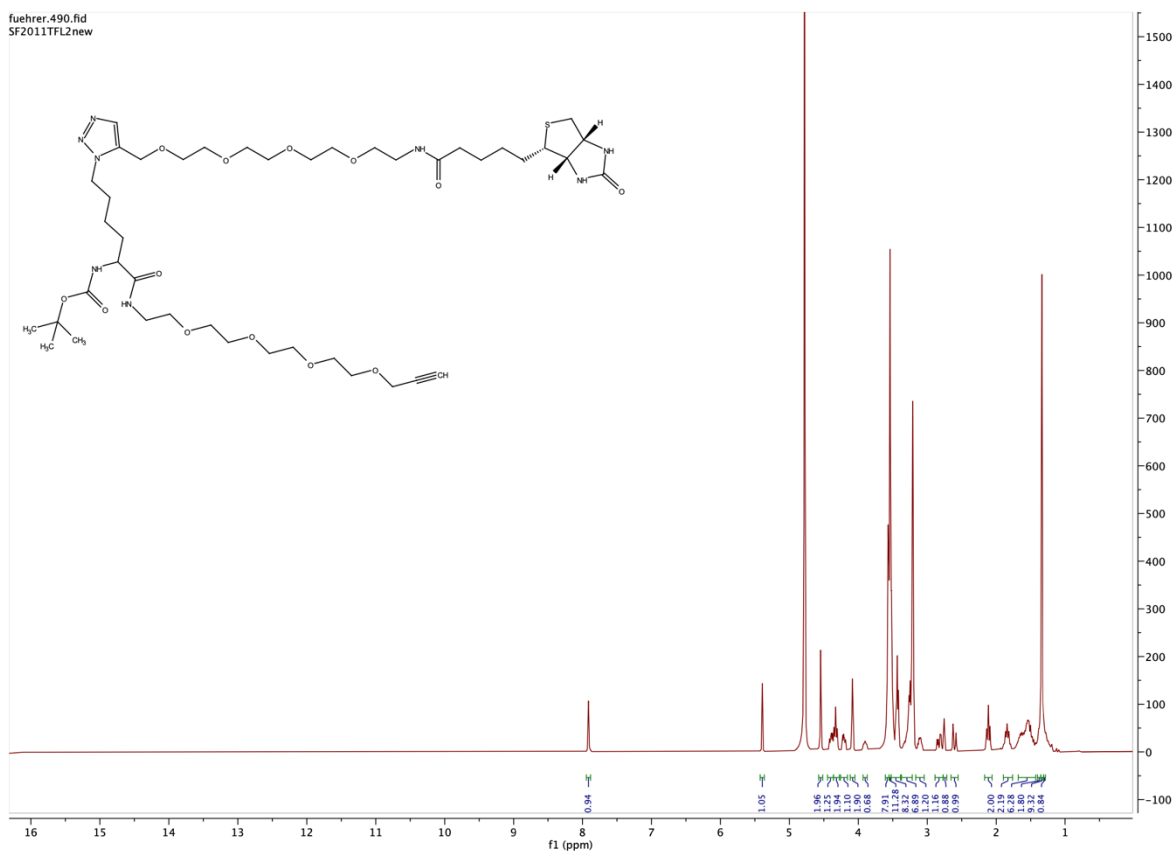
Appendix



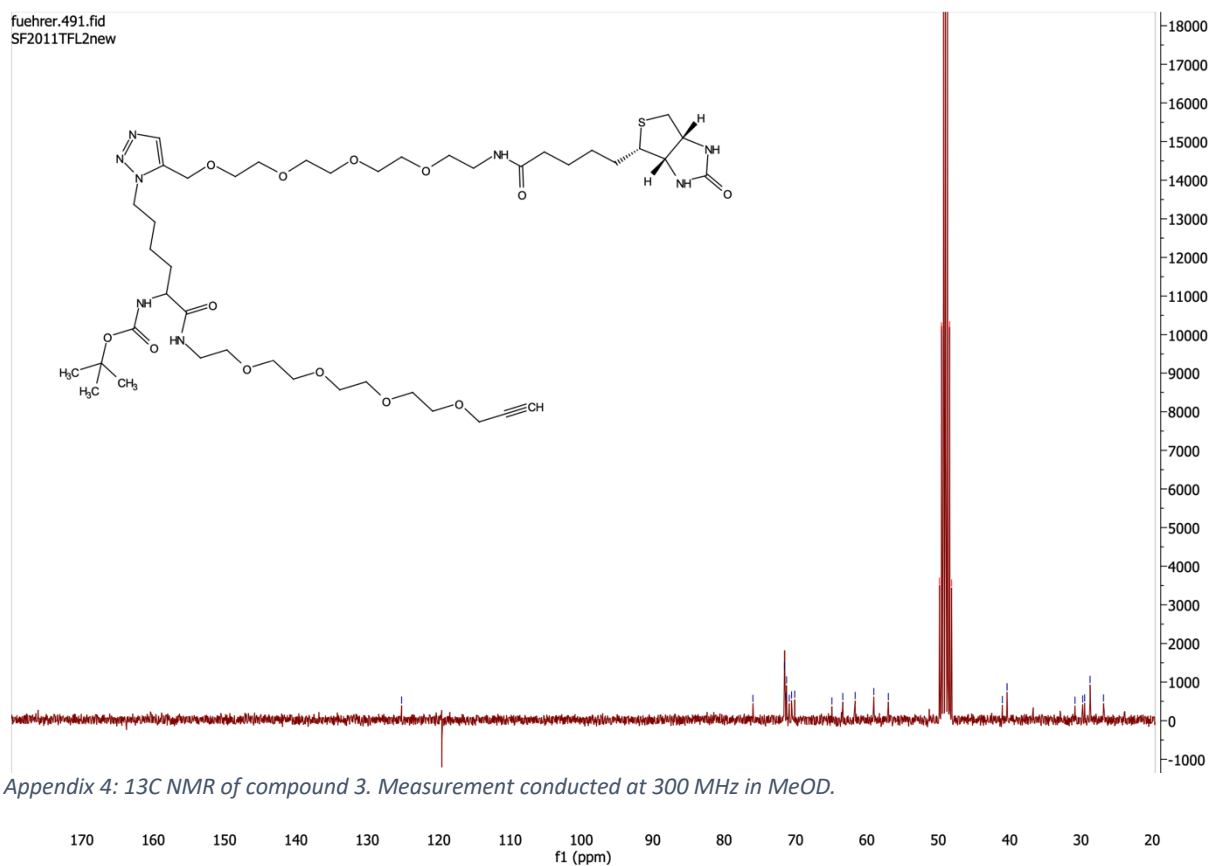
Appendix 1: ^1H NMR of compound 2. Measurement conducted at 300 MHz in MeOD.



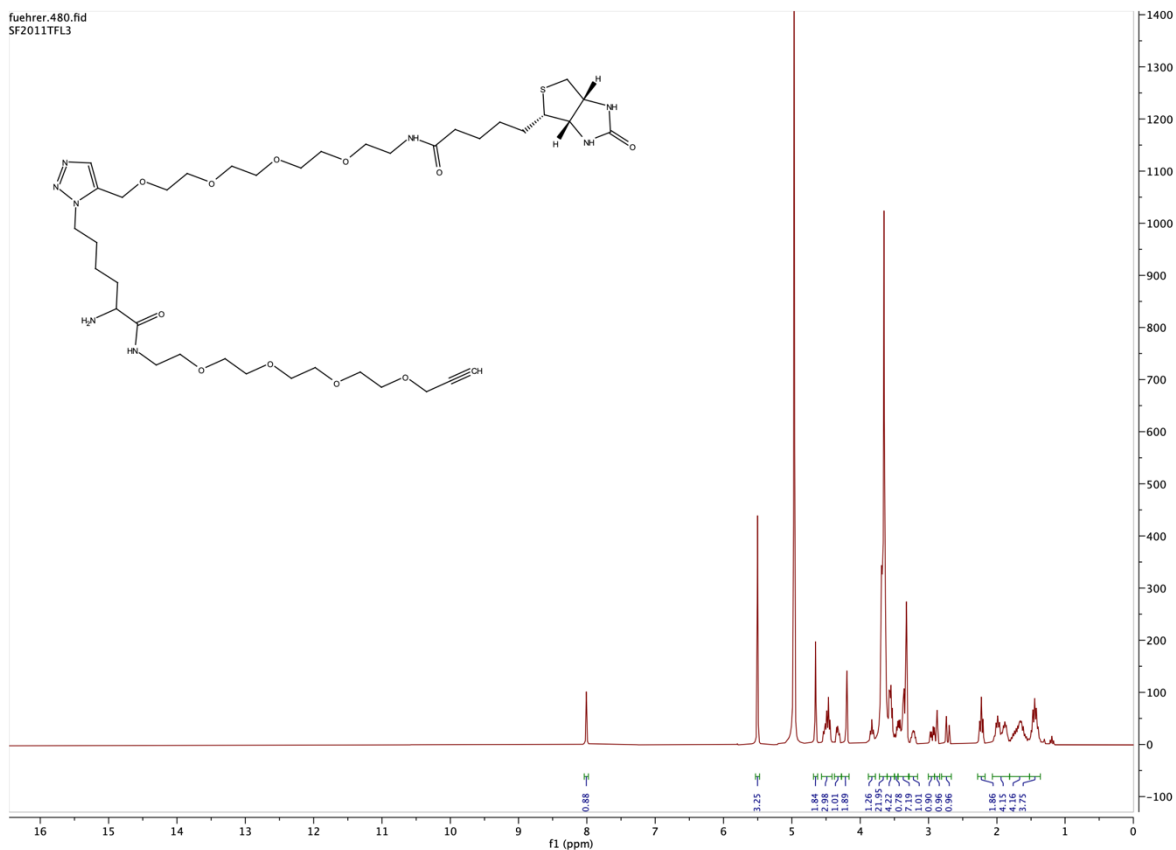
Appendix 2: ^{13}C NMR of compound 2. Measurement conducted at 300 MHz in MeOD.



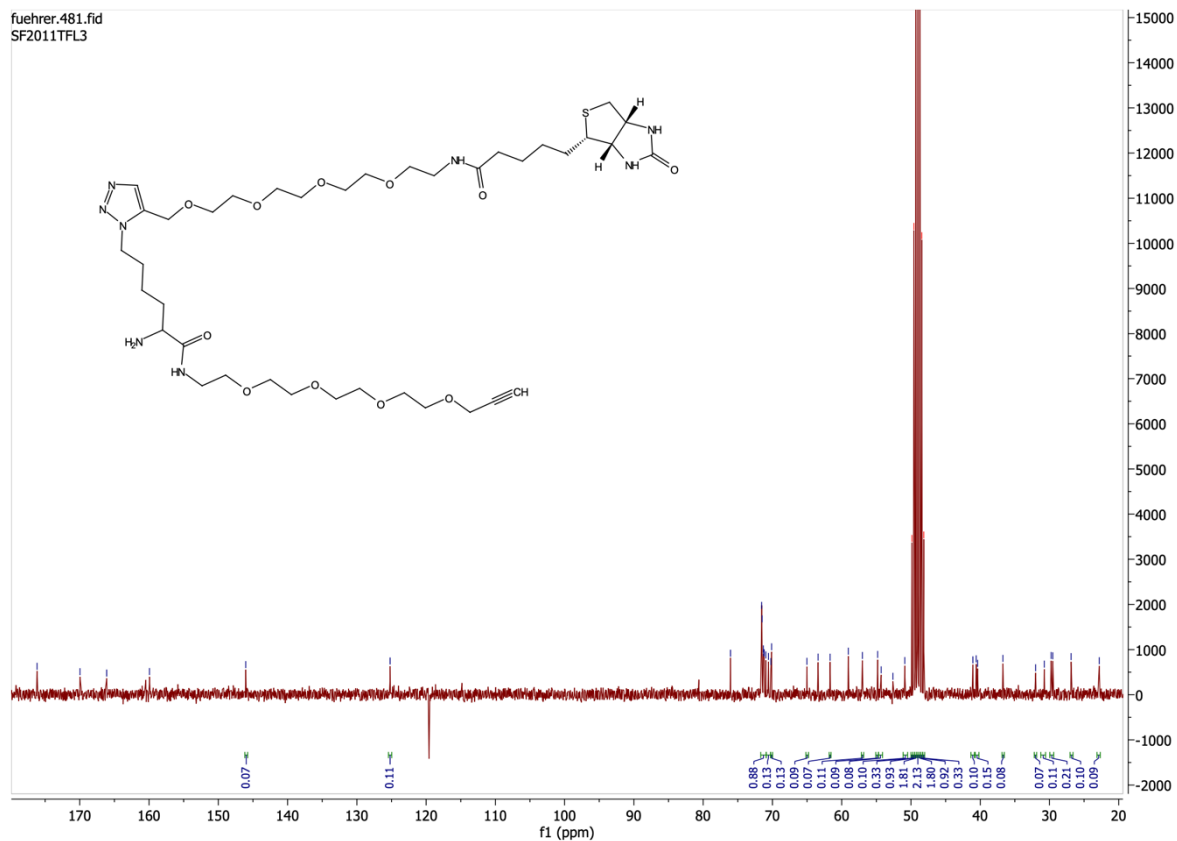
Appendix 3: ^1H NMR of compound 3. Measurement conducted at 300 MHz in MeOD.



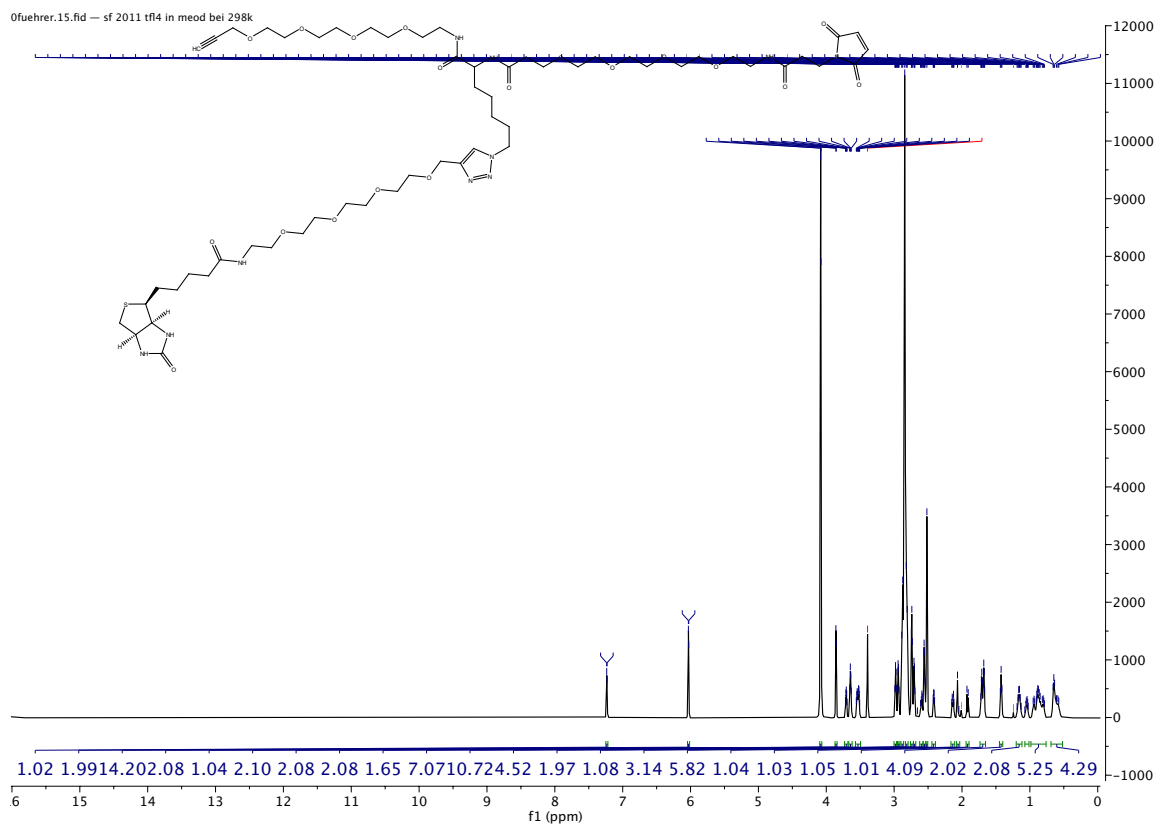
Appendix 4: ^{13}C NMR of compound 3. Measurement conducted at 300 MHz in MeOD.



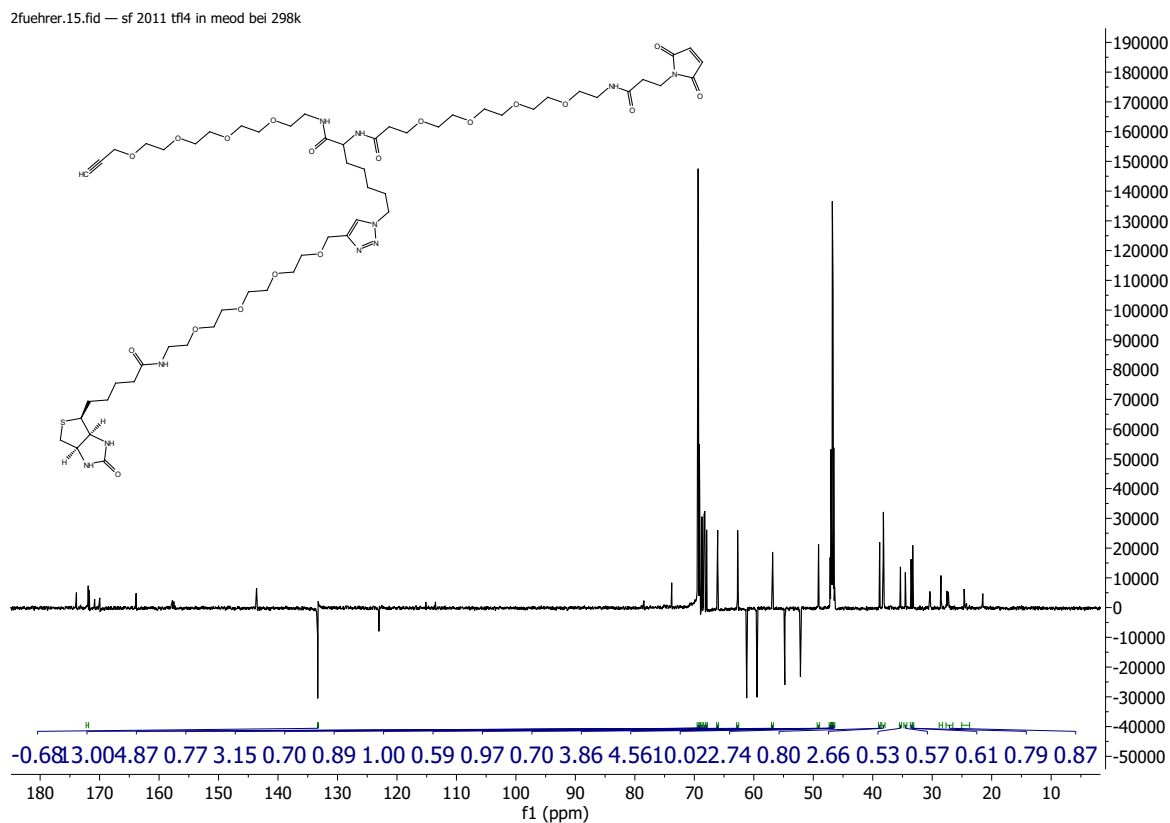
Appendix 6: ¹H NMR of compound 4. Measurement conducted at 300 MHz in MeOD.



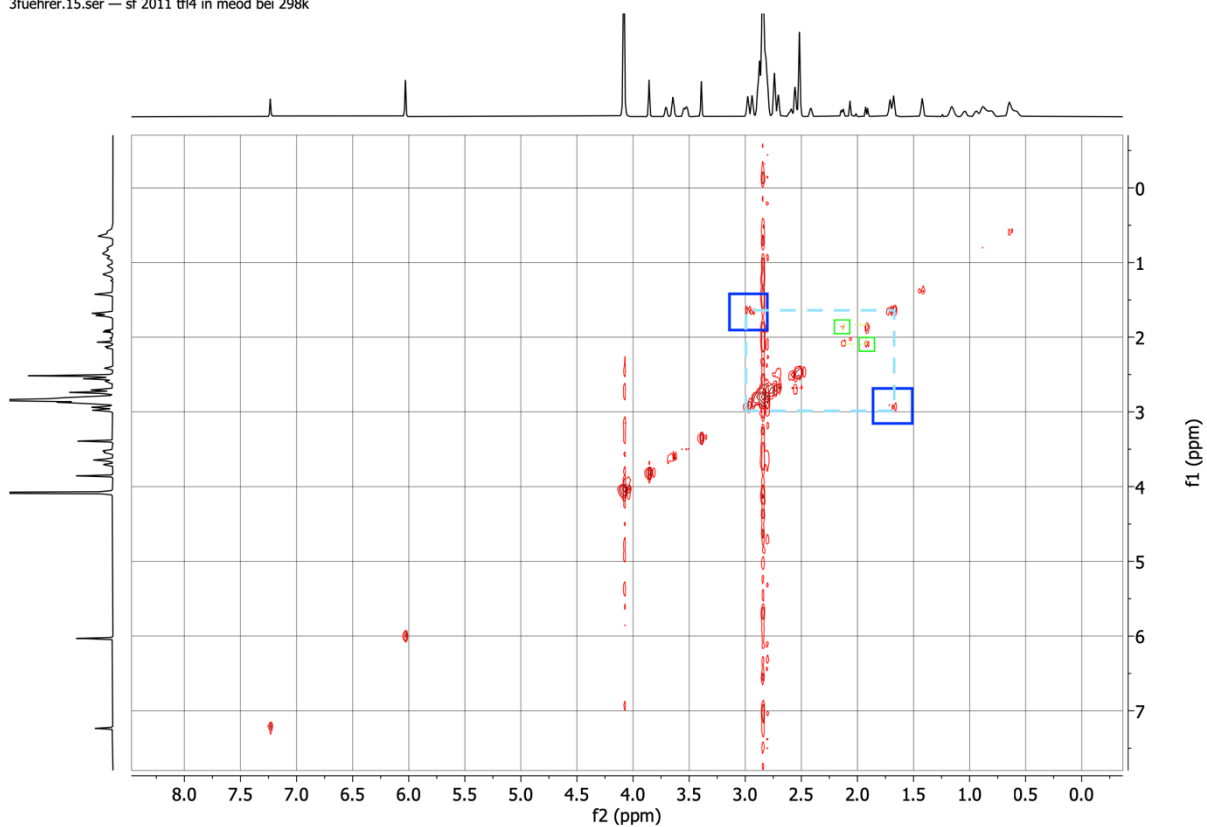
Appendix 5: ¹³C NMR of compound 4. Measurement conducted at 300 MHz in MeOD.



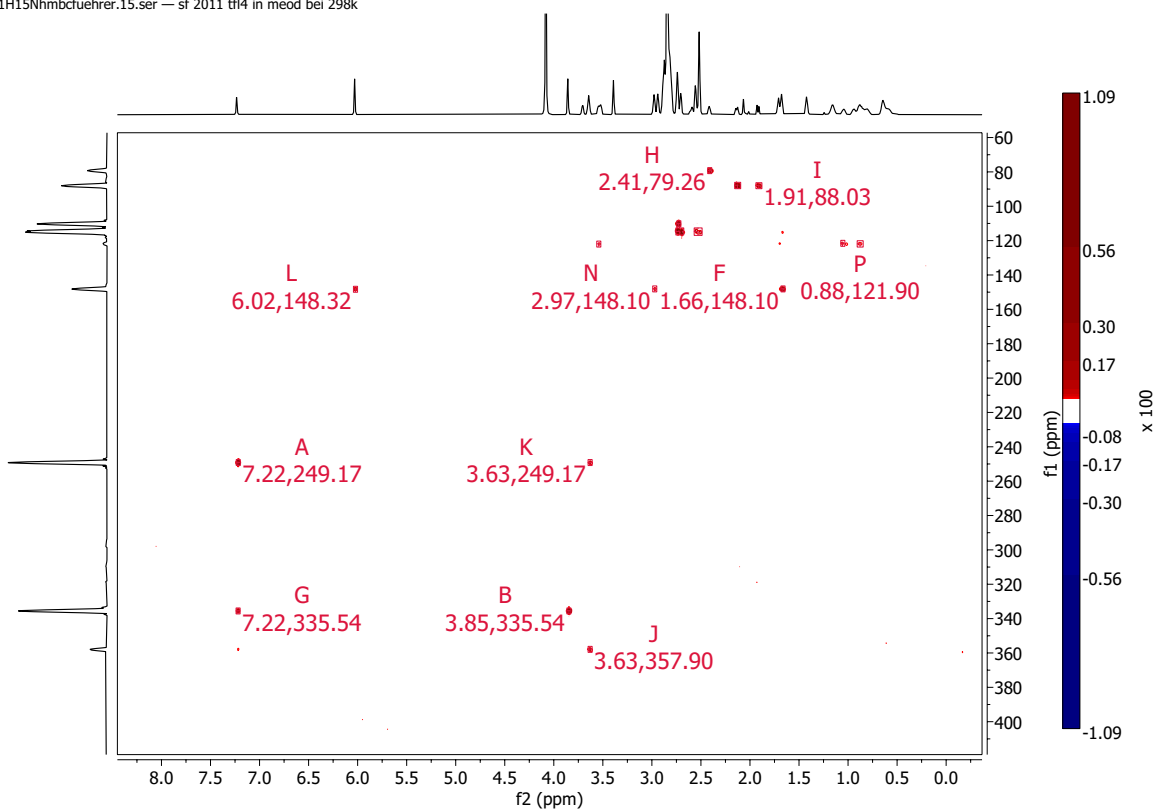
Appendix 8: ^1H NMR of compound 5. Measurement conducted at 700 MHz in MeOD.



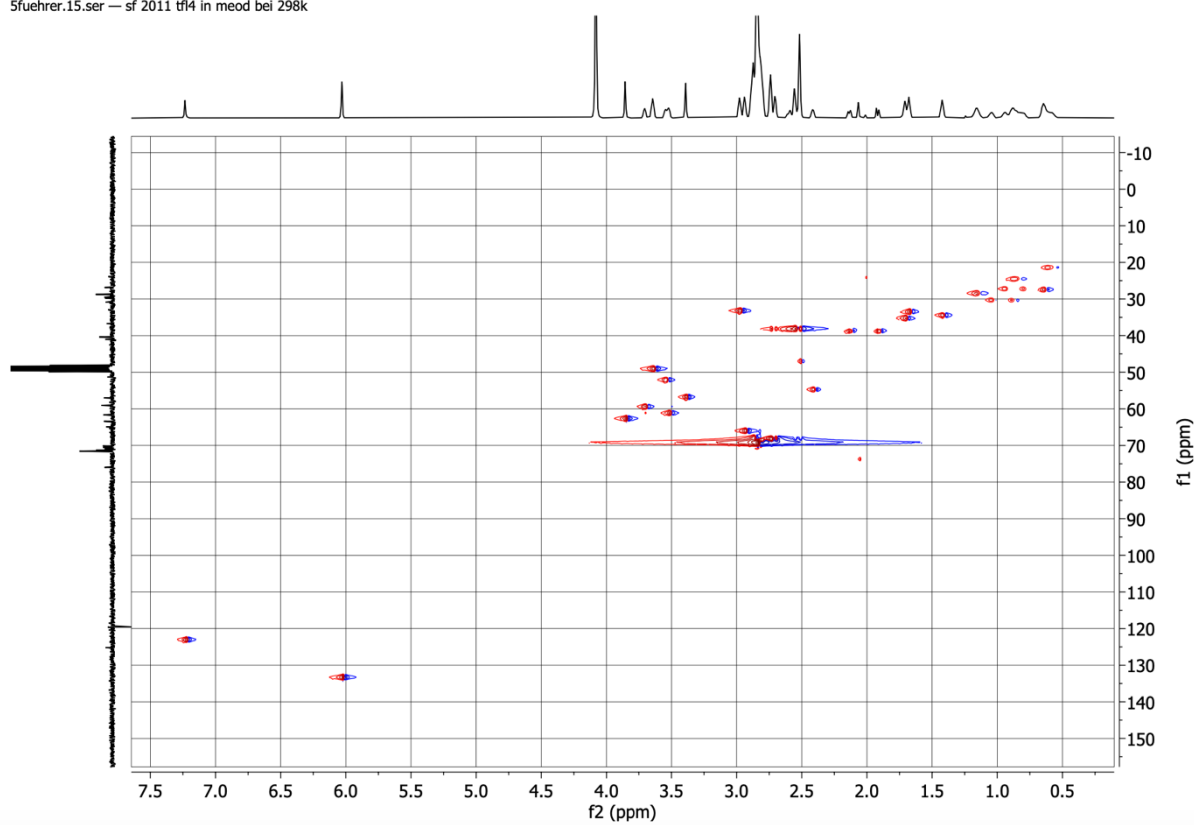
Appendix 7: ^{13}C NMR of compound 5. Measurement conducted at 700 MHz in MeOD.



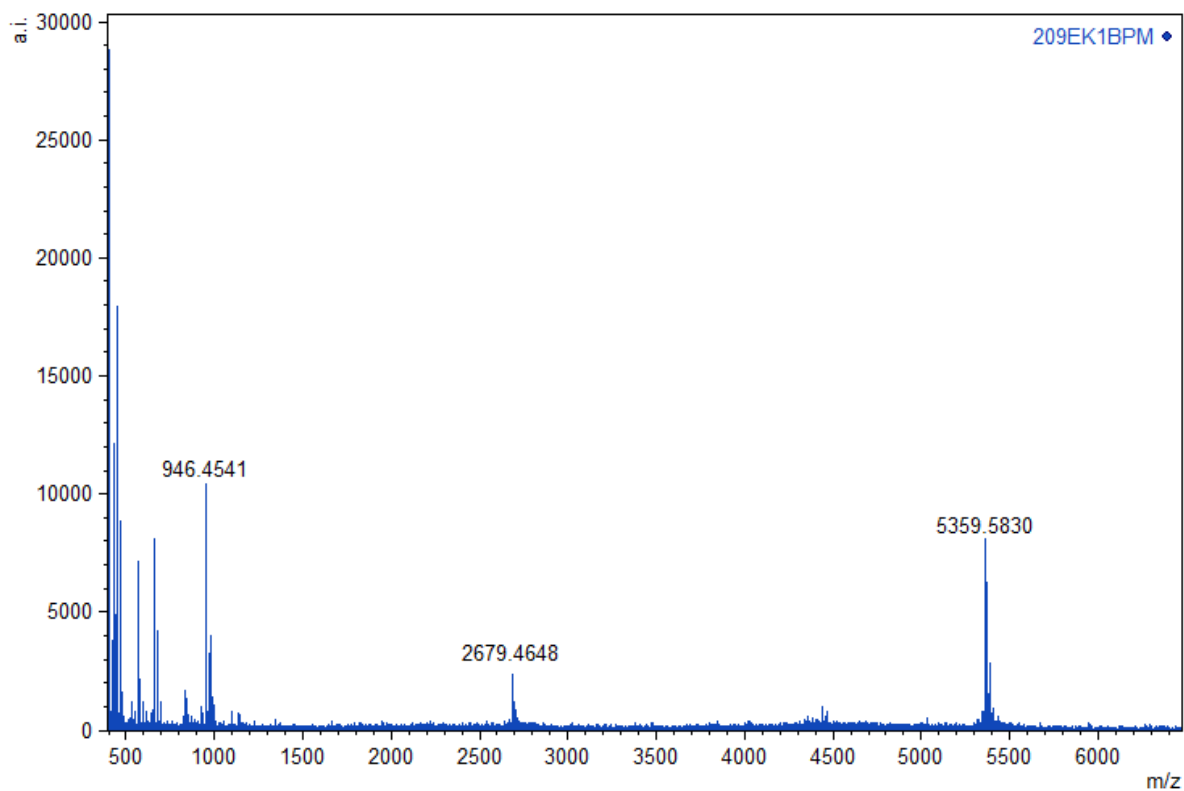
Appendix 9: COSY of compound 5. Measurement conducted at 700 MHz in MeOD.



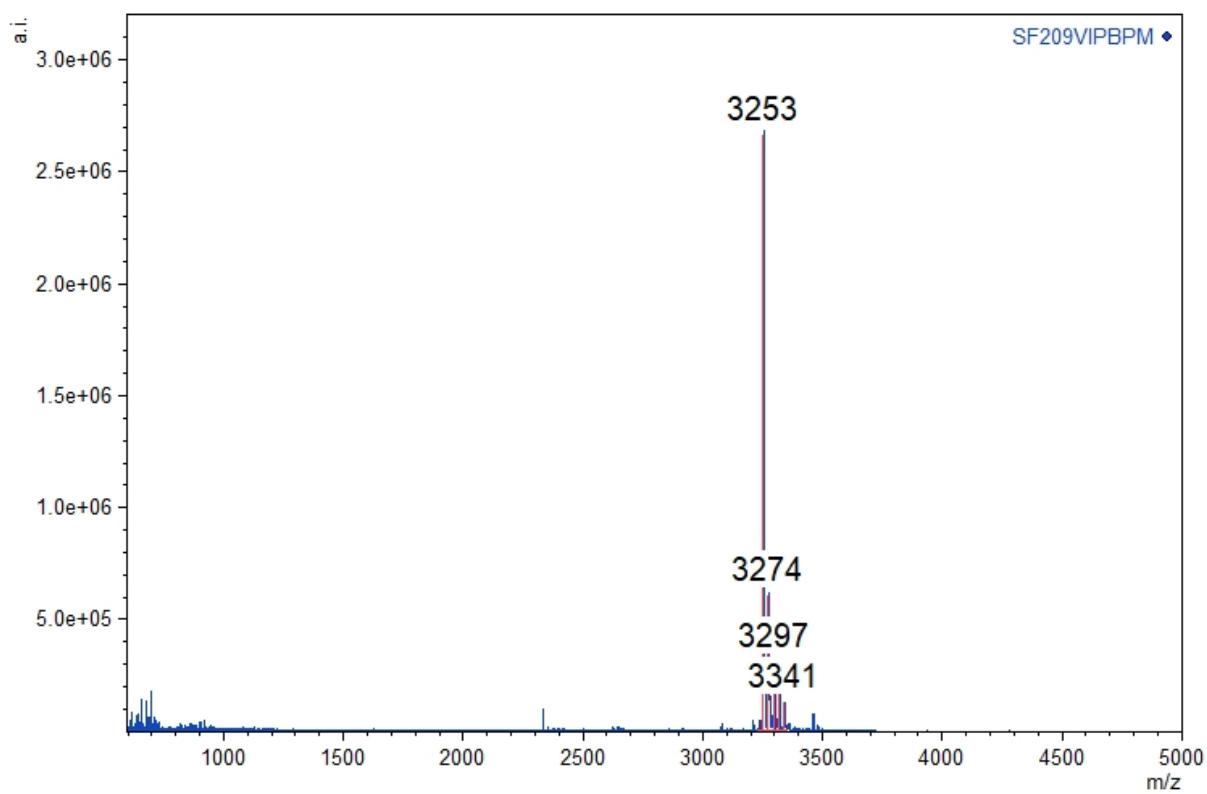
Appendix 10: 1H-13C-HMBC NMR of compound 5. Measurement conducted in MeOD at 700 MHz.



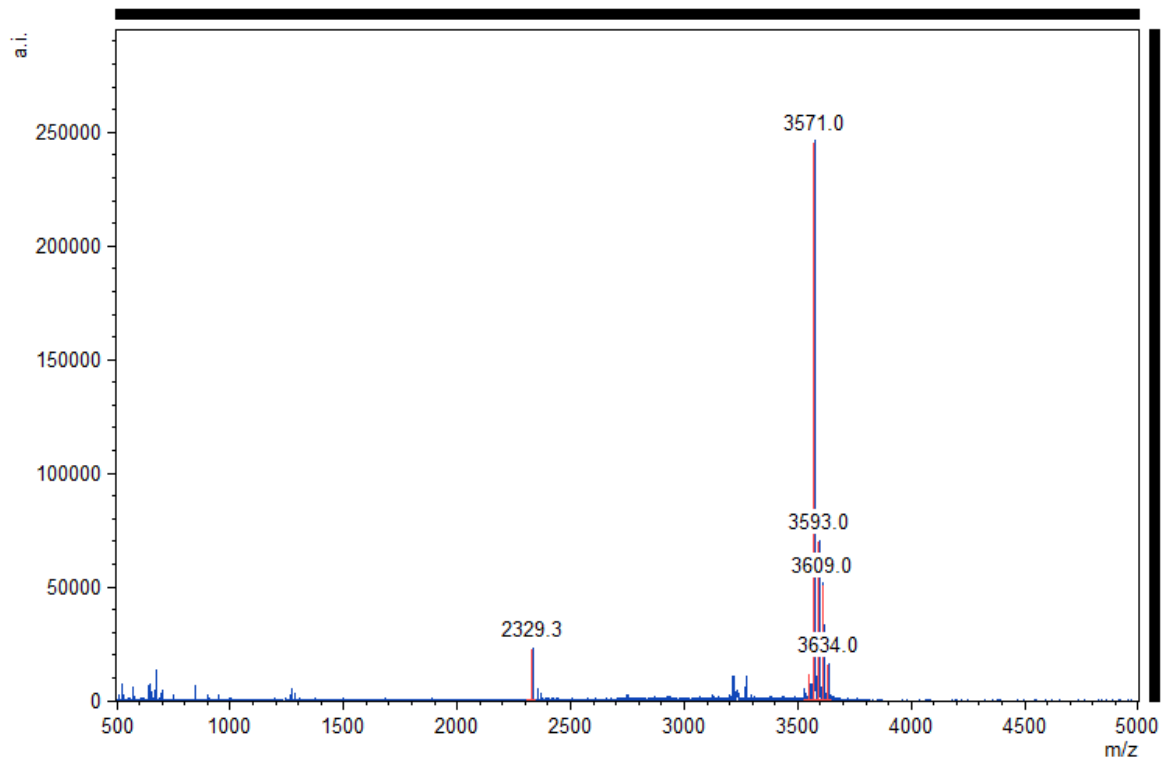
Appendix 11: ¹H-¹³C HSQC NMR spectrum of compound 5. Measurement obtained in MeOD at 700 MHz.



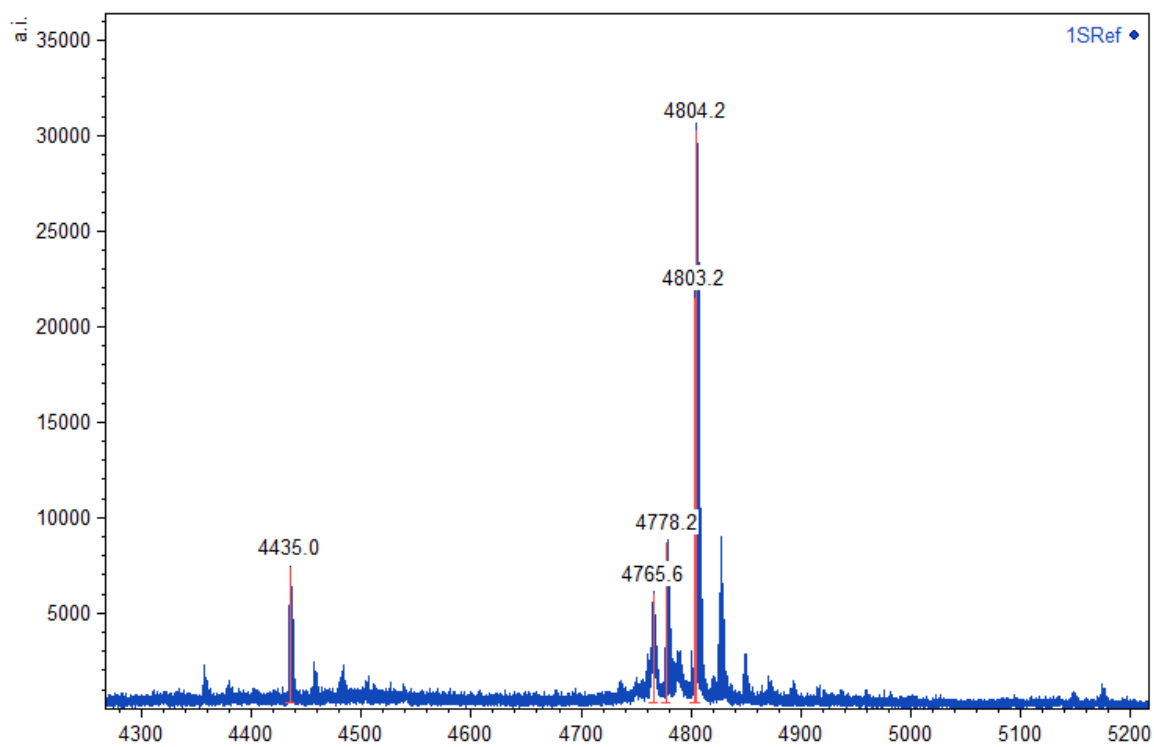
Appendix 12: MALDI TOF spectrum of compound 6. Measurement was performed using SA as a matrix.



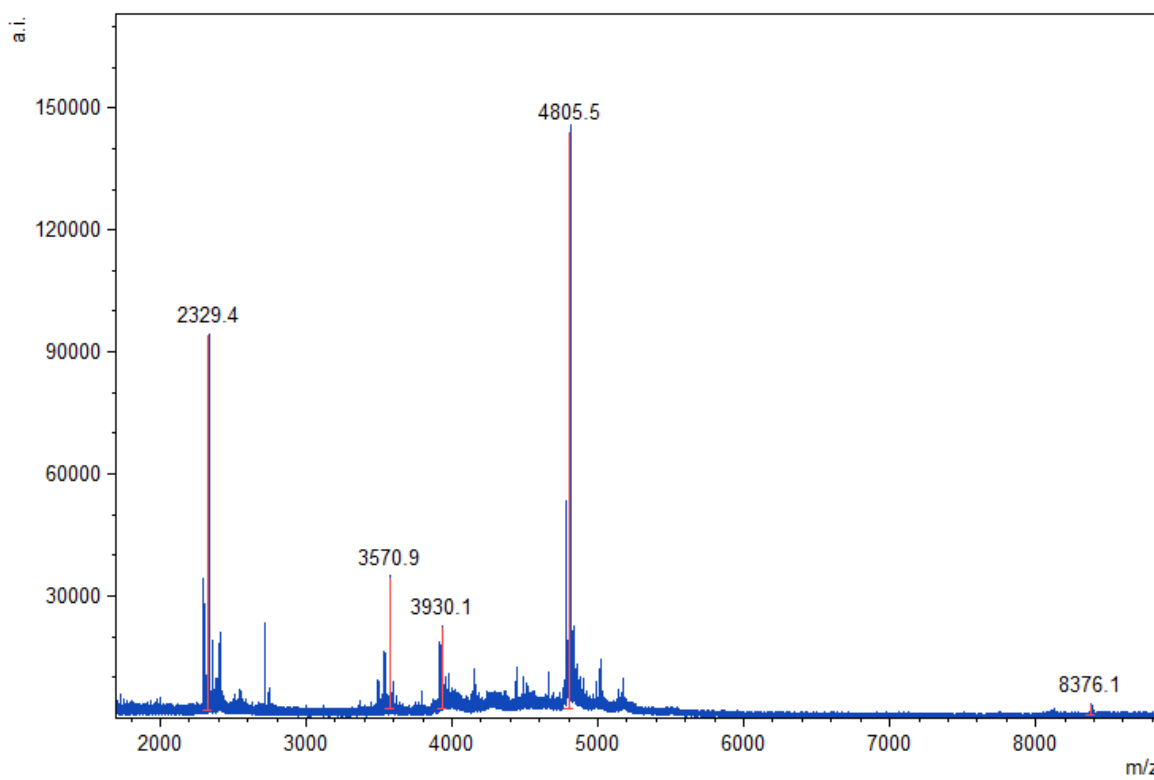
Appendix 13: MALDI TOF analysis of compound 7. Measurement was performed using CHCA as a matrix.



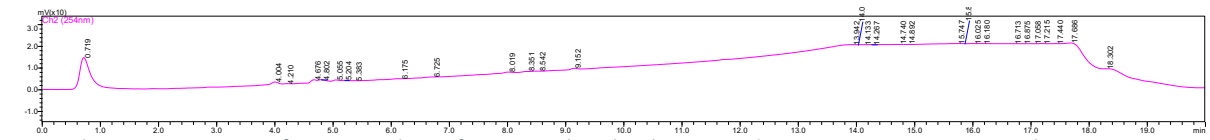
Appendix 14: MALDI TOF analysis of compound 8. Measurement was performed using CHCA as a matrix.

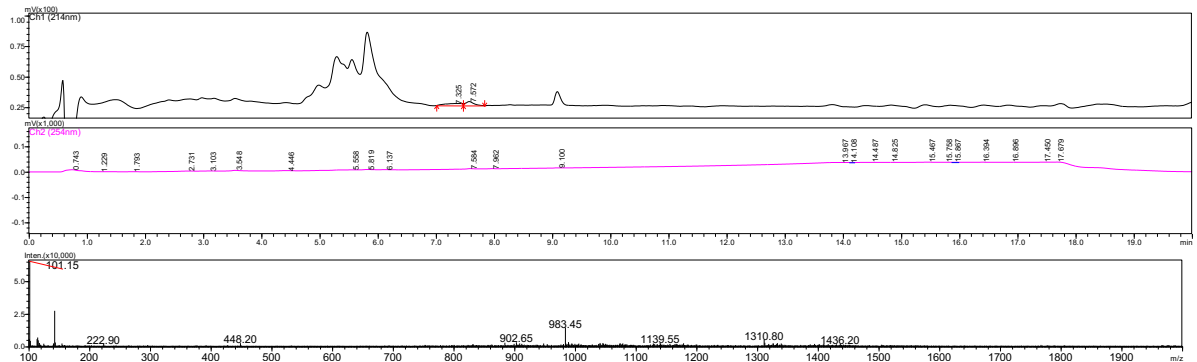


Appendix 15: MALDI TOF analysis of compound 9. Measurement was performed using CHCA as a matrix.

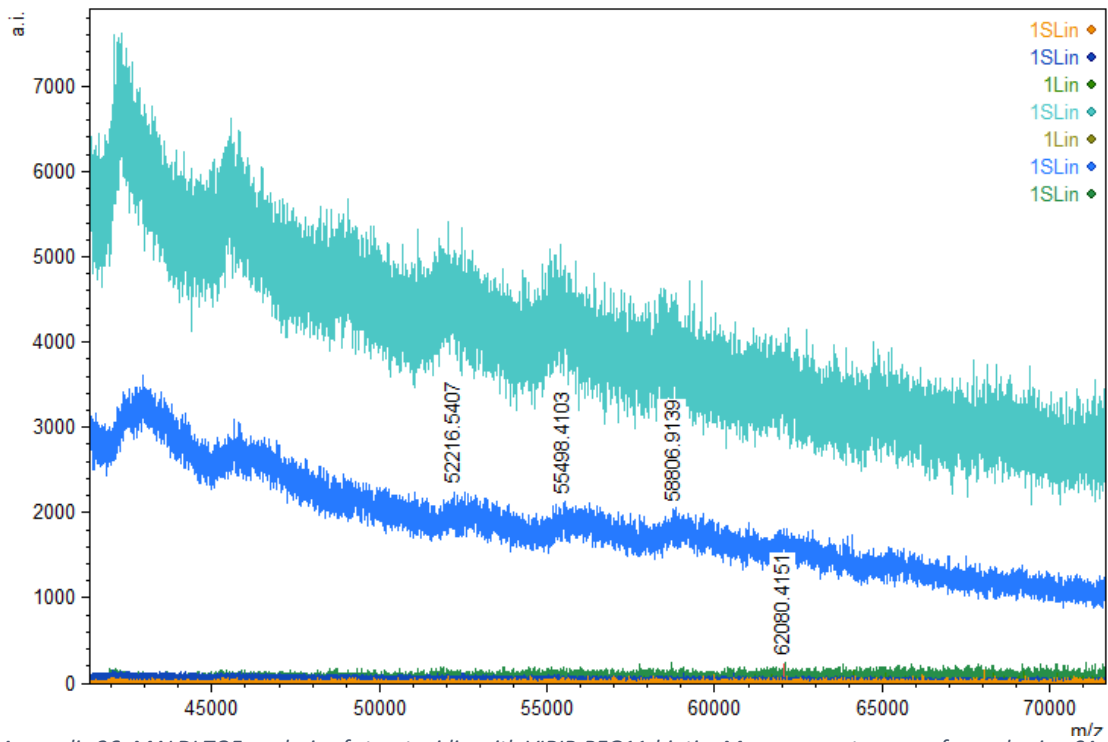


Appendix 16: MALDI TOF analysis of reaction mixture of compound 10. Measurement was performed using SA as a matrix.

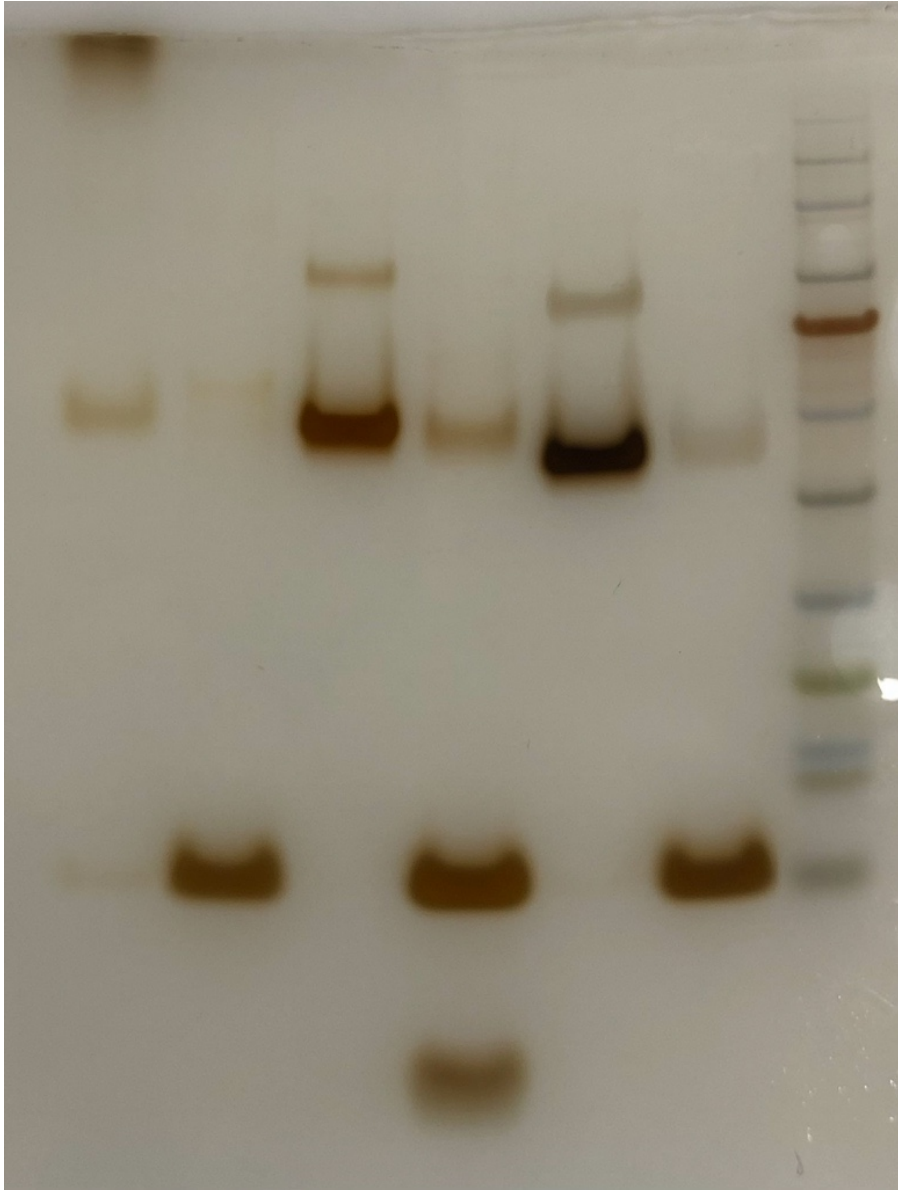




Appendix 25: LC-MS analysis of the reaction mixture of compound 10. The shown chromatogram was measured at 214 nm and 254 nm.



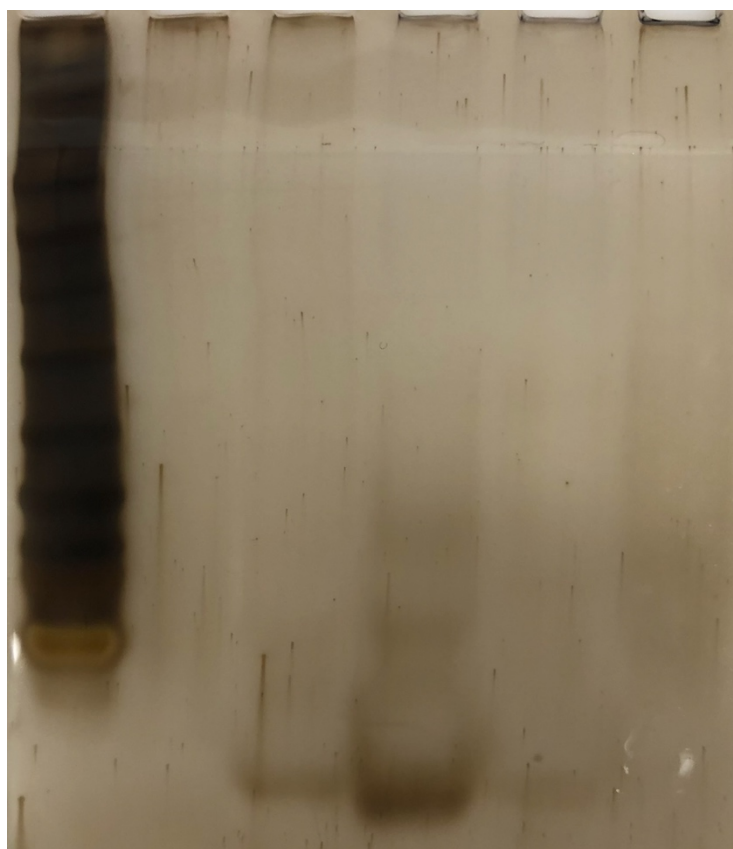
Appendix 26: MALDI TOF analysis of streptavidin with VIRIP-PEG11-biotin. Measurement was performed using SA as a matrix.



Appendix 27: SDS PAGE of purified streptavidin protein hybrids and native streptavidin. Electrophoresis was performed at 120 V in MES running buffer. Band visualization was performed by silver staining.



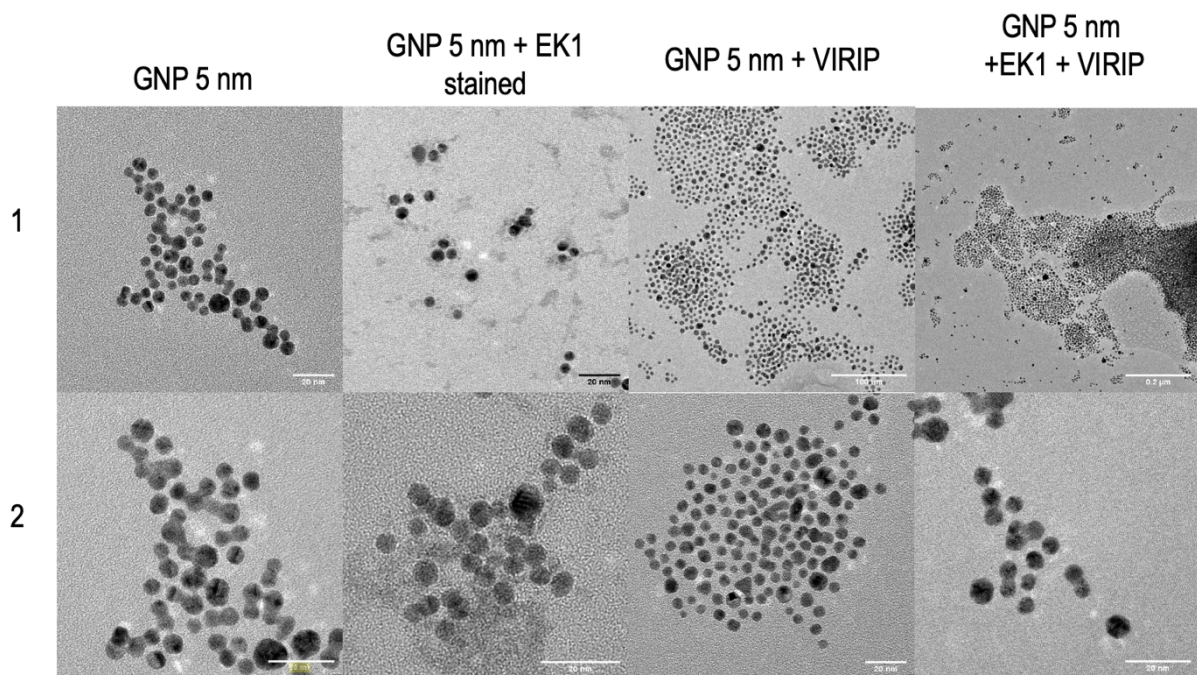
Appendix 28: Visible light photography of gold nanoparticles with EK1. Once purified, once freshly mixed and once each compound alone. Electrophoresis was performed at 130 V in MES running buffer.



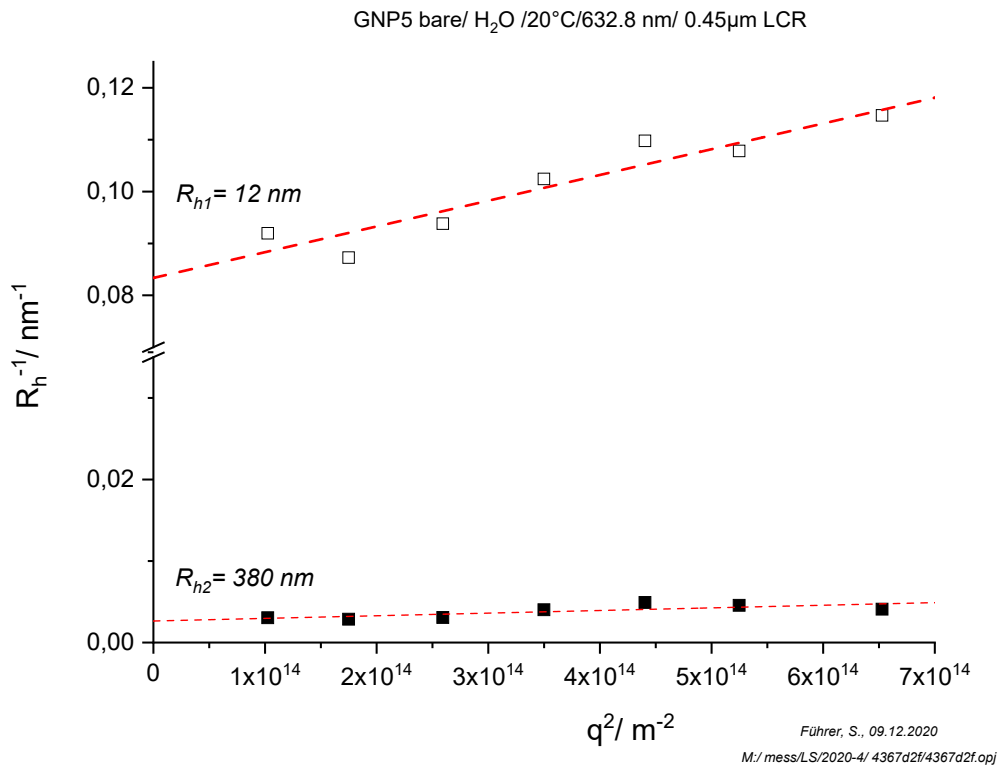
Appendix 29: Silver stained SDS PAGE of gold nanoparticles with EK1. Once purified, once freshly mixed and once each compound alone. Electrophoresis was performed at 130 V in MES running buffer.



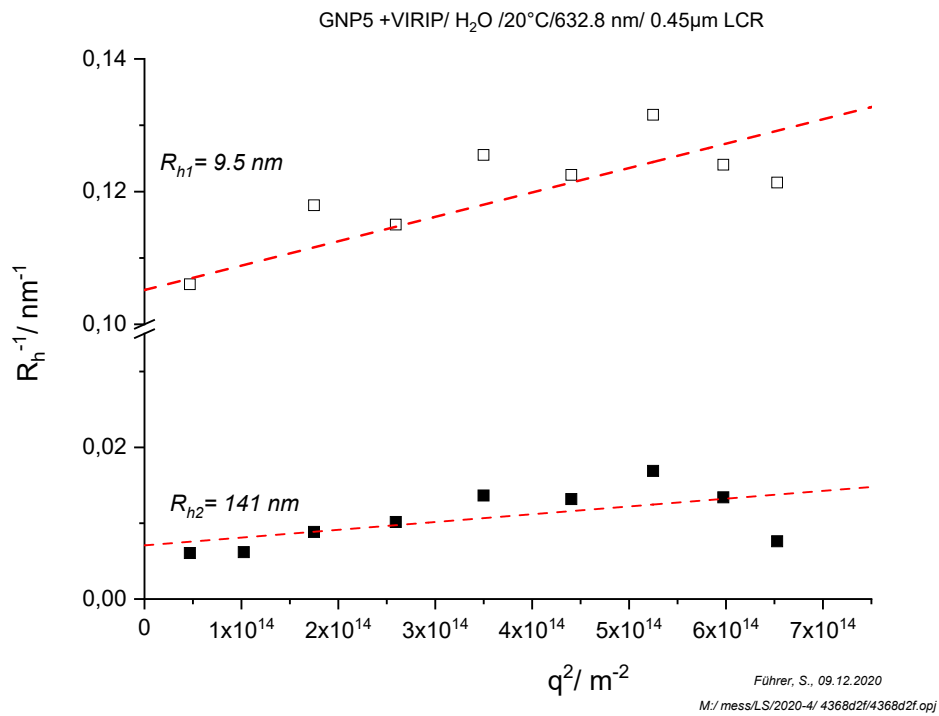
Appendix 30: Visible light photography of agarose gel electrophoresis of peptide coated gold nanoparticles. Electrophoresis was performed using an 1.0% agarose gel in TAE running buffer. Electrophoresis was performed at 50 V.



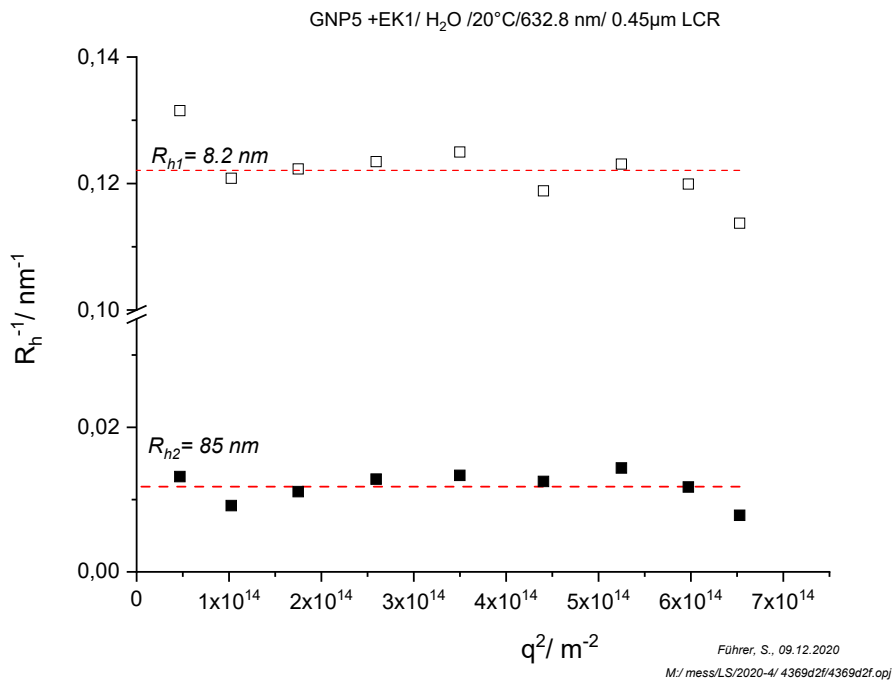
Appendix 31: TEM imaging of peptide coated gold nanoparticles in comparison to untreated GNPs. EK1 coated GNP sample was stained with uranyl acetate. Measurement was performed by Jiaxu Liang..



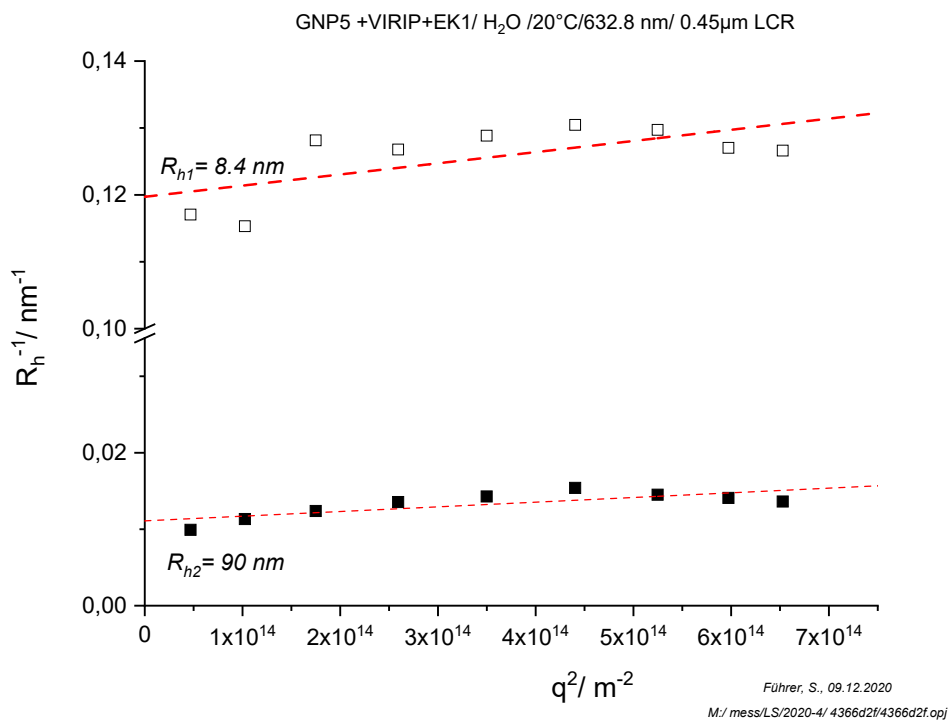
Appendix 32: Multi angle DLS measurement data of blank GNPs. Measurement was performed in ultrapure water by Christine Rosenauer.



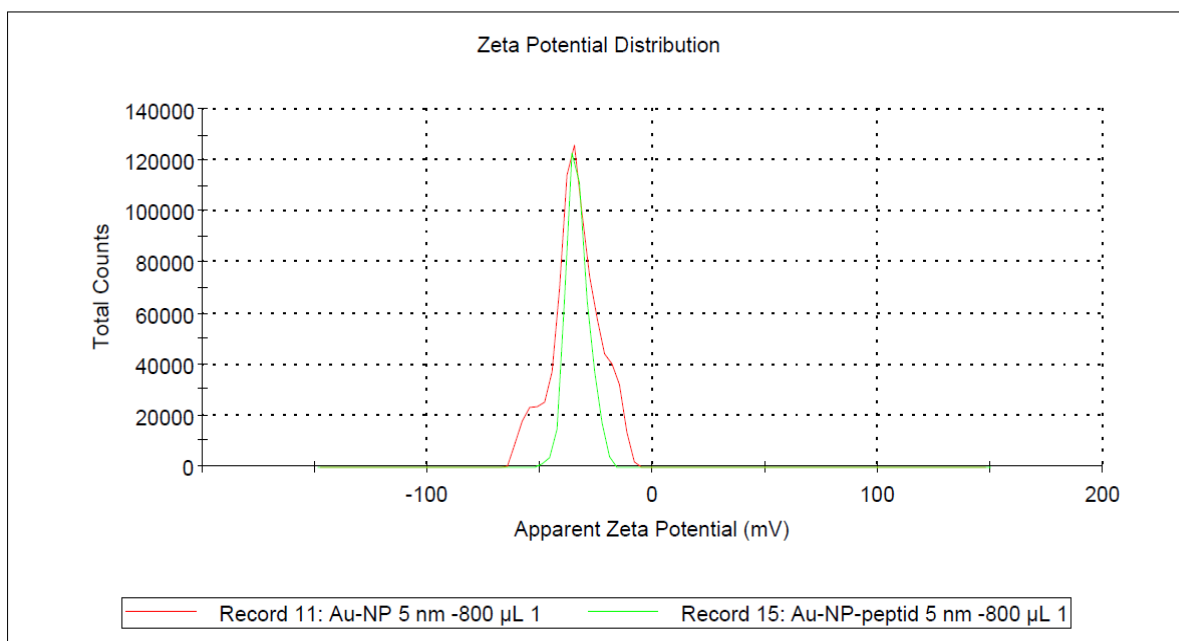
Appendix 33: Multi angle DLS measurement data of VIRIP coated GNPs. Measurement was performed in ultrapure water by Christine Rosenauer.



Appendix 34: Multi angle DLS measurement data of EK1 coated GNPs. Measurement was performed in ultrapure water by Christine Rosenauer.



Appendix 35: Multi angle DLS measurement data of VIRIP and EK1 coated GNPs. Measurement was performed in ultrapure water by Christine Rosenauer.



Appendix 36: Zeta potential measurement of peptide coated GNPs versus citrate stabilized GNPs. Measurement was performed in 1 M KCl solution by Astrid Heck.